

**THE UNIVERSITY OF WESTERN ONTARIO  
DEPARTMENT OF CIVIL AND  
ENVIRONMENTAL ENGINEERING**

**Water Resources Research Report**

**ANEMI 3**

**Tool for investigating impacts of global change**

**By:  
Patrick A. Breach  
and  
Slobodan P. Simonovic**

**Report No: 108  
Date: May 2020**

**ISBN: (print) 978-0-7714-3145-6; (online) 978-0-7714-3146-3**



**ANEMI 3**  
**TOOL FOR INVESTIGATING IMPACTS OF GLOBAL CHANGE**



**By**  
**Patrick A. Breach**  
**And**  
**Slobodan P. Simonovic**

**Department of Civil and Environmental Engineering**  
**Western University, Canada**

**Report No.108**  
**May 2020**

## Executive Summary

The ANEMI3 model is a computer simulation model of global change that emphasizes the role of water resources. Securing water resources for the future is a key issue of global change, and ties into global systems of population growth, climate change carbon cycle, hydrologic cycle, economy, energy production, land use and pollution generation. The current version of the ANEMI integrated assessment model developed at Western University is made up of 11 sectors including: population, land use, food production, carbon cycle, climate, energy-economy, and three water sectors composed of water quality, demand, and availability through modelling of the global hydrological cycle. In this approach the Earth system is modelled as a series of feedback processes linking the 11 sectors or sub-systems. The model is developed using a systems dynamics simulation approach. The model is driven endogenously from an initial state as opposed to the scenario driven approach in most of the available models of global change. The benefit to this approach is that the feedbacks between the model sectors can be studied, allowing for the integrated assessment of global change from an entirely endogenous perspective.

With the new structure of the ANEMI3 model, various experiments can be conducted in order to; examine the impacts of climate change throughout the Earth system, evaluate potential limits to population growth through the depletion of food and water supplies and the generation of pollution, assess the potential impacts of water quality on the development of water supplies, and analyze the role of water supply development of conventional and alternative water supplies in adapting to global water stress. The role of alternative water supplies in the form of desalination and wastewater reuse can be also assessed to fulfill future water demands beyond conventional water supplies of surface and groundwater.

The report presents the ANEMI3 model structure in details and provides discussion of parameter estimation and model validation. The entire model code is provided in the “ANEMI” GitHub repository located at <https://github.com/FIDS-UWO/anemi> as a Vensim model file titled “ANEMI3.mdl”. This file can be opened using the Vensim software in order to view the model structure. A free Vensim PLE licence can be obtained from <https://vensim.com>, which can be used to view the stock and flow diagram that makes up the model structure. Due to the advanced features used in the ANEMI3 model, a Vensim DSS license is required to run the model.

## Table of Contents

List of Figures.....	5
List of Tables.....	7
1 Introduction .....	8
1.1 Analyzing the Earth System.....	8
1.2 Integrated Assessment Models of Global Change .....	9
2 ANEMI Model Evolution.....	10
3 ANEMI3 Model of Global Change – Methodology.....	16
3.1 Intersectoral Feedback Structure .....	17
3.2 Description of the ANEMI3 Model Sectors.....	22
3.2.1 Climate Sector .....	22
3.2.2 Carbon Cycle .....	26
3.2.3 Population Sector.....	31
3.2.4 Land Use Sector.....	36
3.2.5 Food Production Sector.....	39
3.2.6 Sea Level Rise Sector.....	45
3.2.7 Hydrologic Cycle Sector .....	47
3.2.8 Water Demand Sector.....	51
3.2.9 Energy-Economy Sector.....	56
3.2.10 Water Supply Development .....	79
3.2.11 Nutrient Cycles.....	90
3.2.12 Persistent Pollution.....	98
4 Model Validation .....	103
4.1 Parameter Estimation .....	103
4.2 Model Validation.....	105
4.2.1 Behaviour Reproduction.....	105

4.2.2	Future Model Performance .....	111
5	Closing Remarks .....	116
6	References.....	117
	Appendix A: Parameters for the Nutrient Cycles .....	124
	Appendix B: Differential evolution algorithm for parameter estimation.....	126
	Appendix C: Previous Reports in the Series .....	129

## List of Figures

Figure 2.1. Intersectoral feedback structure of ANEMI1 (after Davies and Simonovic 2010). .....	12
Figure 2.2. Intersectoral feedback structure of ANEMI2 (after Akhtar et al. 2013). .....	14
Figure 2.3. Feedback structure of wastewater energy-recovery implementation in ANEMI2 (after Breach and Simonovic 2018).....	15
Figure 3.1. Intersectoral causal loop diagram of the ANEMI3 model. ....	18
Figure 3.2. Causal loop diagram of the ANEMI3 climate sector. ....	23
Figure 3.3. Stock and flow diagram of the ANEMI3 climate sector.....	24
Figure 3.4. Causal loop diagram of carbon cycle sector in ANEMI3. Red, green, and blue arrows and variables represent connections to climate, land use, and energy production sectors respectively. ....	27
Figure 3.5. Stock and flow diagram of carbon cycle in the ANEMI3 model. ....	28
Figure 3.6. Causal loop diagram of the ANEMI3 population sector.....	32
Figure 3.7. Stock and flow diagram of the ANEMI3 population sector. ....	33
Figure 3.8. Causal diagram of the ANEMI3 land use sector.....	36
Figure 3.9. Stock and flow diagram of ANEMI3 land use sector. ....	37
Figure 3.10. Causal loop diagram of the ANEMI3 food production sector.....	39
Figure 3.11. Stock and flow diagram of the ANEMI3 food production sector. ....	40
Figure 3.12. Relationship between global temperature change and change in potential arable land (after King et al. 2018). Error bars represent 95% confidence interval from the GCMs used in calculating global average temperature change.....	43
Figure 3.13. Distribution of crop production for the 4 crop types used in (Searchinger et al. 2019) compared to global totals in the years 1980 and 2017.....	44
Figure 3.14. Causal diagram of the ANEMI3 sea-level rise sector.....	46
Figure 3.15. Causal loop diagram of the ANEMI3 hydrologic cycle sector. ....	47
Figure 3.16. Stock and flow diagram of the AEMI3 hydrologic cycle sector. Items in blue denote processes that have human influence on the hydrologic cycle, while those in red represent the influence of changing climate.....	48
Figure 3.17. Illustration of structural water intensity for domestic water use (after Alcamo et al. 2003). .....	51
Figure 3.18. Causal diagram of the ANEMI3 water demand sector. ....	52
Figure 3.19. GCAM energy production projections for 2005-2100 (after Davies et al. (2013)). .....	53

Figure 3.20. Causal loop diagram for good production and capital sub-system of the energy-economy sector.....	58
Figure 3.21. Stock and flow diagram of the ANEMI3 capital sector of the economy.....	59
Figure 3.22. Causal loop diagram for the energy production sub-system of the ANEMI3 energy-economy sector. ....	62
Figure 3.23. Stock and flow diagram for the ANEMI3 energy production sector .....	64
Figure 3.24. Causal loop diagram for the energy capital sub-sector of the energy-economy sector. ..	65
Figure 3.25. Stock and flow diagram of the ANEMI3 energy capital sector .....	66
Figure 3.26. Causal loop diagram for energy requirements sub-system in the ANEMI3 energy-economy sector. ....	69
Figure 3.27. Stock and flow diagram of energy requirements sub-system of ANEMI3 energy-economy sector.....	70
Figure 3.28. Causal loop diagram of ANEMI3 energy pricing sector.....	73
Figure 3.29. Stock and flow diagram for the energy pricing sub-system of the ANEMI3 energy-economy sector. ....	74
Figure 3.30. Causal loop diagram for the technological change sub-system of the ANEMI3 energy-economy sector. ....	76
Figure 3.31. Stock and flow diagram of energy technology sub-system within the ANEMI3 energy-economy sector. ....	77
Figure 3.32. Causal loop diagram of the ANEMI3 water supply development sector. The dotted arrow from water price to water supply indicates a causality that is neither positive nor negative .....	80
Figure 3.33. Stock and flow diagram of the ANEMI3 water supply development sector.....	81
Figure 3.34. Water pricing component of the ANEMI3 water supply development sector. ....	82
Figure 3.35. Illustration of Wood's algorithm. ....	86
Figure 3.36. Production structure of water supply within the energy-economy-water sector of the ANEMI3. ....	88
Figure 3.37. Goods allocation in the energy-water-economy sector of the ANEMI3. ....	89
Figure 3.38. Stock and flow diagram of the ANEMI3 nitrogen cycle. ....	94
Figure 3.39. Stock and flow diagram of the ANEMI3 phosphorus cycle. ....	95
Figure 3.40. Causal structure of the ANEMI3 persistent pollution sector. ....	98
Figure 3.41. Stock and flow diagram of the ANEMI3 persistent pollution sector. ....	99
Figure 4.1. ANEMI3 model behavior reproduction.....	109

Figure 4.2. ANEMI3 model future behavior.....	113
---	-----

## List of Tables

Table 3.1. Connections between different model sectors in ANEMI3. Highlighted rows represent the intersectoral connections that have been added or modified in this work.....	20
Table 3.2. Initial transfer matrix for area between land use/cover types in [Mha/year].....	38
Table 3.3. Effect of temperature change on crop yields for wheat, rice, maize, and soybean. ....	44
Table 3.4. Initial stock values for hydrologic cycle sector. All values are in units of [km <sup>3</sup> ]. ....	49
Table 3.5. Percentages of water reallocation in the hydrologic cycle after human withdrawal and consumption. ....	49
Table 3.6. Water withdrawal rates for energy production of various types (Larsen and Drews 2019). .....	54
Table 3.7. Parameters used nutrient inputs to nutrient cycles.....	97
Table 3.8. Parameters values used in the persistent pollution sector. ....	103
Table 4.1. Model constants and their optimal values with corresponding sectors.....	104
Table 4.2. Model testing procedures based on Sterman (2000). ....	106
Table 4.3. Comparison datasets for baseline model run. ....	107
Table 4.4. Datasets used for comparison of the ANEMI3 model future behaviour.....	112
Table A.1. Initial values and residence times of carbon, nitrogen, and phosphorus stocks in their respective cycles from Mackenzie et al. (1993).....	124
Table A.2. Rate constants used to describe flow in the cycles of carbon, nitrogen, and phosphorus from Mackenzie et al. (1993).....	125

# 1 Introduction

Human impacts on the environment at global scales are being realized through our ability to alter atmospheric concentrations of greenhouse gases and consequently global climate, creating the need to consider environmental problems and their interactions with the Earth as a system. The Earth system is composed of biological, physical, chemical, and human elements that form a network of feedbacks through their interconnections (Steffan et al. 2004). The concept of global change becomes increasingly important as the components of the Earth system such as population, economic productivity, climate, food production, and hydrology are interlinked through dynamic non-linear feedback processes (Davies 2007). Within this system, changes in one component inevitably lead to changes in another. This is why global change research focusses on interactions between components of the Earth system as a whole, as opposed to only those of climate (Cox and Nakicenovic 2004; Steffan et al. 2004).

## 1.1 Analyzing the Earth System

Assessment of various aspects of global change often requires the use of models from different domains and a way to combine them so that the relationships and interactions between these models can be studied. When it comes to global change research, the goal is often to analyze the effect of policies or scenarios on different aspects of global change. This in turn provides the information necessary to help inform the policies of decision makers. This has necessitated the use of new tools and modelling paradigms to analyze complex interactions in the Earth system at a variety of spatial and temporal scales.

The concept of integrated assessment (IA) has been defined as an interdisciplinary process of bringing together knowledge from different disciplines, adding value in contrast to a single disciplinary approach in order to provide information to decision and policy makers (Rotmans and Dowlatabadi 1998). It is performed to bring about understanding of an issue regardless of the discipline. IA is often applied to issues that involve physical, biological, and/or social elements to bring together knowledge from different fields. Environmental issues have been the main focus of IA, specifically with regards to climate change and natural resource management (Rotmans and van Asselt 1999).

There are many different methods that can be used to form a model for integrated assessment. Connections between disciplinary models can be made statically (output of one model is first obtained then given as input to another), or dynamically (both models running at the same time). The latter of which, is the only way that feedback loops can be created and studied. Dynamic connections can be made by using a computer program to facilitate the exchange of information while the models are running, or both models can be combined into the same computer code (Tol and Vellinga 1998). The field of system dynamics focusses specifically on analyzing the dynamic nature of systems that are composed of feedback loops. Therefore, the use of system dynamics is ideal for the construction of integrated assessment models of global change.

System dynamics simulation implements the principles of systems thinking to decompose real world problems into systems built of interconnected elements. Systems thinking facilitates the conceptualization of system dynamics simulation models through the formulation of dynamic hypotheses (how a system will behave over time). This process involves the use of causal loop diagramming to map out the feedback loops that are driving system behaviour. This is effectively describing the boundary of the problem as well as the components that are responsible for reproducing it. Systems thinking provides a formalized way of implementing Step 2 of the integrated assessment process described in Tol and Vellinga (1998) through the mapping of feedback loops. System dynamics simulation builds from the conceptual models developed through systems thinking by adding structure to them. The addition of stocks or state variables, and the flows that affect them take the system from a conceptual model to a mathematical model through stock and flow diagramming. Stock and flow diagrams illustrate the configuration of stocks and flows which is essentially a visual representation of a system of first order differential equations. Most, if not all, IAMs can be represented in this way from a high level. For these reasons, the system dynamics simulation approach is ideal for the construction of IAMs and provides a formalized way for creating feedback loops between disciplinary models of global change.

## 1.2 Integrated Assessment Models of Global Change

Understanding the interactions between sub-systems of the Earth system is a demanding task and involves communication between diverse areas of study (Hamilton et al. 2015; Dunford et al. 2014; Janetos 2008). To gain an understanding of the interactions between different sub-systems of the Earth system, integrated assessment models are employed. IAMs use simplified representations of

various sectors within the Earth system including; social-economy, climate, ecology, water resources, land use and cover, carbon cycle, and energy production and demand for example, to represent complex feedback structures between them which evolve through time (Akhtar et al. 2013; Hamilton et al. 2015). It is within this framework that global change can be assessed in response to various scenarios regarding policy, technological developments, and socioeconomic trends. IAMs are used to develop scenarios for greenhouse gas emissions and land use/cover for GCMs to simulate climate change (Moss et al. 2010).

The IAMs continue to evolve and therefore the integration between these sectors and biogeophysical cycles of the Earth system (Fiddaman 2002) is becoming tighter. Part of this integration has led to more comprehensive representations of the hydrologic cycle to assess impacts on water stress through comparisons of water availability and demand (Strzepek et al. 2013). The models that currently integrate water availability and demand are: AIM (Asia-Pacific Integrate Model) (Matsuoka et al. 2001), IMAGE (Integrated Model to Assess the Global Environment) (Stehfest et al. 2014), IGSM-WRS which is a modification of the Integrated Global System Model that includes a Water Resource System component (Strzepek et al. 2013), GCAM (Global Change Assessment Model) (Calvin et al. 2019), and ANEMI (Davies and Simonovic 2010; Akhtar et al. 2013). Complete review of relevant literature is provided in Breach (2020).

## **2 ANEMI Model Evolution**

The word *anemi* is a Greek word that translates to “the winds of change”. The choice of this word for the integrated assessment model used in this work was to capture the dynamic and feedback driven nature of the model which makes it unique in the domain of integrated assessment modelling. The ANEMI model was inspired by the WorldWater model of Simonovic (2002), which was based on the WORLD3 model of Meadows and Jorgen (1992). The WORLD model was created to assess potential limits to the growth of human civilization through natural resource and pollution effects which were explored using system dynamics simulation techniques. This work showed that overshoot and collapse behaviours in our global system are expected in the future due to the coupling of economic growth and material consumption. This was later expanded upon in the WorldWater model to include the World’s water resources as another potential limit to growth. Conceptually, the ANEMI model builds upon that of WorldWater by developing a model that is purely based on system dynamics (model is

constructed using stocks and flows to represent feedback processes), which an emphasis on the role of water resources in the Earth system.

The ANEMI model is developed at the Facility for Intelligent Decision Support, at Western University. It started with integration of 8 global models of climate, carbon, land use, population, energy-economy, water use, water quality and the natural hydrologic cycle. The climate sector models the change and interaction between atmospheric and ocean temperatures in response to radiative forcing from changes in atmospheric greenhouse gas concentrations. The carbon sector provides atmospheric carbon dioxide concentrations to the climate sector by modelling the carbon cycle on a globally aggregated scale. This includes carbon stocks for land biomass, litter, humus, stable humus and charcoal, and several ocean layers. The transfer of carbon in the carbon cycle is influenced anthropogenically by changes in land use, and industrial carbon dioxide emissions. The changes in land use are driven primarily by population growth rates resulting in conversion of temperate forest, and semi-desert and tundra biomes to agricultural land, and agricultural land to human developed areas. Anthropogenic greenhouse gas emissions are driven by the production of energy which is closely tied to economic development. The economic sector models economic output as a function of the global capital stock, and labor from the working population.

In the ANEMI model, water resources are represented through the three water sectors, including water quality, water demand, and the hydrologic cycle. The hydrologic cycle component determines the amount of water resources available for human consumption, by modelling the movement of water through atmosphere, land, groundwater, ice, and ocean stocks. Water demand is driven through population and economic development as well as irrigation in the case of agricultural demand. A portion of water withdrawals and consumption are driven by the water demand and act to reallocate water in the hydrologic cycle. Water quality is represented simply by allowing for polluted water in the form domestic and industrial wastewaters, as well as agricultural returnable waters to displace freshwater resources. This is done by using the rule of thumb mentioned in Shiklomanov (2000), where 1 unit of polluted water renders 8-10 units of water unsuitable for human consumption, contributing to water stress. Water stress acts as the primary driver for the development of alternative water resources in the form of wastewater reuse and desalination. However, it is assumed that these resources can be established immediately without any consideration for the cost of implementation.

The first version of the ANEMI model (ANEMI1) established the basic feedback structure of the society-biosphere-climate system by bringing together separate sub-systems available in the literature in order to represent the model sectors listed above, and establish inter-sectoral feedbacks used to drive the system (Figure 2.1).

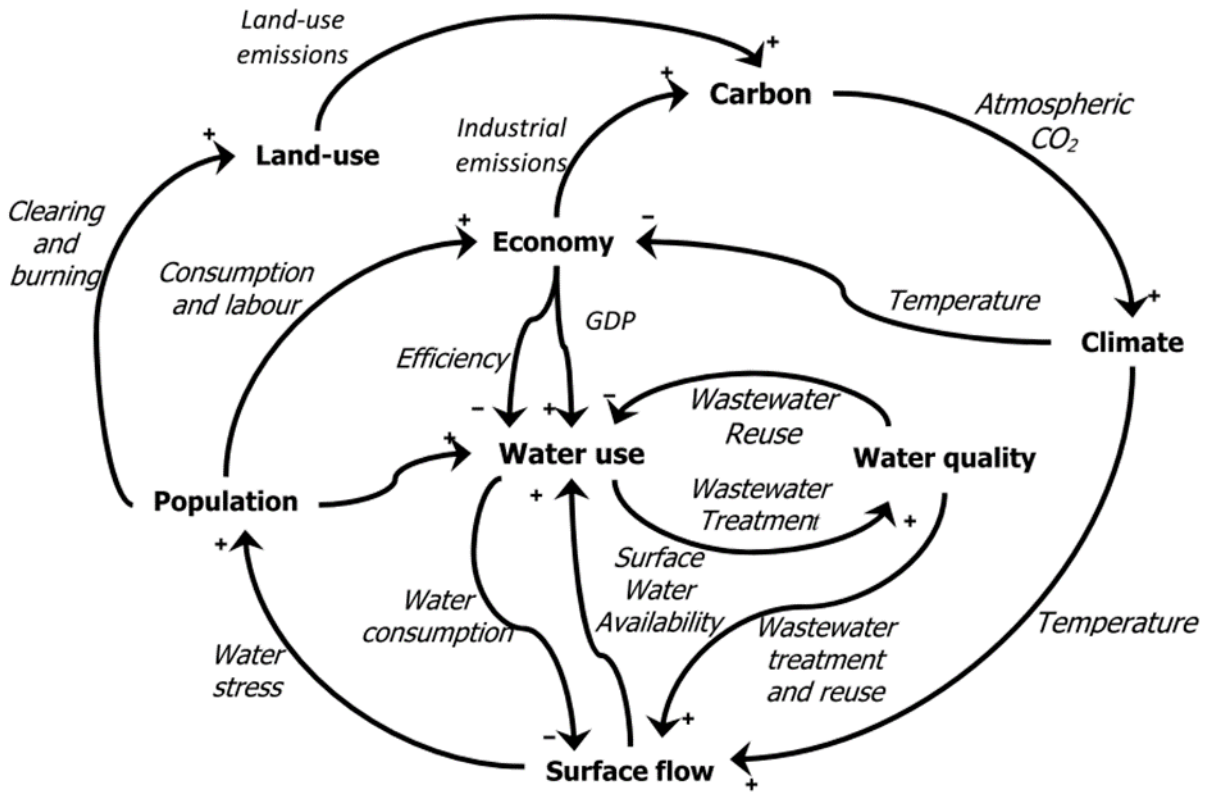


Figure 2.1. Intersectoral feedback structure of ANEMI1 (after Davies and Simonovic 2010).

The purpose of this work was to increase the understanding of socio-economic policies and scientific uncertainties of the Earth system by focusing on system structure and function rather than specific predictions (Davies and Simonovic 2010). Using several policy scenarios and sensitivity simulations it was found that water pollution resulting from low levels of wastewater treatment may lead to severe levels of water stress. It was recommended that greater reuse of treated wastewater and slowing the rate of irrigation expansion could help alleviate water stress in the future. In this work the role of feedbacks on the development of global change are emphasized as feedback interactions between

socio-economic and physical systems are used to drive the model. The feedback structure of ANEMI1 is shown in Figure 2.1.

In Davies and Simonovic (2011) the first version ANEMI model was improved by incorporating more detail into the agricultural and food production sectors as well as how this relates to water pollution. Food production was made to be driven by per capita caloric consumption which varies over time, along with the total caloric consumption which with population. Fodder crops and pasture-based production are simulated separately from food crops due to different water requirements. This allows for more accurate quantification of virtual or green water requirements needed from the agricultural sector of the model. The dilution of green water from agricultural runoff was then incorporated into the definition of water stress by acting as an additional source of water consumption. The results from this study showed that increased levels of irrigation versus rain-fed crops reduced green water consumption and agricultural area by the year 2100. This in turn led to higher water stress values from greater consumption of blue water and more water pollution from agricultural runoff. In other words, in order to meet the demands for food of a growing population water becomes increasing scarce.

The second version of ANEMI (ANEMI2), published in Akhtar et al. (2013) incorporates a computable general equilibrium model to represent energy production within the global economy as well as a new disaggregated population sector, sea-level rise impacts on agriculture, and includes the effect of more greenhouse gases on climate. The disaggregation of the population sector into four age demographics allowed for the working population (ages 15 to 64) to represent the labor force in the economic model, and allowed for heat stress effects driven by changes in climate to affect mortality rates in the old and young (ages 15 or less and 65+). The energy-economy sub-system allowed for a carbon tax scenario to be analyzed. The application of a carbon tax on fossil fuels initially showed a heavier reliance on hydropower and nuclear energy production, as well as a drop in energy consumption due to higher prices. This policy resulted in a 0.4°C by the year 2085 compared to baseline. However, carbon emissions were only delayed, leading to higher emission rates by the year 2100. The feedback structure of ANEMI2 is in Figure 2.2.

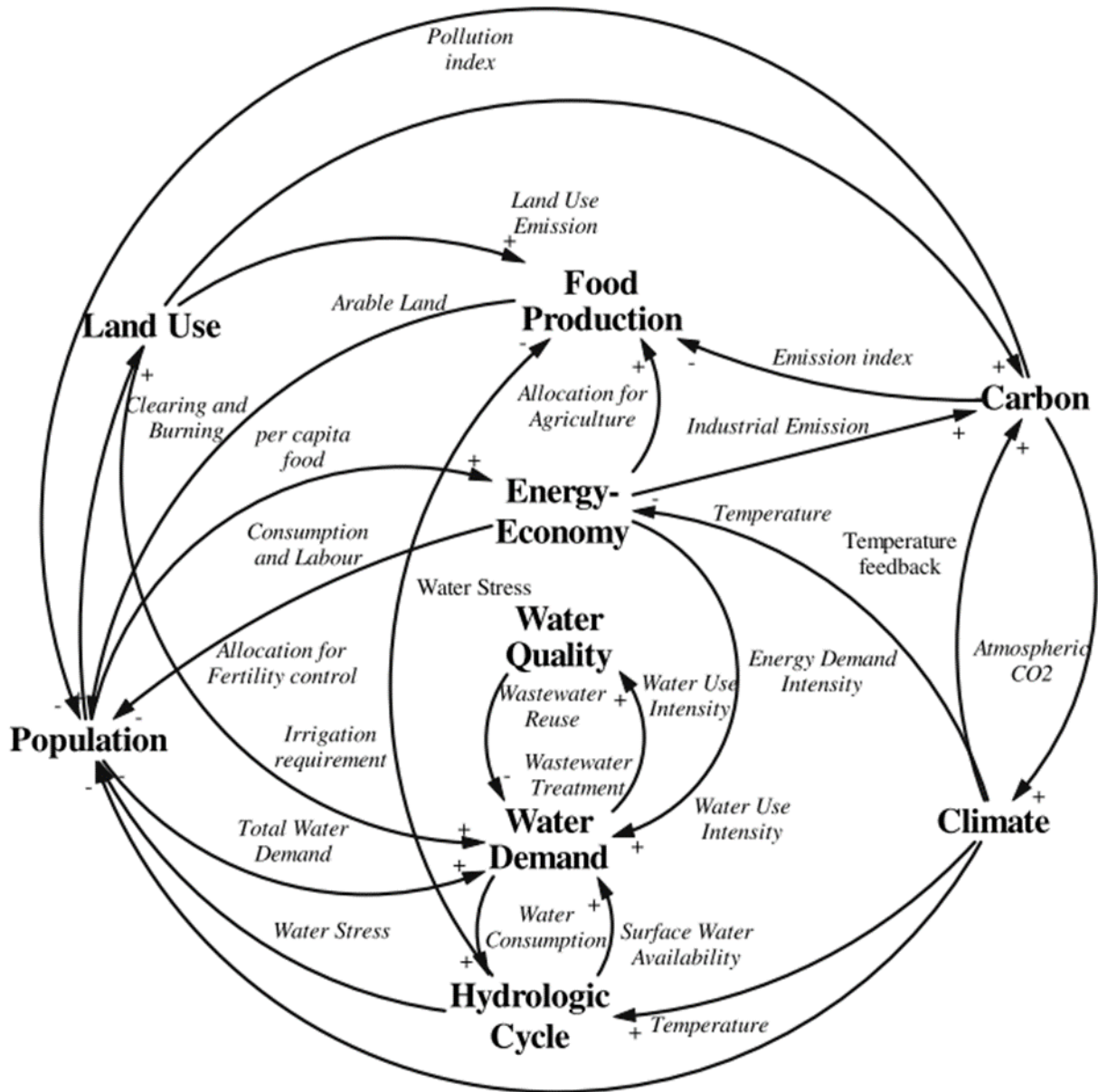


Figure 2.2. Intersectoral feedback structure of ANEMI2 (after Akhtar et al. 2013).

Building from the structure of ANEMI2, Breach and Simonovic (2018) added energy recovery from wastewater in the form of biosolids incineration and biogas utilization. The recovered energy is treated as an additional energy source in the energy-economy sector of ANEMI2, creating a feedback that acts to boost wastewater treatment over time with re-investment from energy recovery. In this work, the level of wastewater treatment is represented by a stock that contains a number of uniform treatment plants providing a level of wastewater treatment capacity. Investment boosts the number of

plants while the processes of aging and decommissioning causes the stock to decrease. Energy-recovered from the wastewater treatment processes provides for a portion of energy production in the energy-economy sector and re-investment is proportional to the energy supplied. The feedback structure of this work is shown in Figure 2.3. Feedback structure of wastewater energy-recovery implementation in ANEMI2 (after Breach and Simonovic 2018). The results show that by viewing the construction of wastewater treatment plants as a type of investment in recovered energy, wastewater treatment could increase globally by 34% despite increases in wastewater volumes due to a growing population with improved access to sanitation.

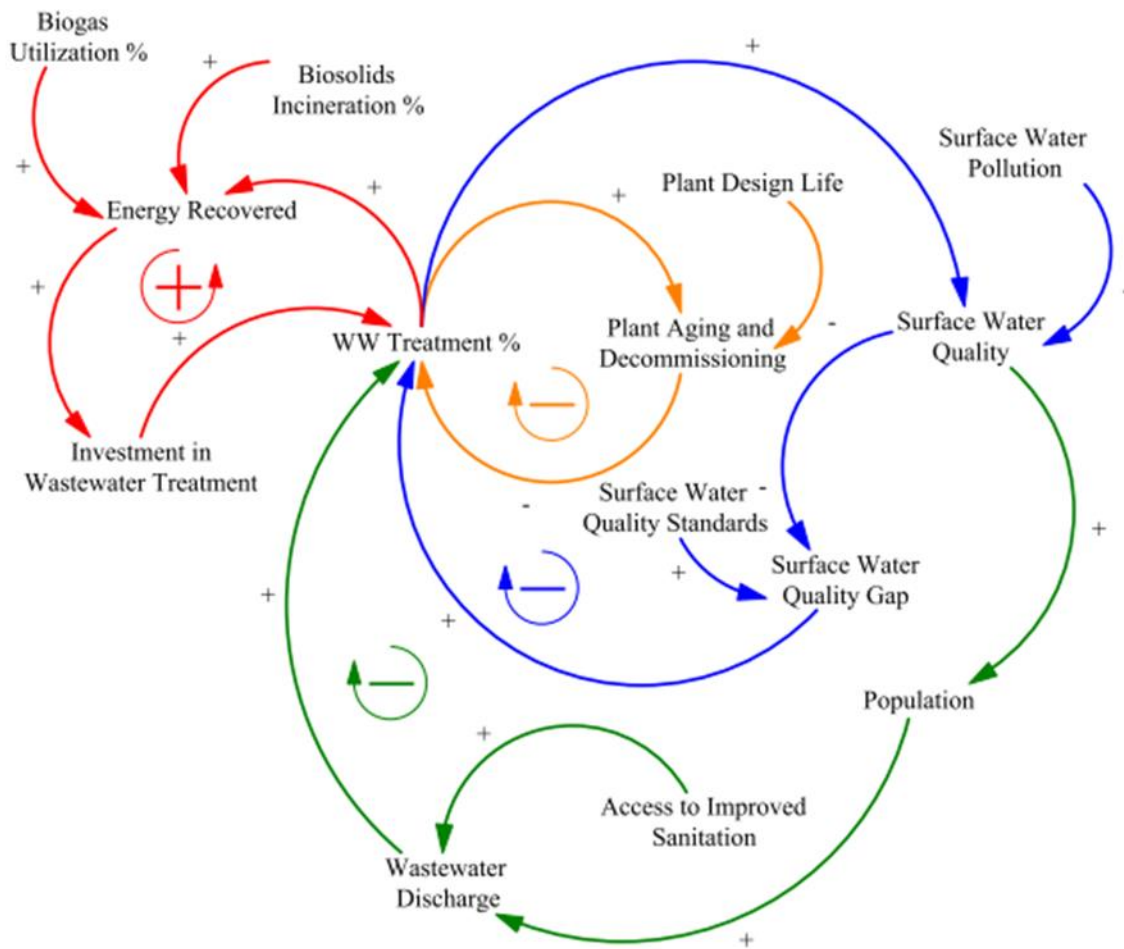


Figure 2.3. Feedback structure of wastewater energy-recovery implementation in ANEMI2 (after Breach and Simonovic 2018).

### **3 ANEMI3 Model of Global Change – Methodology**

This section of the report presents the ANEMI3 model, which is built upon the first two iterations of ANEMI. The model shares the same system dynamics simulation paradigm that was used in the previous iterations of ANEMI, in that feedbacks and delays are used to drive system behaviour. ANEMI3 is a type of integrated assessment model that describes the state of and interactions between model sub-systems that compose the Earth system. The main sub-systems or ‘sectors’ used that of the climate system, carbon, nutrient, and hydrologic cycles, population dynamics, land use, food production, sea level rise, energy production, global economy, persistent pollution, water demand, and water supply development.

Each individual sector in the model describes the relevant feedbacks that drive the state variables in the sector. Connections between sectors form intersectoral feedbacks responsible for the functioning of the Earth system. It is the intersectoral feedbacks that allow us to represent feedbacks that drive global changes in the Earth system. Some of which are evident today while others may become more prominent in the future. From a system dynamics perspective, effective policymaking should be based on addressing the feedback structure of a system, not only on modifying the system parameters. This viewpoint is what makes the ANEMI3 model unique and useful in a time when global modelling is becoming progressively more complex.

The boundary of the model is defined by the problem that is being explored. In this case, we are modelling the role of water resources in various aspects of global change. Therefore, the spatial scale of the model is mainly one that is global. In some sectors, the stocks are disaggregated to capture material flows on a sub-global scale, but not at a level that is location specific. For example, in the nutrient cycles different stocks are used to denote the flow of nutrients from atmosphere to land, humus, rivers, coastal water, and oceans, however each of these individual stocks are globally aggregated. This spatial scale limits the level of detail that can be used to describe the flows that act to change the model stocks, however it allows us to accomplish our research objective to analyze feedbacks between water resources and other model sectors on a global scale.

The time horizon used in the model is from the year 1980-2100. This is in part due to the incorporation of models from different studies into the sub-sectors of ANEMI which had initial time horizons close to the year 1980, while the year 2100 is one that is often used as a benchmark for global change

phenomenon such as climate change. Results are aggregated to an annual time step; however the stocks are integrated using a time step of  $1/128^{\text{th}}$  of a year. This is done because the time step should be sufficiently larger than the smallest time constant in order to avoid instabilities when integrating a system of first order differential equations (Roberts et al. 1983). Simple Euler integration is used to solve the system of equations in the model. This was done to reduce model computation time when performing sensitivity analyses.

One of the objectives of this work is to examine the development of global water supplies from an economic perspective, allowing for the role of both conventional and alternative water supplies to be assessed with regards to offsetting future water stress on a global scale. Another is to assess the potential influence of water quality degradation on the development of surface water supplies. With the assembled model, experiments are to be carried out in order to; a) assess the relationship between water supply and food production to sustain a growing population, b) assess the potential impacts of water quality on the development of water supplies, and c) analyze the impacts of climate change on various aspects of the Earth system.

### 3.1 Intersectoral Feedback Structure

The highly endogenous structure and coupling of sub-systems in the ANEMI3 model are part of its novelty in the realm of integrated assessment modelling. Because of this, feedback processes are responsible for the behaviour that is exhibited in model runs. The model sectors that comprise the ANEMI3 model are that of the climate system, carbon, nutrient, and hydrologic cycles, population dynamics, land use, food production, sea level rise, energy production, global economy, persistent pollution, water demand, and water supply development. Feedback loops between sectors, or intersectoral feedback loops are responsible for global change in this Earth system.

Creating a causal loop diagram from these connections between model sectors allows us to view the feedbacks that are created by combining model sectors in this way (Figure 3.1). Intersectoral feedbacks in the ANEMI3 model allow for the representation of various aspects of global change. In this diagram alone there is a total of 89 possible intersectoral feedback loops. The size of the feedback loops range from 2 to 9 sectors included out of the 10 that are shown.



and structures lost to coastal flooding, for example. This feedback loop is present in other feedback-based integrated assessment models. With the modified feedback structure of the ANEMI3 model in this report, global scale feedbacks are created in addition to those present in the previous iterations. These include:

- Water supply development increases water consumption, thereby reducing water availability, resulting in reduced water supply development.
- Increased water supply development results in a decrease in water stress, allowing for more population growth and water demand thereby increasing production pressure on water supply.
- Investment in water supply capital stocks increases the global aggregate capital stock, thereby increasing water usage intensity and water demand, creating more pressure for the development of water supply.
- The development of water supplies alleviates water stress on food production thereby increasing agricultural runoff to the nutrient cycles. This in turn has a negative impact on water supply through reduced water quality and increased cost of water supply for surface water.
- Persistent pollution adds additional negative feedbacks to population growth by acting as a multiplier of life expectancy. With increased population, the total use of resources and pollution generation increase. The increase in persistent pollution levels after some time and reduces population growth.
- Increased population has a positive effect on global economy by boosting the labor force, resulting in more industrial pollution generation. This in turn has a limiting effect on population growth through the life expectancy multiplier from persistent pollution.
- Increased population also provides more labor input which supports the economic growth. This affects water demand by reducing withdrawal intensities in the domestic and industrial sectors, resulting in less water consumption and more available water resources. This supports

water supply development thereby limiting water stress and supporting further population growth.

One of the goals of this work is to identify new feedback processes that may be of importance to global change, particularly with regards to water supply development. All the connections between model sectors in the ANEMI3 model are listed below in Table 3.1.

Table 3.1. Connections between different model sectors in ANEMI3. Highlighted rows represent the intersectoral connections that have been added or modified in this work.

<b>Influencing Model Sector</b>	<b>Affected Model Sector</b>	<b>Types of Influence</b>
Climate	Hydrologic Cycle	<ul style="list-style-type: none"> <li>• Surface temperature change increases evapotranspiration and melting of ice and snow</li> </ul>
Climate	Economy	<ul style="list-style-type: none"> <li>• Reduces economic output through temperature change in climate damage function</li> </ul>
Climate	Population	<ul style="list-style-type: none"> <li>• Surface temperature change increases heat stress effects on young and old</li> </ul>
Climate	Food Production	<ul style="list-style-type: none"> <li>• Increased global temperature have a positive effect on potentially arable land thus more food production</li> </ul>
Climate	Carbon Cycle	<ul style="list-style-type: none"> <li>• Increased surface temperatures stimulate carbon uptake from litter, humus, charcoal sinks, and ocean sinks</li> </ul>
Climate	Sea Level Rise	<ul style="list-style-type: none"> <li>• Surface temperature change is used as an indicator for the relationship used to represent sea level rise</li> </ul>
Carbon Cycle	Climate	<ul style="list-style-type: none"> <li>• Higher atmospheric carbon concentration increases radiative forcing on the climate system</li> </ul>
Hydrologic Cycle	Water Supply	<ul style="list-style-type: none"> <li>• Available water resources determine depletion effect in supply development</li> </ul>
Hydrologic Cycle	Nutrient Cycles	<ul style="list-style-type: none"> <li>• Changes in streamflow, rainfall, and groundwater percolation rates affect nutrient transfer rates</li> <li>• Increased river flow rates reduce the concentration of nutrients</li> </ul>
Water Supply	Population	<ul style="list-style-type: none"> <li>• Water stress increases mortality rates through life expectancy</li> </ul>
Water Supply	Economy	<ul style="list-style-type: none"> <li>• Water supply development is aggregated within total economic capital and output</li> <li>• A portion of global investment funds are allocated to water supply development</li> </ul>

Water Supply	Food Production	<ul style="list-style-type: none"> <li>• Water stress acts as a limit to food production</li> </ul>
Water Demand	Water Supply	<ul style="list-style-type: none"> <li>• Increased water demand creates water stress thereby increasing production pressure on water supplies</li> </ul>
Water Demand	Nutrient Cycles	<ul style="list-style-type: none"> <li>• Higher industrial and domestic water demand result in the generation of more nitrogen and phosphorus in the form of wastewater</li> </ul>
Water Demand	Hydrologic Cycle	<ul style="list-style-type: none"> <li>• Domestic, industrial, and agricultural water demands consume available water resources</li> </ul>
Nutrient Cycles	Water Supply	<ul style="list-style-type: none"> <li>• Water quality influences surface water supply development</li> </ul>
Population	Water Demand	<ul style="list-style-type: none"> <li>• Growing population increases domestic water demands</li> </ul>
Population	Land Use	<ul style="list-style-type: none"> <li>• Growing population increase forest and grassland clearing and burning for agriculture</li> </ul>
Population	Economy	<ul style="list-style-type: none"> <li>• Increased population boosts available labour</li> </ul>
Population	Food Production	<ul style="list-style-type: none"> <li>• Increased population creates the need for more food production</li> </ul>
Population	Persistent Pollution	<ul style="list-style-type: none"> <li>• Greater population increases the generation of industrial persistent pollution amounts</li> </ul>
Economy	Population	<ul style="list-style-type: none"> <li>• Increased economic output results in higher quality health services and life expectancy thereby reducing mortality rates</li> </ul>
Economy	Water Demand	<ul style="list-style-type: none"> <li>• More economic output increases domestic water demands</li> </ul>
Economy	Food Production	<ul style="list-style-type: none"> <li>• Higher economic output results in greater agricultural input per hectare and higher food production</li> </ul>
Economy	Energy Production	<ul style="list-style-type: none"> <li>• Increased global capital results in higher energy requirements thus boosting energy production</li> </ul>
Economy	Persistent Pollution	<ul style="list-style-type: none"> <li>• Increased consumption results in higher per capita persistent pollution generation</li> </ul>
Energy Production	Emissions	<ul style="list-style-type: none"> <li>• Energy production from fossil fuels increases carbon emissions</li> </ul>
Energy Production	Economy	<ul style="list-style-type: none"> <li>• Increased energy capital boosts total capital and economic output</li> </ul>
Energy Production	Water Demand	<ul style="list-style-type: none"> <li>• Production of energy is used as an indicator of industrial activity and associated water demands</li> </ul>
Land Use	Food Production	<ul style="list-style-type: none"> <li>• Increased agricultural lands boosts potential food production</li> </ul>

Land Use	Carbon Cycle	<ul style="list-style-type: none"> <li>Clearing and burning of forest and grasslands release carbon stored in litter, humus, and charcoal stocks to the atmosphere</li> </ul>
Land Use	Persistent Pollution	<ul style="list-style-type: none"> <li>Increased agricultural lands result in greater persistent pollution generation from agriculture</li> </ul>
Food Production	Water Demand	<ul style="list-style-type: none"> <li>More food production results in higher agricultural water demands</li> </ul>
Food Production	Population	<ul style="list-style-type: none"> <li>Greater food per capita results in higher life expectancy</li> </ul>
Food Production	Nutrient Cycles	<ul style="list-style-type: none"> <li>More net arable land results in higher emissions of nutrients from agricultural effluents</li> </ul>
Emissions	Carbon Cycle	<ul style="list-style-type: none"> <li>More CO<sub>2</sub> emissions boost atmospheric carbon content</li> </ul>
Emissions	Climate	<ul style="list-style-type: none"> <li>Increased emission of methane, nitrogen dioxide, and chlorofluorocarbons increases radiative forcing on the climate system</li> </ul>
Persistent Pollution	Population	<ul style="list-style-type: none"> <li>Higher levels of persistent pollution act as a multiplier to decrease life expectancy</li> </ul>
Persistent Pollution	Food Production	<ul style="list-style-type: none"> <li>Increased persistent pollution has a negative effect on land fertility thus reducing food production rates</li> </ul>
Sea Level Rise	Food Production	<ul style="list-style-type: none"> <li>Sea level rise reduced net arable land for food production</li> </ul>

### 3.2 Description of the ANEMI3 Model Sectors

#### 3.2.1 Climate Sector

The climate sector of ANEMI3, as in previous versions, is based on the DICE model of Nordhaus (1994). In this sector, the dynamics of heat exchange between the deep ocean and the combined upper ocean and atmospheric layers are modelled, along with a cooling effect that acts to limit the rate of temperature increase. Identifying the feedbacks that drive this simple climate system allow us to speculate on how the system will function over time. The climate sub-system is driven by two feedback loops (Figure 3.2). The first being a feedback cooling effect, while the second represents the diffusion of heat in the atmospheric stock to the ocean stock. Both negative feedbacks act to dampen the systems response to radiative forcing which comes from increased greenhouse gas concentrations in the carbon cycle and greenhouse gas sub-systems. Based on the structure of this simplified climate system, one might expect it to predict global temperature values on the lower end of the spectrum. This is because positive feedbacks related to climate change such as methane release from tundra

regions and change in albedo as global ice cover melts are not included, which have the potential to accelerate increases in global temperatures.

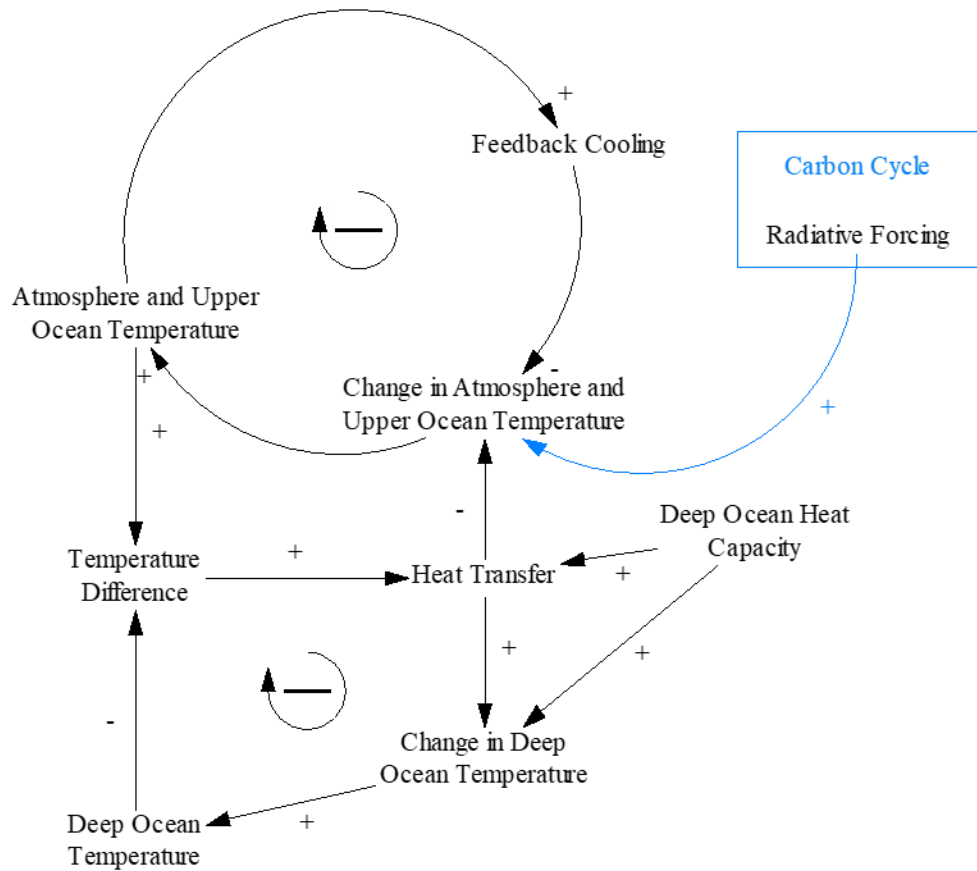


Figure 3.2. Causal loop diagram of the ANEMI3 climate sector.

The stock and flow diagram of this model is given in Figure 3.3. Two stocks are used to quantify the current global temperature of the atmosphere and oceans in response to external radiative forcing caused by greenhouse gases that are divided into CO<sub>2</sub>, methane, nitrogen dioxide, chlorofluorocarbons, and others. Diffusion of heat between these two stocks results in heat being transferred from the atmosphere stock to the ocean stock which acts as a heat sink.

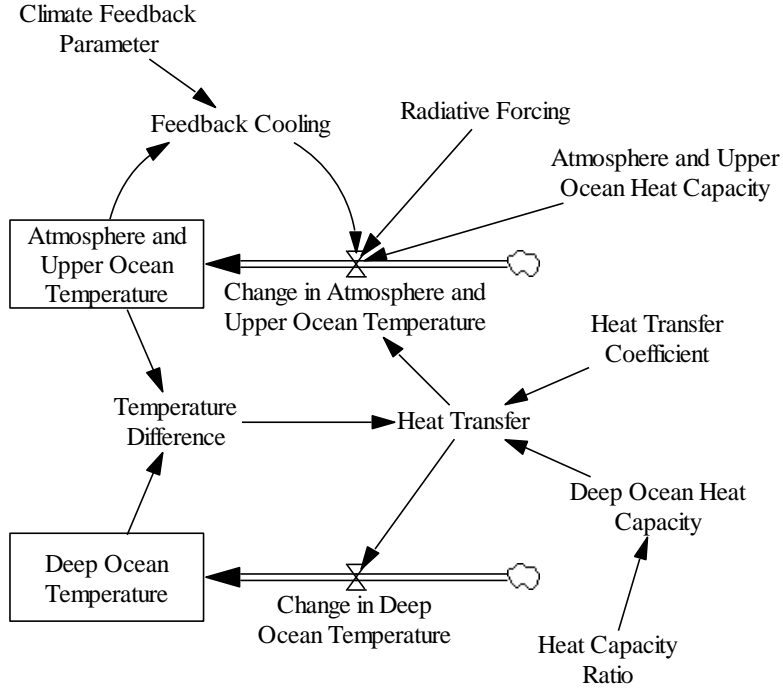


Figure 3.3. Stock and flow diagram of the ANEMI3 climate sector.

Radiative forcing acts to increase the flow that changes the temperature of the atmosphere stock and is based on the relative change of the greenhouse gases considered from their preindustrial levels. The mathematical description of the atmospheric and upper ocean temperature stock is given by,

$$T_{AUO} = \int CT_{AUO} \cdot dt \quad [^{\circ}C] \quad (3.1)$$

Where  $T_{AUO}$  represents the temperature of the atmosphere and upper ocean and  $CT_{AUO}$  is the rate at which  $T_{AUO}$  is changing ( $^{\circ}C/year$ ). The deep ocean temperature,  $T_{DO}$  is defined as,

$$T_{DO} = \int CT_{DO} \cdot dt \quad [^{\circ}C] \quad (3.2)$$

Where  $CT_{DO}$  is the change in temperature of the deep ocean stock ( $^{\circ}C/year$ ). The change in temperature of the atmospheric and upper ocean stock is calculated based on the difference between

radiative forcing, heat transfer from the deep ocean stock and the heat capacity of the atmospheric and upper ocean stock,

$$CT_{AUO} = \frac{F - f_H - HT}{HC_{AUO}} \quad [^{\circ}C/year] \quad (3.3)$$

$F =$  Radiative forcing [ $W/m^2$ ]

$f_H =$  Feedback cooling effect [ $W/m^2$ ]

$HT =$  Heat transfer between atmosphere and upper ocean to deep ocean [ $W/m^2$ ]

$HC_{AUO} =$  Heat capacity of atmosphere and upper ocean [ $W \cdot \frac{year}{^{\circ}C \cdot m^2}$ ]

The change in temperature of the deep ocean stock,  $CT_{DO}$  depends on the heat transfer from the atmosphere and upper ocean layer above, and the heat capacity of the deep ocean stock,

$$CT_{DO} = \frac{HT}{HC_{DO}} \quad [^{\circ}C/year] \quad (3.4)$$

$HC_{DO} =$  Heat capacity of deep ocean layer [ $W \cdot \frac{year}{^{\circ}C \cdot m^2}$ ]

Heat capacity of the deep ocean layer is calculated by,

$$HC_{DO} = R_{HC} \cdot C_{HT} \quad \left[ W \cdot \frac{year}{^{\circ}C \cdot m^2} \right] \quad (3.5)$$

$R_{HC} =$  Heat capacity ratio [ $W/(m^2 \cdot ^{\circ}C)$ ]

$C_{HT} =$  Heat transfer coefficient [ $year$ ]

The transfer of heat between the atmosphere and upper ocean and deep ocean layers is dependent upon the difference in temperature between them, the heat capacity of the deep ocean layer and heat transfer coefficient.

$$HT = (T_{AUO} - T_{DO}) \frac{HC_{DO}}{C_{HT}} \quad [W/m^2] \quad (3.6)$$

### 3.2.2 Carbon Cycle

The carbon cycle in the ANEMI3 model is based on Goudriaan and Ketner (1984b). It is used to model the flow of carbon through the Earth system from atmosphere to land and oceans. By incorporating the entire carbon cycle, atmospheric concentration can more realistically be simulated to drive changes in climate through the greenhouse effect. Feedbacks between the carbon cycle and climate system can also be represented through increased solubility of carbon dioxide in the ocean and fertilization effects of plant material with increased global temperatures. Finally, by modelling the cycle of carbon, connections can be made with the land use sector by separating the land stock of carbon into different biome types. This allows for changes in land use such as the burning and clearing of grasslands and forests, to contribute CO<sub>2</sub> emissions to the atmosphere.

The causal loop diagram of the carbon cycle sector is given in Figure 3.4. The chain of negative feedback loops passing through each of the terrestrial carbon stocks from the atmosphere and back again act as positive feedback loop in the carbon cycle. This is because more atmospheric carbon results in higher uptake of carbon in the biomass, which results in greater transfer of carbon through the chain (litter, humus, stabilized humus and charcoal) thereby resulting in more decay and transfer of carbon back to the atmosphere. Although these are positive feedback loops, carbon in this cycle is conserved, but the release or storage of carbon in the terrestrial stocks will be dependent on the balance between uptake and decay. The last feedback loop in the diagram is a negative feedback loop that represents the diffusion of carbon dioxide between the two ocean layers.

The cycle of carbon from the atmosphere through land and oceans is shown in the stock and flow diagram of Figure 3.5. The atmosphere, ocean layers, and terrestrial components of the carbon cycle are represented as stocks while the processes of net primary production (carbon uptake by living biomass), rates of dead biomass decay, and dissolution of carbon into the ocean are represented as flows.

The biome (or land use) types that are represented in the model are 1) tropical forests, 2) temperate or boreal forests, 3) grasslands, 4) agricultural lands, 5) deserts and tundra, and 6) settled areas. Living biomass of each biome is sub-divided into leaves, branches, stems and roots. Decaying biomass is separated in litter, humus, charcoal, and stabilized humus and charcoal. This subdivision allows for atmospheric carbon uptake and decay rates to be specified for each carbon sink. The ocean stock of

carbon is sub-divided into two separate layers; one mixed layer and one deep ocean layer. The mixed layer is used to represent diffusion of carbon between ocean and atmosphere based on the difference in concentration. CO<sub>2</sub> is highly soluble in seawater and dissolves into the mixed layer from the atmosphere according to Henry's Law (Masterson and Hurley 2009).

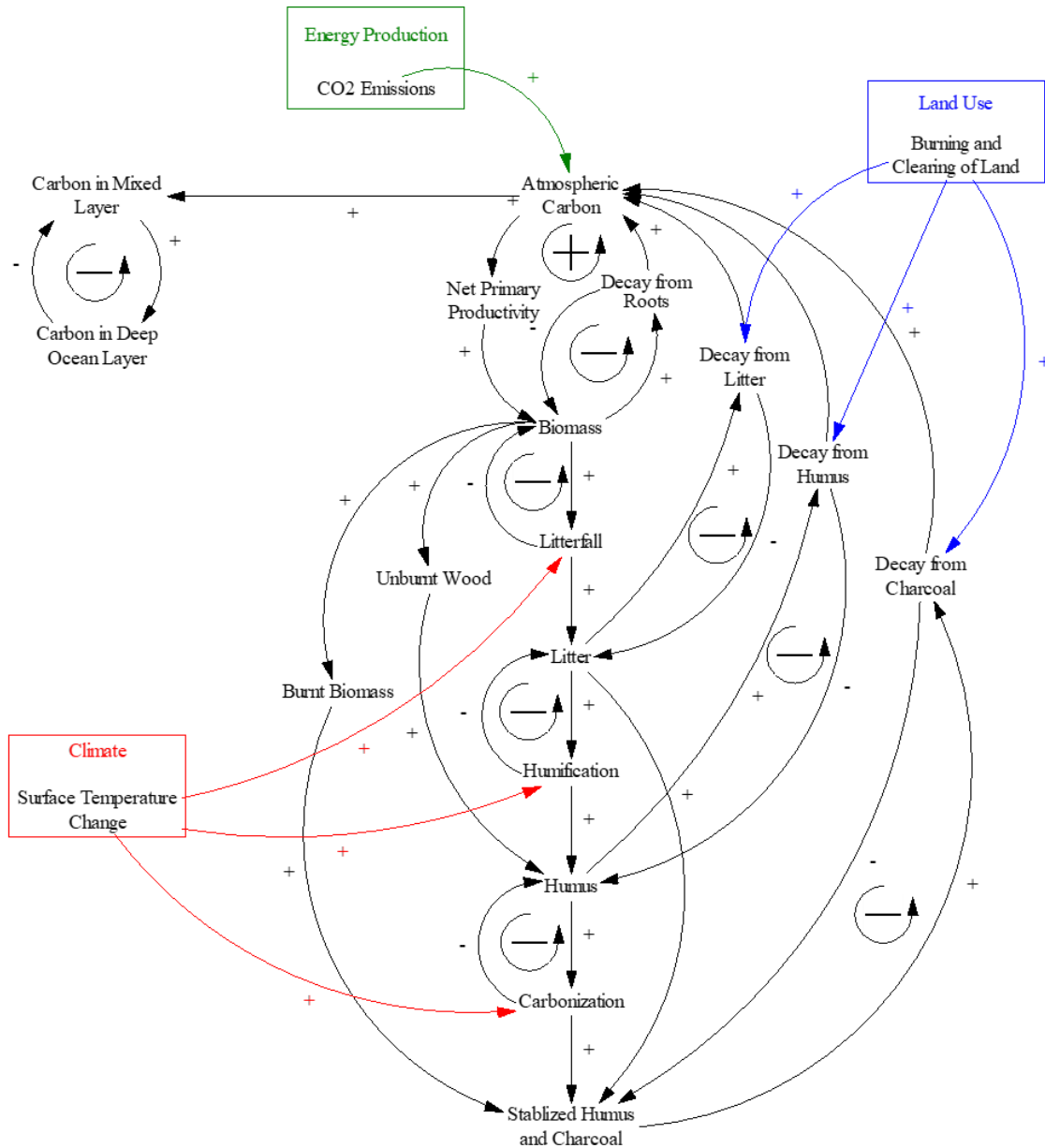


Figure 3.4. Causal loop diagram of carbon cycle sector in ANEMI3. Red, green, and blue arrows and variables represent connections to climate, land use, and energy production sectors respectively.

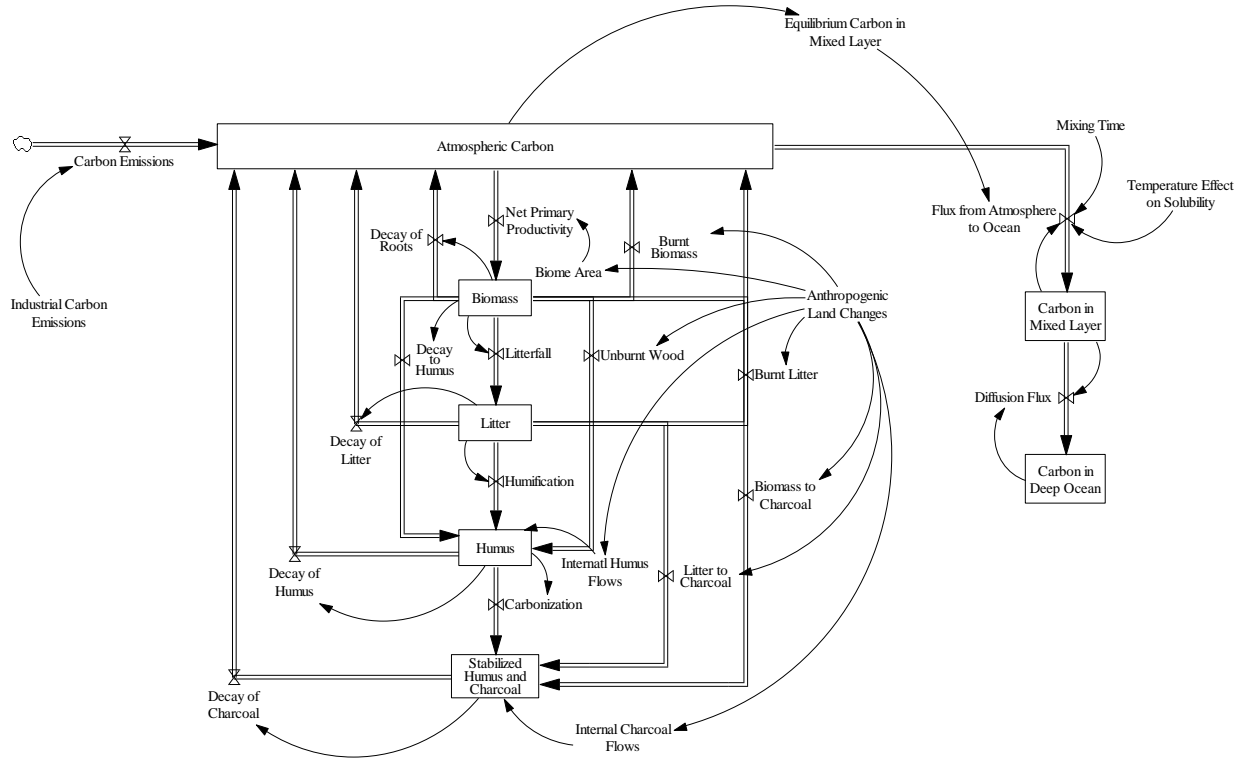


Figure 3.5. Stock and flow diagram of carbon cycle in the ANEMI3 model.

The mathematical description of the carbon cycle sector is summarized from Davies (2007). The accumulation of carbon in the atmosphere can be expressed as,

$$N_A = \int (D_B + D_L + D_H + D_K - NPP + B_B + B_L + E - F_0) \cdot dt \quad [Gt C] \quad (3.7)$$

$N_A$  = Atmospheric carbon [Gt C]  
 $D_B$  = Decay of biomass [Gt C/y]  
 $D_L$  = Decay of litter [Gt C/y]  
 $D_H$  = Decay of humus [Gt C/y]  
 $D_K$  = Decay of charcoal [Gt C/y]

$NPP$  = Net primary productivity [Gt C/y]  
 $B_B$  = Burning of biomass [Gt C/y]  
 $B_L$  = Burning of litter [Gt C/y]  
 $E$  = Industrial emissions [Gt C/y]  
 $F_0$  = Carbon absorption by oceans [Gt C/y]

Net primary productivity is computed as,

$$NPP_{jk} = p_{jk} \cdot \sigma(NPP_j) \cdot \frac{A_j}{10^{15}} \quad [Gt C/y] \quad (3.8)$$

$j = \text{Biome type}$

$k = \text{Biomass component}$

$p_{jk} = \text{Fraction of biomass partitioned to component } k \text{ of biome } j$

$\sigma(NPP_j) = \text{Variable surface density of net primary production [Gt C/(m}^2 \cdot \text{y)]}$

$A_j = \text{Biome area [m}^2\text{]}$

The biome (or land use) type  $j$  refers to the set of biomes represented in the model and the biomass component  $k$  refers to the leaves branches stems and roots that make up a given biome type. The variable surface density of net primary production is represented as,

$$\sigma(NPP_j) = \sigma(NPP_j)_0 \cdot \left( 1 + \beta \cdot \ln \left( \frac{C_A}{C_{A_0}} \right) \right) \quad [\text{Gt C}/(\text{m}^2 \cdot \text{y})] \quad (3.9)$$

$\sigma(NPP_j)_0 = \text{base surface density [Gt C}/(\text{m}^2 \cdot \text{y})\text{]}$

$\beta = \text{CO}_2 \text{ fertilization factor}$

$C_A = \text{Current atmospheric CO}_2 \text{ [Gt C]}$

$C_{A_0} = \text{Initial atmospheric CO}_2 \text{ [Gt C]}$

The amount of carbon stored within each component the biomass stock for each biome type is represented as,

$$B_{jk} = \int \left( NPP_{jk} - FL_{B_{jk}} - FH_{B_{jk}} - FK_{B_{jk}} - B_{B_{jk}} - UB_{B_{jk}} \right) \cdot dt \quad [\text{Gt C}] \quad (3.10)$$

$FL_{B_{jk}} = \text{Amount of litter falling from biomass to litter layer [Gt C/y]}$

$FH_{B_{jk}} = \text{Decay of biomass to humus [Gt C/y]}$

$FK_{B_{jk}} = \text{Burning of biomass [Gt C/y]}$

$B_{B_{jk}} = \text{Burning of biomass from human land use [Gt C/y]}$

$UB_{B_{jk}} = \text{Unburned remainder of biomass [Gt C/y]}$

Carbon accumulation in the litter stock is represented as,

$$L_j = \int \left( \sum_{k=1}^4 FL_{B_{jk}} - D_{L_j} - FH_{L_j} - BL_j - FL_{K_j} \right) \cdot dt \quad [\text{Gt C}] \quad (3.11)$$

$\sum_{k=1}^4 FL_{B_{jk}} = \text{Total litter fall [Gt C/y]}$   
 $D_{L_j} = \text{Decay of carbon from litter to atmosphere [Gt C/y]}$   
 $FH_{L_j} = \text{Decomposition of litter into humus [Gt C/y]}$   
 $B_{L_j} = \text{Flow of carbon from litter to atmosphere [Gt C/y]}$   
 $FL_{K_j} = \text{Carbon flow from litter directly to charcoal [Gt C/y]}$

The humus carbon stock can be expressed as,

$$H_j = \int \left( \sum_{k=1}^4 FH_{B_{jk}} + FH_{L_j} - FK_{H_j} - D_{H_j} + \sum_{k=1}^4 UB_{jk} + FH_{H_j} \right) \cdot dt \quad [\text{Gt C}] \quad (3.12)$$

$\sum_{k=1}^4 FH_{B_{jk}} = \text{Decay of biomass to humus [Gt C/y]}$   
 $FH_{L_j} = \text{Decomposition of litter to humus [Gt C/y]}$   
 $FK_{H_j} = \text{Decomposition of humus to charcoal [Gt C/y]}$   
 $D_{H_j} = \text{Decay of humus to the atmosphere [Gt C/y]}$   
 $\sum_{k=1}^4 UB_{jk} = \text{Unburned remainder of biomass [Gt C/y]}$   
 $FH_{H_j} = \text{Internal flow of humus [Gt C/y]}$

The charcoal carbon stock can be expressed as,

$$K_j = \int \left( FK_{H_j} - D_{K_j} + \sum_{k=1}^4 FK_{B_{jk}} + FK_{L_j} - FK_{K_j} \right) \cdot dt \quad [\text{Gt C}] \quad (3.13)$$

$FK_{H_j} = \text{Flow of carbon from humus to charcoal [Gt C/y]}$   
 $D_{K_j} = \text{Decay of charcoal [Gt C/y]}$   
 $\sum_{k=1}^4 FK_{B_{jk}} = \text{Burning of biomass [Gt C/y]}$   
 $FK_{L_j} = \text{Carbon flow from litter to charcoal [Gt C/y]}$   
 $FK_{K_j} = \text{Internal flow of charcoal from one biome to another [Gt C/y]}$

For initial values for each of the carbon stocks as well as parameters used in defining the flows from one to another the reader is referred to (Davies 2007). The mixed layer ocean carbon stock is represented as,

$$C_{ML} = \int (FO_A - DF_o(0)) \cdot dt \quad [Gt C] \quad (3.14)$$

$C_{ML}$  = Carbon in mixed layer ocean stock [Gt C/y]

$FO_A$  = Absorbtion of carbon dioxide from atmosphere [Gt C/y]

$DF_o(0)$  = Diffusive flow of carbon dioxide to deep ocean [Gt C/y]

The deep ocean carbon stock is divided into 10 layers of varying depth with the top 5 layers having a thickness of 200m and the bottom 5 layers having a thickness of 560m each. This is done to slowly transfer carbon deep into the ocean carbon stock based on diffusive flow. The deep ocean carbon stock is represented mathematically by,

$$C_o(h) = \int (DF_o(h) - DF_o(h + 1)) \cdot dt \quad [Gt C] \quad (3.15)$$

$DF_o(h)$  = Diffusive flow of carbon from upper layer to current layer [Gt C/y]

$DF_o(h + 1) =$

Diffusive flow of carbon to lower layer from current layer [Gt C/y]

$h$  = current layer of 10 deep ocean layers

### 3.2.3 Population Sector

The causal loop diagram in Figure 3.6 illustrates the feedbacks associated with the population sector. There is one positive feedback loop which drives the system and is responsible for exponential growth of the human population. A higher population results in a higher growth rate through more births and therefore a higher population. The rest of the population sector details a series of negative feedbacks that act as limits to population growth. The negative feedbacks include from the effects of crowding, water stress, extreme temperatures, food production, persistent pollution, and wealth represented as global GDP. All of which are always active but to different degrees and affect either the life expectancy and thus mortality rates of the population, or fertility thereby reducing birth rates. Each of these effects act as multipliers and are related through look-up tables that could be associated with a significant amount of uncertainty, the degree of which is tested in the model experimentation section of this thesis.

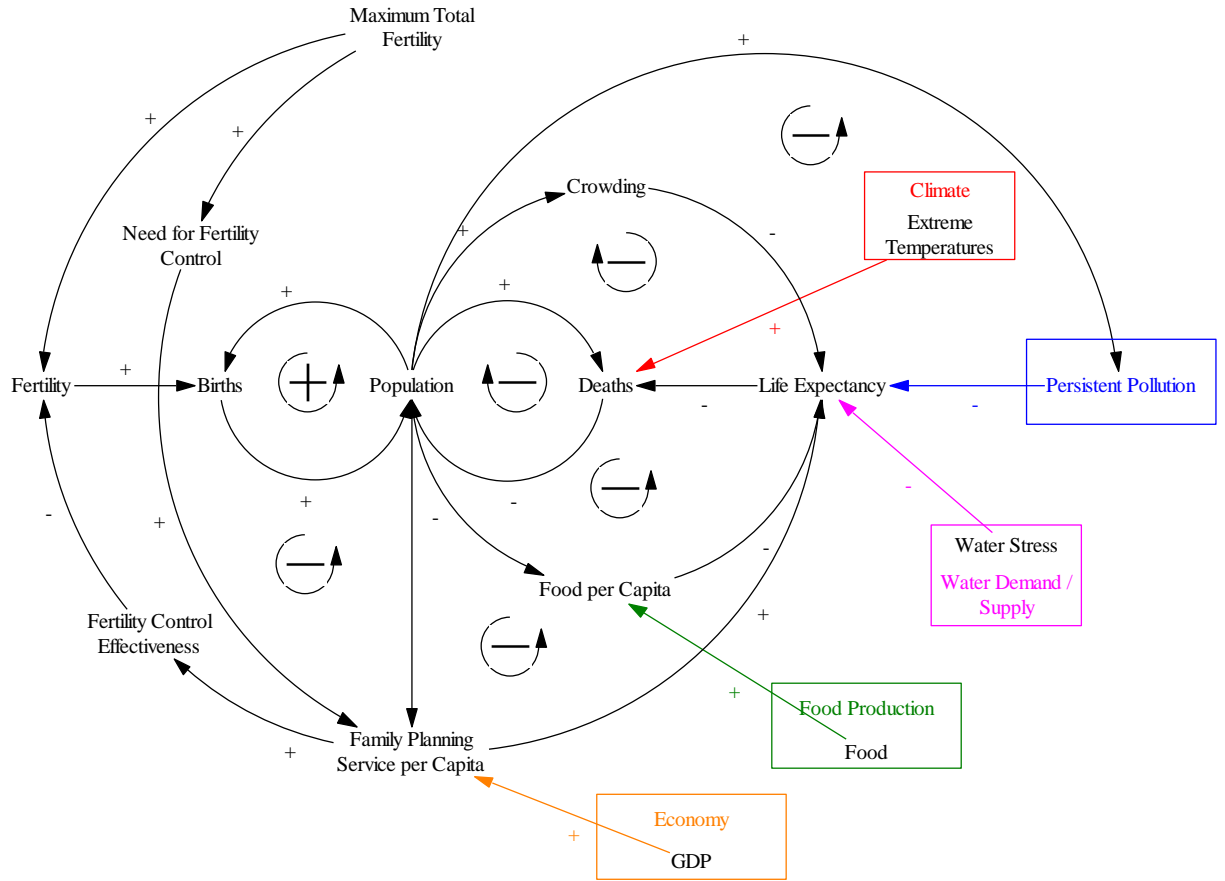


Figure 3.6. Causal loop diagram of the ANEMI3 population sector.

The population sector of ANEMI3 uses separate stocks to split the population into different demographics of ages 0 to 14, 15 to 44, 45 to 65, and 65+. This was done to capture the effects of delays in demographic responses to changes in external conditions which thereby affect birth and death rates. It allows for the growth of the total population to retain some inertia as external conditions change which more closely captures the dynamics of population growth in the real world. This structure also allows for the population of different age groups to be used in other areas of the model. For example, the 15 to 44 and 45 to 65 population groups are combined and used as the labour force in the energy-water economy sector. Another reason as to why these groups were used is so that age group specific factors that influence mortality can be applied. Climate change is included as an influence on mortality rate through the use of a temperature multiplier that acts to influence deaths due to the presence of more frequent heat waves causing heat stress. Factors influencing fertility and birth rates are also included and will be discussed further below.

The stock and flow structure of the population sector includes stocks that represent the number of people currently in each age group (Figure 3.7). Flows are used to move people from the younger to older age groups over time, and the flow of people from each stock outside of the model boundary denotes deaths. This structure of stock and flows is often referred to as an “aging chain”, which is used to capture delays in the movement of information or material from one cohort to another over time. This is a generic structure that can be applied to a range of problems capturing higher order delays of material or information. It is often used in production processes representing the movement of a product through different production stages but could also be used to represent physical processes such as the routing of streamflow in a semi-distributed hydrologic model. Applied to population cohorts the aging chain takes a more literal meaning and represents the delay associated with individuals in each population cohort aging over time and moving in older cohort groups.

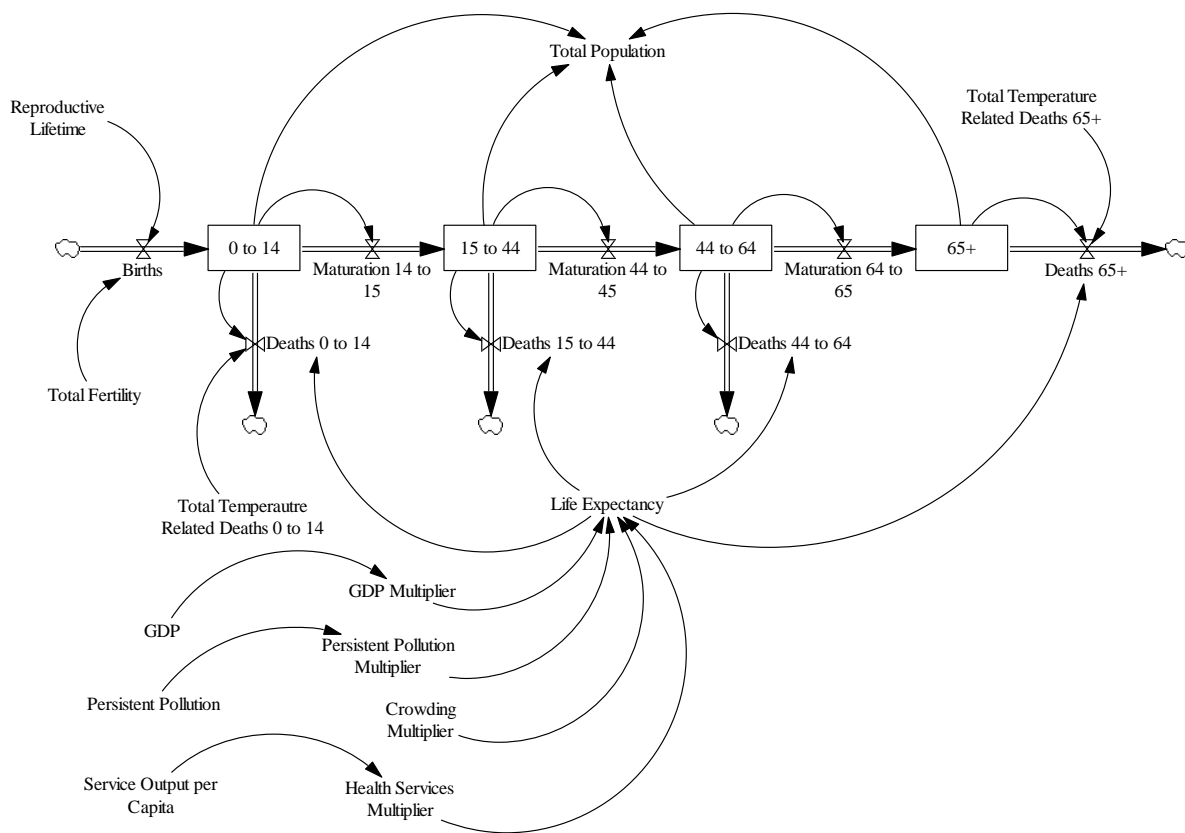


Figure 3.7. Stock and flow diagram of the ANEMI3 population sector.

The aging chain of population groups can be represented mathematically by,

$$P_1 = \int Births - P_1 M_1 - \frac{P_1(1 - M_1)}{\tau_1} - T_{deaths_1} \quad [persons] \quad (3.16)$$

$$P_2 = \int P_1 M_1 - \frac{P_2(1 - M_2)}{\tau_2} - P_2 M_2 \quad [persons] \quad (3.17)$$

$$P_3 = \int P_2 M_2 - \frac{P_3(1 - M_3)}{\tau_3} - P_3 M_3 \quad [persons] \quad (3.18)$$

$$P_4 = \int P_3 M_3 - P_4 M_4 - T_{deaths_4} \quad [persons] \quad (3.19)$$

$P_i = Population [persons]$

$M_i = Mortality rate [1/y]$

$\tau_i = Length of time spent in sub-demographic [y]$

$T_{deaths_i} = Temperature related deaths [persons]$

Where  $i$  refers to the sub-demographic in the aging chain (1 being 0 to 14 age group and 4 being 65+). The birth rate is dependent on fertility rate, and the half of the size of the reproductive population (assumes equal proportion of gender),

$$Births = F_{total} \cdot \frac{P_2}{2\tau_2} \quad [persons/y] \quad (3.20)$$

$F_{total} = Total fertility$

Total fertility is calculated based on the maximum fertility rate multiplied by the level of desired total fertility and fertility control effectiveness.

$$F_{total} = MIN(F_{M_{total}}, F_{M_{total}} \cdot (1 - F_{e_{cont}}) + F_{e_{cont}} \cdot F_{D_{total}}) \quad (3.21)$$

$F_{M_{total}} = Maximum total fertility$

$F_{e_{cont}} = Fertility control effectiveness$

$F_{D_{total}} = Desired total fertility$

Mortality rates for each sub-demographic are based on empirical relationships adopted from Meadows et al. (1974) and Keyfutz and Flieger (1971) which are a function of life expectancy,

$$L_E = L_{EN} \cdot L_{MF} \cdot L_{MHS} \cdot L_{MP} \cdot L_{MC} \quad [y] \quad (3.22)$$

$L_E$  = Life expectancy

$L_{EN}$  = Life expectancy normal [y]

$L_{MF}$  = Lifetime multiplier from food

$L_{MHS}$  = Lifetime multiplier from health services

$L_{MP}$  = Lifetime multiplier from pollution

$L_C$  = Lifetime multiplier from crowding

$L_{WS}$  = Lifetime multiplied from water stress

The calculation of life expectancy is based on a “normal” life expectancy that is multiplied by several factors that increase or decrease it from the normal value based on a set of empirical relationships.  $L_{MF}$  is a function of food supply from the food production sector,  $L_{MHS}$  is a function of GDP from the economic sector,  $L_{MP}$  is a function of persistent pollution from the pollution sector,  $L_C$  is a function of urban population which varies with the total population, and  $L_{WS}$  varies based on the current level of water stress from the water demand and water supply sectors in ANEMI3. Temperature related deaths  $T_{deaths_i}$ , are only applicable to the 0 to 14 and 65+ age groups because they are the most susceptible to heat stress induced by climate change related increases in severe heat waves. This is dependent on another empirical relationship that is a function of global temperature change in the climate sector.

An increasingly important dynamic that is currently not included in the ANEMI3 model is the migration of human population driven by the climate change. The issue is not new, and there are examples of climate driven migrations dating back as far as 45,000 years in the past (Ionesco et al. 2017). However, changes in climate are occurring much faster than they have been in the recent past, accelerated through anthropogenic greenhouse gas emissions. It has been estimated that the number of climate migrants could reach 200 million by the year 2050 as a result of shoreline erosion, coastal flooding, and agricultural displacement (Piguet et al. 2008). Climate migration on such a scale could have far reaching effects on all aspects of the Earth system. Water demands will shift to accommodate changes in the spatial distribution of water resources due to climate change. However, barriers that prevent migration such as political or economic boundaries may exacerbate the impacts on affected populations that are not able to relocate from areas that experience climate related disasters. This is



Changes in land use and cover are modelled using a transfer matrix which contains the rate at which one land use and cover type changes into another. This matrix only considers anthropogenic influence on each biome type and the rates of change are a linear function of population. This formulation assumes that the natural ecosystem is resilient to disturbance. It is adopted from ANEMI1 (Davies 2007) which was originally based on the model of Goudriaan and Ketner (1984). The stock and flow diagram of the land sector in ANEMI3 is given in Figure 3.9.

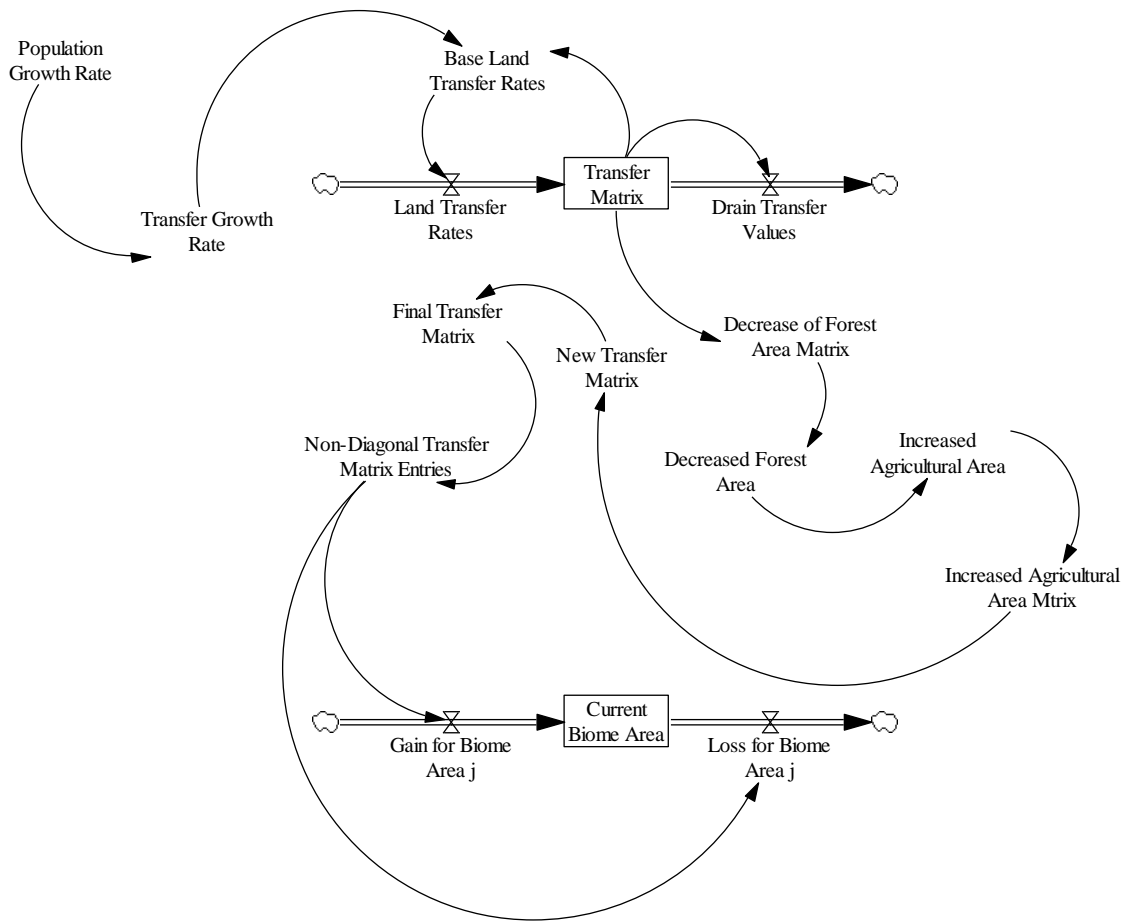


Figure 3.9. Stock and flow diagram of ANEMI3 land use sector.

There are two stocks in this formulation. The first is the transfer matrix which represents the current rate of change for each biome. This is then altered by population growth and temperature change which represent anthropogenic influence on each biome. The values of the updated transfer matrix are then applied to the current biome area. The initial transfer matrix shown in Table 3.3. The values in this table can be interpreted as the rate of transfer from the biome type in row  $i$ , to biome type in

column  $j$ . The non-diagonal elements are the base land transfer rates from one biome type to another, while diagonal elements are used to represent shifts in biome areas that do not change from one type to another.

Table 3.2. Initial transfer matrix for area between land use/cover types in [Mha/year].

	<b>Tropical Forest</b>	<b>Temperate Forest</b>	<b>Grassland</b>	<b>Agricultural Land</b>	<b>Human Area</b>	<b>Semi-Desert and Tundra</b>
<b>Tropical Forest</b>	15	0	0	0	0	0
<b>Temperate Forest</b>	0	2	0	0	0	0
<b>Grassland</b>	6	1	400	0	0	0
<b>Agricultural Land</b>	6	0	0	400	0	2
<b>Human Area</b>	0.5	0.5	1	1	0	0
<b>Semi-Desert and Tundra</b>	0	0	0	0	0	0

The land transfer rate of the non-diagonal elements is represented as,

$$L_{trans (non-diag)} = L_{tm} \cdot r \quad [Mha/y^2] \quad (3.23)$$

$L_{trans (non-diag)}$  = Land transfer rate of non-diagonal elements [Mha/y<sup>2</sup>]

$L_{tm}$  = Land transfer matrix [Mha/y]

$r$  = Population growth rate [1/y]

Land transfer rates along the diagonal direction are calculated as,

$$L_{trans (diag)} = L_{tm} \cdot r^{\frac{1}{2}} \quad [Mha/y^2] \quad (3.24)$$

The land transfer matrix is considered as a stock, which represents the state of land transfer at a given point in time. The land transfer matrix changes based on the land transfer rates in Equations 13 and 14 and drain transfer values ( $L_{tdr}$ ), which are used to eliminate the possibility of negative transfer rates.

$$L_{tm} = \int (L_{trans} - L_{tdr}) \cdot dt \quad [Mha/y] \quad (3.25)$$

The land transfer matrix is ultimately used to drive the change in biome area at a rate equal to the sum of the transfer rates from biome  $i$  to biome  $j$ , minus the sum of transfer rates from biome  $j$  to biome  $i$ ,

$$\frac{dA_j}{dt} = \sum_{i=1}^6 (a_{ij} - a_{ji}) \quad [Mha/y] \quad (3.26)$$

$A_j =$  Current area of biome  $j$  [Mha]

$a_{ij} =$  Rate of transition of area from biome  $i$  to biome  $j$  [Mha/y]

### 3.2.5 Food Production Sector

The food production sector in ANEMI3 models global food production which is ultimately used to determine the level of food per capita as an indicator for limitations of population growth. The production of food is affected by several factors including land fertility, arable land, water, and nutrients. The food production sector is based on that of the WORLD3 model (Meadows et al. 1974). The feedback structure of the food production sector is shown by the causal loop diagram in Figure 3.10.

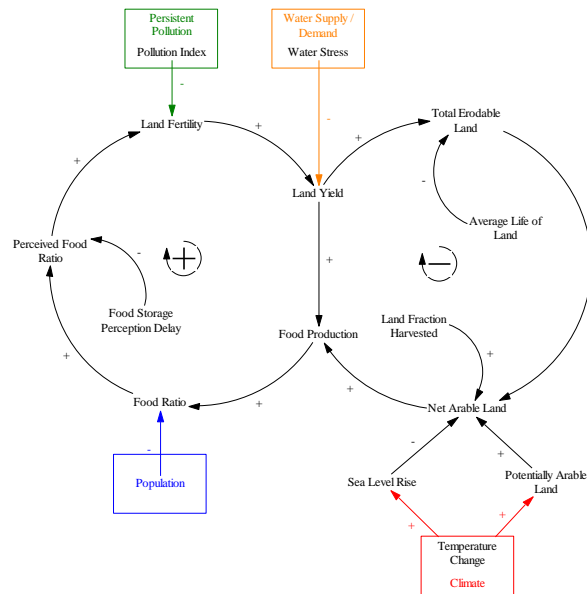


Figure 3.10. Causal loop diagram of the ANEMI3 food production sector.

There are two main feedback loops which drive the food production. The positive loop represents the effect of increased food production driving more reinvestment in increasing land fertility and thus food production again. The negative loop represents decreasing land yield due to food production which lead to more land erosion and then less arable land available for food production. The corresponding stock and flow structure is shown in Figure 3.11.

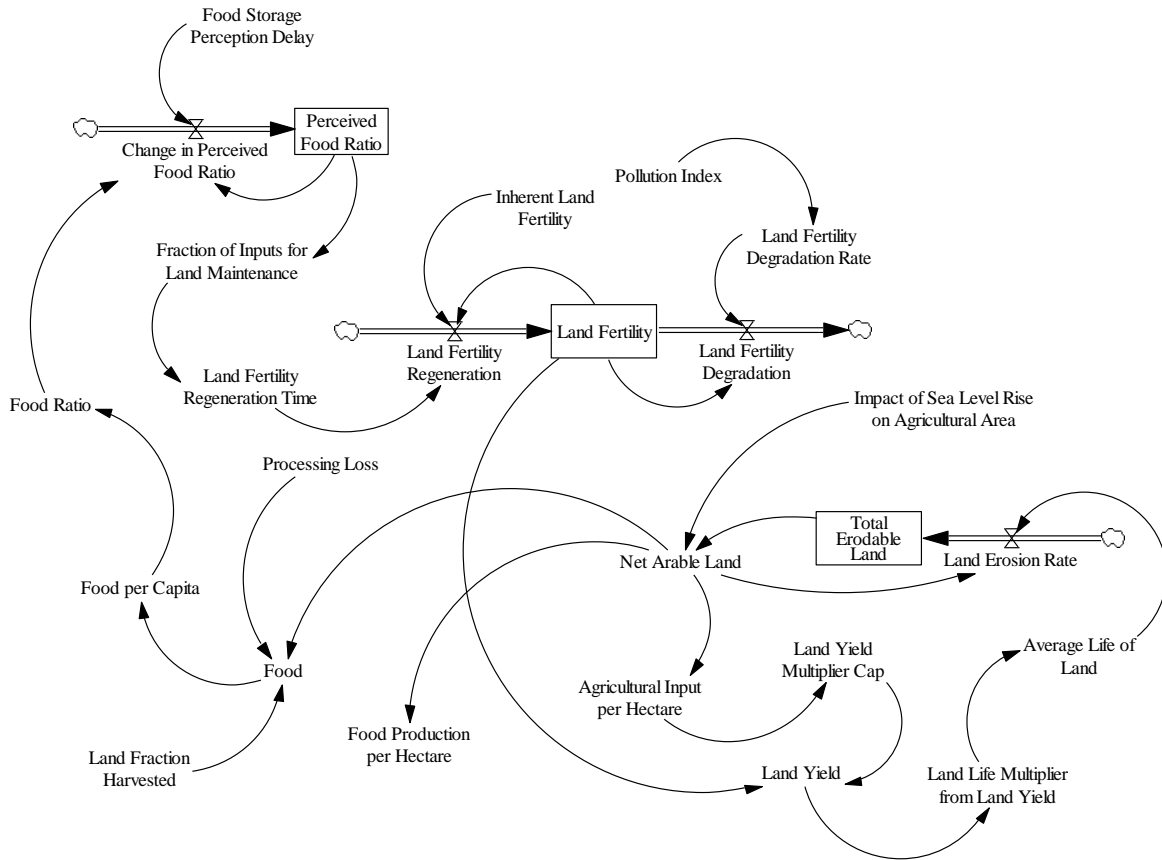


Figure 3.11. Stock and flow diagram of the ANEMI3 food production sector.

Food production can be increased in two ways through this representation. Either the amount of arable land can be increased by cultivating more land for agriculture, or the yield of that land can be increased through the application of modern agricultural inputs. In ANEMI3, climate change through increased temperatures can affect the level of potentially arable land, as changes in the number of growing days available in a given region can allow for agricultural activities to become feasible in areas where they were not. Two main factors limit the food production in the model. The first being that the production of food is reduced by land erosion, which limits the ability to produce food from the

stock of arable land. The second is reduced land fertility, which arises from water stress as well as pollution.

Food production in units of vegetable equivalent kilograms per year is calculated based on the equations from Meadows et al. (1974),

$$F_p = L_y \cdot A_l \cdot L_{fh} \cdot (1 - P_l) \quad [\text{Veg. eq. kg/y}] \quad (3.27)$$

$F_p$  = Amount of food production [Veg. eq. kg/y]

$L_y$  = Land yield [Veg. eq kg/(ha · y)]

$A_l$  = Net arable land [ha]

$L_{fh}$  = Land fraction under harvesting

$P_l$  = Processing loss (assumed as 10%)

The land yield represents the total weight of crop production on average per hectare of land each year. The base amount of land yield is the land fertility, which can be modified by capital inputs which represent the use of modern agricultural inputs such as fertilizers and the efficiency for which they are applied. Water stress is also included as a factor that affects the land yield because insufficient water resources needed for irrigated agriculture will reduce crop output.

$$L_y = L_{yf} \cdot L_{fert} \cdot L_{ymc} \cdot L_{ymw} \quad [\text{Veg. eq. kg}/(\text{ha} \cdot \text{y})] \quad (3.28)$$

$L_{yf}$  = Land yield factor

$L_{fert}$  = Land fertility [Veg. eq. kg/(ha · y)]

$L_{ymc}$  = Land yield multiplier from capital

$L_{ymw}$  = Water stress to land yield factor

The fertility of the land used for food production is dependent on several different factors including soil chemistry, moisture content, and the type of crops being grown. Any processes that affect these factors will in turn influence the rate of degradation and regeneration of land fertility. Land fertility is represented as a stock, governed by the following equation,

$$L_{fert} = \int (L_{fr} - L_{fd}) \cdot dt \quad [\text{Veg. eq. kg}/(\text{ha} \cdot \text{y})] \quad (3.29)$$

$L_{fr}$  = Land fertility regeneration [Veg.eq.kg/(ha · y<sup>2</sup>)]

$L_{fa}$  = Land fertility degradation [Veg.eq.kg/(ha · y<sup>2</sup>)]

The net amount of arable land that can be used for food production depends on the level of arable or agricultural land from the land use sector, the amount of erodible land which progresses over time with food production, as well as the amount of agricultural land that has been impacted by sea level rise. The amount of land area used for fodder and animal crop is subtracted from this value, as only that used for crop production is considered.

$$A_l = (L_{ar} - L_{ero}) \cdot L_{obs} - L_{slr} - L_{fa} \quad [ha] \quad (3.30)$$

$A_l$  = Net Arable Land [ha]

$L_{ar}$  = Arable land [ha]

$L_{ero}$  = Net erodible land [ha]

$L_{obs}$  = Obstacle to land conversion [ha]

$L_{slr}$  = Impacted agricultural land due to sea level rise [ha]

$L_{fa}$  = Land area used for fodder and animal crop [ha]

Climate change is expected to bring warmer climates to northerly regions over time, and may create the potential for regions that have not been exploited for agricultural purpose in the past to be considered for the future (Zabel et al. 2014; King et al. 2018). The WORLD3 model, from which the food production sector in ANEMI3 comes from, did not include a sector for climate change, let alone the potential effects of climate change on food production. King et al. (2018) used a set of seven global climate models to estimate the changes in land area that has growing degree days above 5 degrees Celsius with an annual sum of over 1200 degrees Celsius as an indicator of potentially arable land. Based on this study the change in global temperature from the same set of GCMs used in the study is related to the change in potentially arable land. Figure 3.12 shows this relationship.

This relationship is used as a multiplier to the land transfer rates from the semi-desert and tundra biome to the biome for agricultural land. However, this relationship is only between surface temperature change and *potential* arable land. In order to become agricultural land, the newly discovered amounts of potential arable land would need to be cultivated based on updated information of the land becoming available for cultivation as the climate changes. Therefore, an information delay

is applied to this relationship with a baseline value of 20 years. The sensitivity to this assumed information delay is tested in Section 3.4.4.

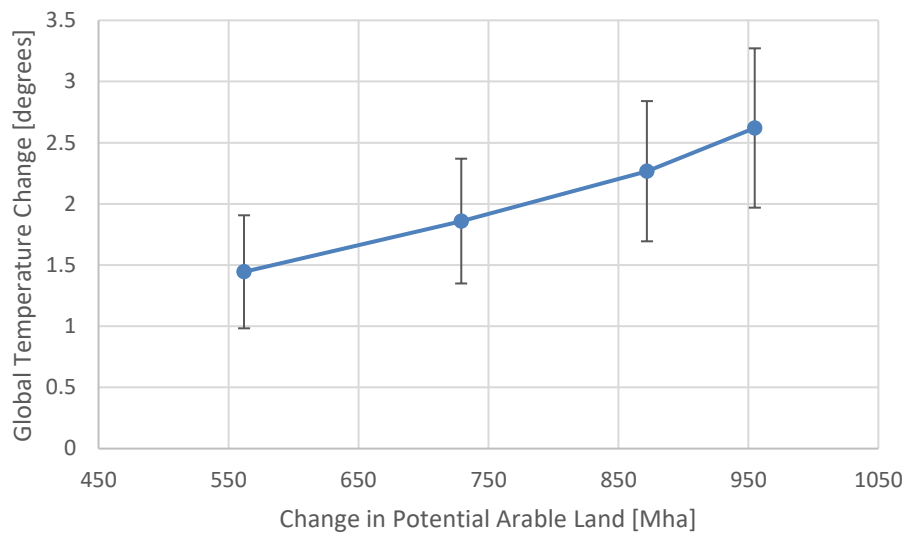


Figure 3.12. Relationship between global temperature change and change in potential arable land (after King et al. 2018). Error bars represent 95% confidence interval from the GCMs used in calculating global average temperature change.

In addition to increasing potentially arable land as a result of climate change mentioned in Section 3.2.3, it is expected that global crop yields will decrease to the occurrence of more severe and frequent temperature extremes, thereby causing heat and water stress (Zhao et al. 2017; King et al. 2018; Searchinger et al. 2019). In Searchinger et al. (2019), a comprehensive analysis was carried out to examine the impact of changes in climate on crop yields of four major crop types including wheat, rice, maize, and soybean. The analysis compiled, results from different methods that include: global grid and point based models, statistical regressions, and field warming experiments. The results showed that on average, for each degree of temperature change global yields of wheat, rice, maize, and soybean would be reduced by 6.0%, 3.2%, 7.4%, and 3.1%, respectively. The ANEMI3 model only includes the total food production including all crop types. In order to incorporate these potential climate related effects on land yield, a weighted average was taken from these percentage reductions based on the total number of tonnes produced in the model base year of 1980. Crop production data was taken from the FAOSTAT database (FAO 2019b).

Table 3.3. Effect of temperature change on crop yields for wheat, rice, maize, and soybean.

Crop Type	Temperature Yield Reduction	Production Levels in 1980	Weighted Average of Temperature Yield Reduction
	%/°C	billion tonnes	%/°C
Wheat	6.0	1.98	5.34
Rice	3.2	1.96	
Maize	7.4	1.75	
Soybean	3.1	0.33	

The weighted average of temperature yield reductions for wheat, rice, maize, and soybean crops based on the 1980 production levels is 5.34% per degree Celsius of global surface temperature change (Table 3.4.). These four crops are only a subset of the all crop types grown. However, their use in the ANEMI3 model for total yield reduction values is justified by the fact that their proportion of global food production has remained relatively constant over time (Figure 3.13).

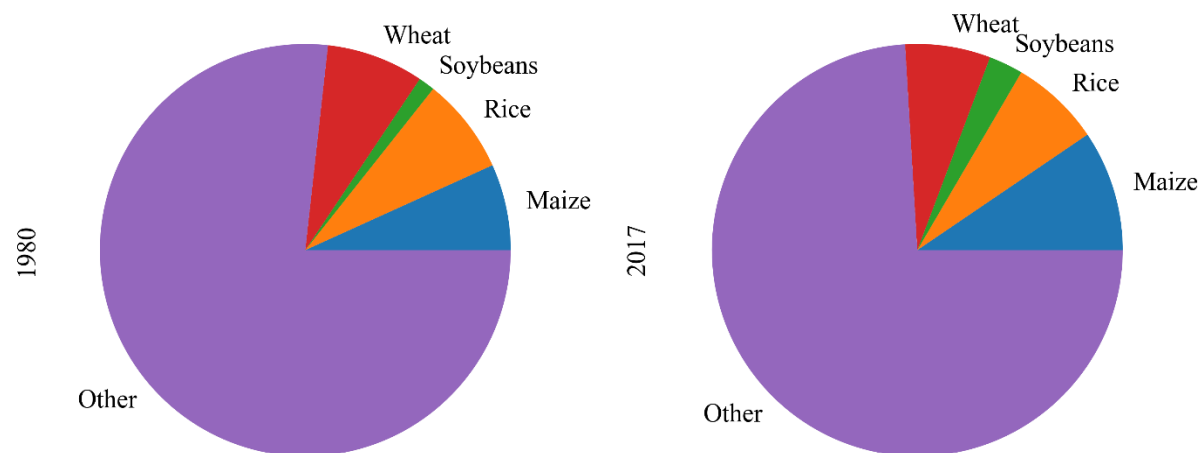


Figure 3.13. Distribution of crop production for the 4 crop types used in (Searchinger et al. 2019) compared to global totals in the years 1980 and 2017.

This number is used as a scenario to assess the influence of climate change on food production, along with the effect of increased potentially arable land derived from King et al. (2018).

The previous model versions included irrigation as an exogenous driver of water demands for agriculture. However, evidence has shown that crop yields from irrigated agriculture are consistently higher than those from rain-fed agriculture in the developing world (Lipton et al. 2003; Dowgert 2010; Jin et al. 2012). Increasing levels of irrigation in the future are a key factor to increasing agricultural land yields despite limited expansion potential for agricultural land use. Irrigated agriculture allows for increased land yields by allowing crops to receive a constant stream of dissolve nutrients from soils for optimal vegetative growth and development for crop production. Irrigation has the most potential to increase crop yields in areas where large seasonal and interannual fluctuation in rainfall patterns exist (Klohn et al. 2003). Due to the potential for shifts in the spatial and temporal distributions of rainfall patterns as a result of climate change, it is possible that the potential for irrigated agriculture may increase in the future. In the ANEMI3 model, a tighter coupling of irrigation and food production is made to assess the ability of intensified irrigation and agricultural land use to satisfy the increased demand on food production in the future. The effect of irrigation on food production is incorporated through a multiplier effect on land yield, based on the fact that crop yields from irrigated agriculture are higher than rainfed by a factor of 2.3 on average (Dowgert 2010). The effect of changes in food production and agricultural water demand are tested by implementing exogenous scenarios taken from FAO (2018). For the results please see Breach (2020).

In this sector the effects of climate change on food production have been enhanced from the previous version of ANEMI, which only considered the the impact of sea level rise through reduced arable land. In ANEMI3, the effect of changes in global air temperatures now affect food production by reducing land yields through the effect of heat stress based on the findings of Dowgert (2010). In addition, air surface temperatures now have an affect on food production through the northward shift of potentially arable lands into boreal forests based the functional relationship derived from King et al. (2018).

### 3.2.6 Sea Level Rise Sector

During the period of 1901 to 2010, the average sea level has risen approximately 0.2m due to the melting of arctic sea ice and ocean expansion (IPCC 2013). The rate at which polar ice is melting and sea levels are rising is projected to accelerate in the 21<sup>st</sup> century with climate change. The amount of projected sea level rise under a variety of different scenarios is likely to be between 0.26m and 0.82m relative to the baseline (1986 – 2005) period. Rising sea levels has the potential to impact agriculture

and fresh groundwater resources through the inundation of agricultural lands and saltwater intrusion into groundwater aquifers. The resulting impacts to the global economy are projected to be on the scale of 14 trillion USD per year by 2100 due to flood damages if no adaptation measures are adopted (Jevrejeva et al. 2018). Additional economic impacts may arise on the municipal level from increased water elevations in coastal outfalls for drainage systems, causing the potential for backups in stormwater drainage systems and wastewater treatment plants (IPCC 2014).

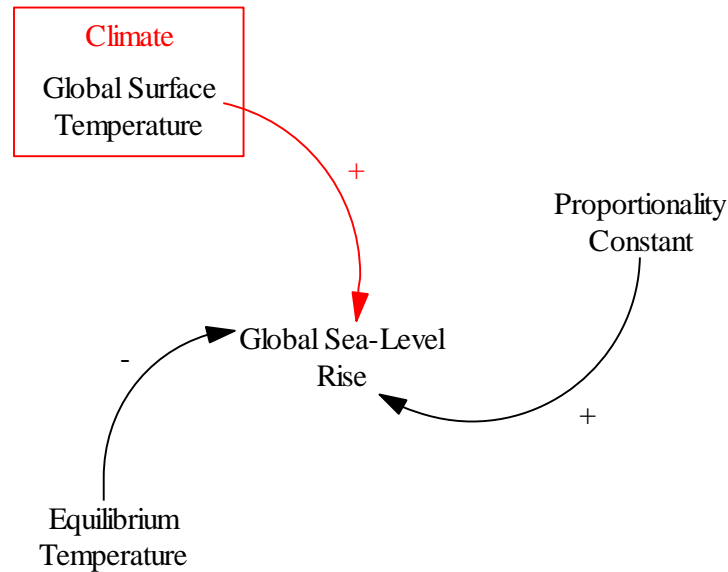


Figure 3.14. Causal diagram of the ANEMI3 sea-level rise sector.

In ANEMI3, the global average near surface air temperature change is used as a driver for sea level rise. The projected mean sea level rise is approximated as linear function of the temperature change,

$$H = a(T - T_0) \quad [m] \quad (3.31)$$

$H$  = Mean sea level rise [m]

$T$  = Global mean temperature [°C]

$T_0$  = Reference temperature [°C]

$a$  = Slope of correlation [m/°C]

This equation is based on the work of Rahmstorf (2007) who demonstrated a highly significant correlation of global temperature changes and mean sea level rise ( $r=0.88$ ,  $p=1.6e-8$ ). The slope ( $a$ ) of which was found to be 3.4mm/(year.degC). Although this representation of mean sea level rise is

simple, the impacts of which are important for food production in ANEMI3 by limiting the amount of land available for agriculture.

### 3.2.7 Hydrologic Cycle Sector

The hydrologic cycle describes the flow of water from oceans to atmosphere, onto the land surface and through the groundwater back to the ocean again as a continuous cycle. Each point in the hydrologic cycle can be considered as a kind of reservoir from which water flows to and from. The causal loop diagram in Figure 3.15 illustrates the feedback loops at work that drive the hydrologic cycle.

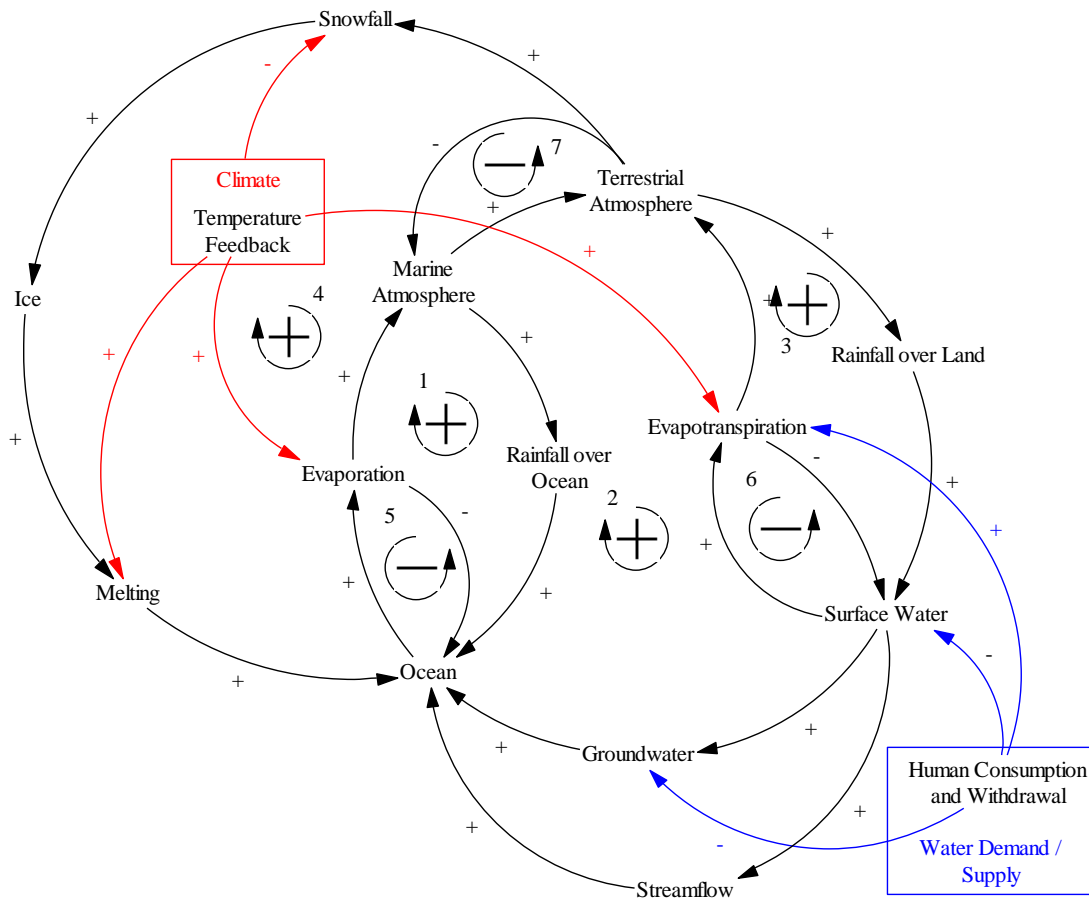


Figure 3.15. Causal loop diagram of the ANEMI3 hydrologic cycle sector.

Feedback loops number 1- 4 in Figure 3. 15 illustrate the movement of water from the atmosphere (terrestrial or marine) to the surface (ocean or land) as rainfall or snowfall and then back to the

atmosphere (through evaporation and evapotranspiration). These are positive feedback loops because more water in oceans and surface waters results in larger surface area and thus more evaporation leading to more atmosphere and rainfall then more water in oceans and surface waters once again. The positive loops are balanced by negative loops 5 and 6 which regulate increases in land and ocean water volumes by increased evaporation. Loop number 7 illustrates the balance between advection of atmospheric water over oceans and land surfaces as this process depends upon the difference in water content between them. The configuration of stocks and flows in the hydrologic cycle sector of the model are shown in Figure 3.16.

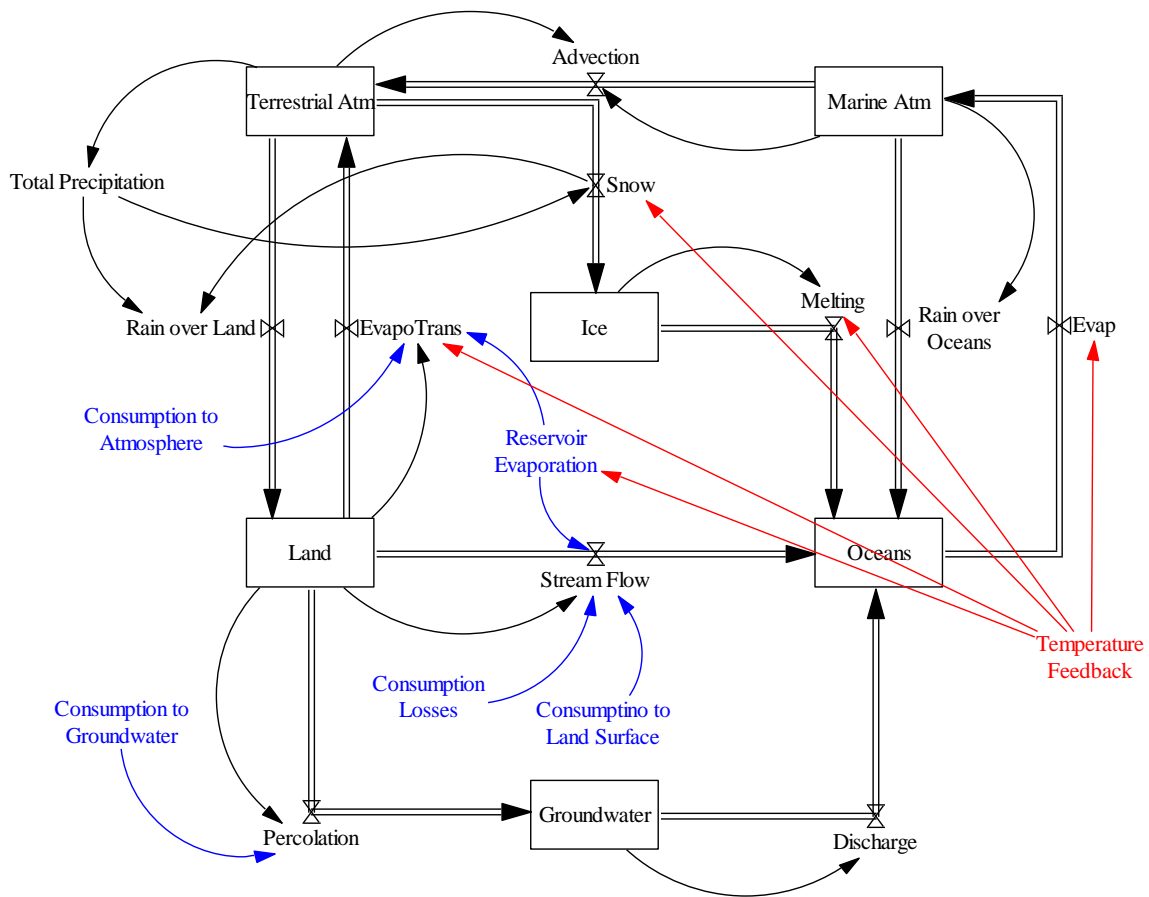


Figure 3.16. Stock and flow diagram of the AEMI3 hydrologic cycle sector. Items in blue denote processes that have human influence on the hydrologic cycle, while those in red represent the influence of changing climate.

In the ANEMI3, six reservoirs or stocks are used consisting of oceans, ice, land, groundwater, terrestrial atmosphere, and marine atmosphere. The processes modelled that move water to and from these stocks are snowfall, ice melt, evaporation and evapotranspiration, rain over land and oceans,

stream flow, percolation, and groundwater discharge. These processes all act as flows that influence the stocks. Initial values for the stocks in the hydrologic cycle are chosen in a way that allows the system to start at a pseudo steady state condition in Table 3.5. from Davies (2007). From this initial point, the hydrologic cycle is influenced by anthropogenic means.

Table 3.4. Initial stock values for hydrologic cycle sector. All values are in units of [km<sup>3</sup>].

Hydrologic Stock	Literature Value	ANEMI3 Model Value
Marine Atmosphere	9.4 – 11 * 10 <sup>3</sup>	9.4 * 10 <sup>3</sup>
Terrestrial Atmosphere	4.0 – 4.5 * 10 <sup>3</sup>	4.0 * 10 <sup>3</sup>
Oceanic Water Content	1338 * 10 <sup>6</sup>	1338 * 10 <sup>6</sup>
Land Surface Water	118 – 360 * 10 <sup>3</sup>	200 * 10 <sup>3</sup>
Ice and Permafrost	24 – 43 * 10 <sup>6</sup>	24.5 * 10 <sup>6</sup>
Groundwater	10.5 – 23.4 * 10 <sup>6</sup>	10.6 * 10 <sup>6</sup>

Anthropogenic influence on the hydrologic cycle is implemented in two ways. The first, takes into consideration water withdrawals and consumption, while the second represents the influence of changing climate. The effect of withdrawals and consumption for domestic, industrial, and agricultural water users involves the removal of water resources in the form of surface water (from stream flow) and groundwater (from the groundwater stock). The total amount of withdrawals is based on water production in the water supply sector, while the way that withdrawals are allocated across the hydrologic cycle is based on the composition of water demand across users. The proportions of which are given in Table 3.6..

Table 3.5. Percentages of water reallocation in the hydrologic cycle after human withdrawal and consumption.

Water User	Evaporation	Land	Groundwater	Lost
Agriculture	70	10	20	0
Domestic	50	0	50	0
Industry	70	0	15	15

Most of the water is not removed from the cycle at any point, it is only reallocated among the different stocks in order to maintain conservation of mass. However, in the case of industrial water

consumption, water can be effectively “locked” away in cases where water makes up a portion of the final product in the production process. Climate change influences the hydrologic cycle by superimposing a temperature feedback effect that affects a number of processes within it as the temperature change increases by acting as a multiplier. As a result, a larger portion of precipitation becomes rainfall instead of snow, and the melting of ice is increased along with evaporative processes.

The mathematical formulation of the hydrologic cycle in the ANEMI3 starts with the water content stored in the atmosphere over land and oceans,

$$A_M = \int (E_M - Adv - P_O) \cdot dt \quad [km^3] \quad (3.32)$$

$A_M =$  Marine atmospheric moisture [ $km^3$ ]

$E_M =$  Evaporation from oceans [ $km^3/y$ ]

$Adv =$  Advective flow of moisture between land and oceans [ $km^3/y$ ]

$P_O =$  Precipitation over oceans [ $km^3/y$ ]

$$A_L = \int (Adv + ET - P_R - P_S) \cdot dt \quad [km^3] \quad (3.33)$$

$A_L =$  Atmospheric moisture over land [ $km^3$ ]

$ET =$  Evapotranspiration from land surface [ $km^3/y$ ]

$P_R =$  Precipitation over land in the form of rain [ $km^3/y$ ]

$P_S =$  Precipitation over land in the form of snow [ $km^3/y$ ]

Water storage in the terrestrial environment or land surface is represented as,

$$LS = \int (P_R - ET - SF - GP) \cdot dt \quad [km^3] \quad (3.34)$$

$LS =$  Water storage on land surface [ $km^3$ ]

$SF =$  Streamflow of water from land surface to ocean [ $km^3/y$ ]

$GP =$  Groundwater percolation [ $km^3/y$ ]

Water storage in the oceans is given by the following equation,

$$O = \int (SF + GD + P_O + M - E_M) \cdot dt \quad [km^3] \quad (3.35)$$

$GD = \text{Groundwater discharge } [km^3/y]$

$M = \text{Melting of ice sheets } [km^3/y]$

Finally, groundwater and ice storage are expressed as,

$$GS = \int (GP - GD) \cdot dt \quad [km^3] \quad (3.36)$$

$GS = \text{Groundwater storage } [km^3]$

$$IS = \int (P_S - M) \cdot dt \quad [km^3] \quad (3.37)$$

$IS = \text{Ice storage } [km^3]$

### 3.2.8 Water Demand Sector

Water demand sector in the ANEMI3 is based on the desired water withdrawals of agricultural, domestic, and industrial water users. Base domestic water withdrawals are dependent on structural water intensities which relate economic factors such as GDP to withdrawal rates per person. This concept is based on the conceptual model presented in Alcamo et al. (2003), and has been confirmed by the IHP (2000) data (see Figure 3.17).

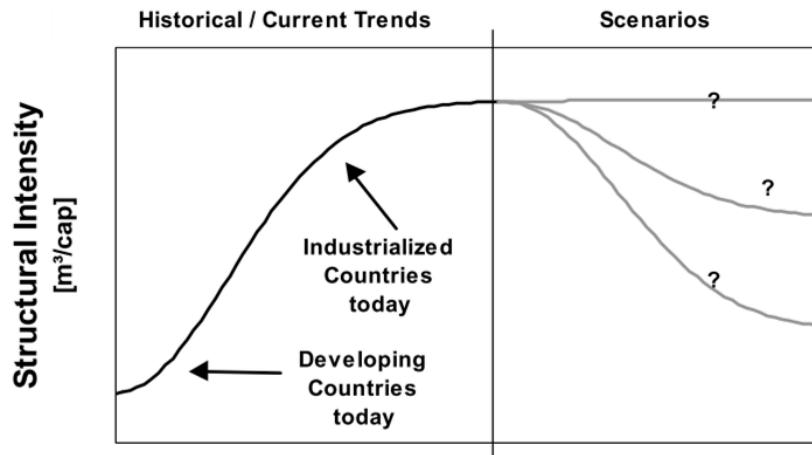


Figure 3.17. Illustration of structural water intensity for domestic water use (after Alcamo et al. 2003).

The relationships presented indicate that there are established trends in water usage as countries become developed using an indicator of economic development such as GDP per capita. Domestic water use in terms of water volume per capita tends to increase as more water is needed for improved sanitation and use of more water-using appliances such as dishwashers and washing machines. This trend stabilizes in the developed countries. The causal diagram in Figure 3.18 shows the water demand sector as a whole including domestic, industrial, and agricultural water users.

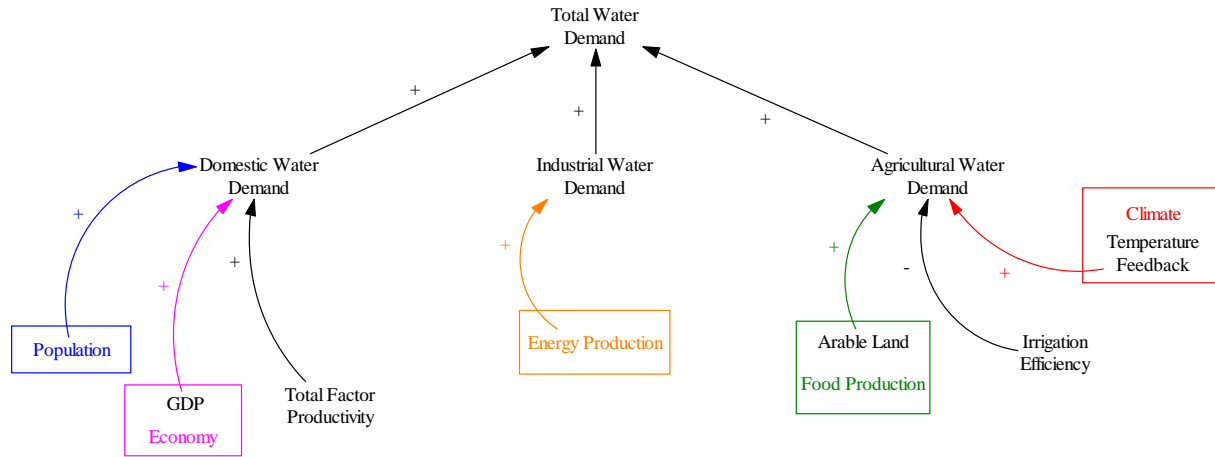


Figure 3.18. Causal diagram of the ANEMI3 water demand sector.

Although there are no feedback loops within the water demand sector itself, there are many intersectoral connection and feedbacks associated with water demand discussed previously in Section 3.1.

Domestic structural water intensity from this conceptual model is represented by the following equation,

$$DSWI = DSWI_{min} + DSWI_{max}(1 - \exp(-\gamma_d GDP^2)) \quad [m^3/person] \quad (3.38)$$

*DSWI* = Domestic structural water intensity [ $m^3/person$ ]

Where domestic structural water intensity is a function of GDP and  $DSWI_{min}$ ,  $DSWI_{max}$ , and  $\gamma_d$  are calibrated parameters based on the country for which the domestic structural water intensity is to be estimated. This equation is designed for the use of country level inputs, however in the ANEMI3

it is calibrated and applied to the global scale. The reasoning behind this is that conceptually this equation fits the trends that are taking place globally domestic water use as discussed above. This concept is also ideal for application to the global scale as the input of global GDP is readily available in the ANEMI3 model. Using the domestic structural water intensity, water demand is calculated as,

$$W_{dom} = DSWI \cdot P_{total} \cdot \Delta TFP \quad [km^3] \quad (3.39)$$

$W_{dom}$  = Domestic water demand [ $km^3$ ]  
 $P_{total}$  = Total population [persons]  
 $\Delta TFP$  = Change in total factor productivity

The change in total factor productivity is from the economic sector in the ANEMI3 and represents changes in domestic water use efficiency. This can be in the form of more efficient water distribution systems and water-using home appliances, for example.

The generation of electricity typically dominates water withdrawals in the industrial sector as a country develops. The trend in energy use starts with a high usage of water per unit of energy consumption due to the usage of mostly thermal power plants and water for cooling. Over time, more developed countries generally have a mix of thermal and non-thermal power generation plants thus reducing water usage per unit of energy consumption. The representation of industrial water withdrawal in the ANEMI3 takes into consideration projected changes in the mix of energy supply by incorporating projections from the Global Change Assessment Model (GCAM) presented in Figure 3.19.

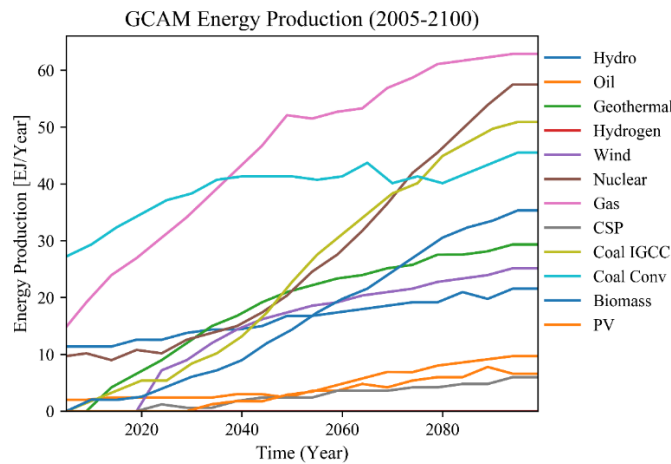


Figure 3.19. GCAM energy production projections for 2005-2100 (after Davies et al. (2013)).

In the ANEMI3 energy sector, energy production is considered for four different energy sources consisting of coal, oil and gas, hydro and nuclear power, and renewables. The fuel types from GCAM shown in Figure 3.19 were aggregated to their corresponding types in the ANEMI3, along with the water withdrawals for each of the GCAM energy production type as shown in Table 3.7.

Table 3.6. Water withdrawal rates for energy production of various types (Larsen and Drews 2019).

ANEMI3 Energy Type	GCAM Energy Type	Water Withdrawal Factor (L/MWh)
Coal	Coal IGCC (Integrated Gasification Combined Cycle)	1612
	Coal Conv (Conventional Coal)	103694
Oil and Gas	Oil	95890
	Gas	43502
Hydro and Nuclear	Hydro	0
	Nuclear	151628
Renewables	Geothermal	7586
	Hydrogen	0
	Wind	0
	CSP (Concentrated Solar Power)	3165
	Biomass	104806
	PV (Photovoltaic)	10

The industrial water demand is therefore represented by the following equation,

$$W_{ind} = \sum_{i=1}^4 \left( E_{p_i} \cdot \sum_{j=1}^n EWF_j \cdot \left( \frac{GCAM_j}{Total\ GCAM_i} \right) \right) \quad [km^3/y] \quad (3.40)$$

$W_{ind}$  = Industrial water demand [ $km^3/y$ ]

$E_{p_i}$  = Energy production in ANEMI3 for energy source  $i$  [ $GJ/y$ ]

$EWF_j$  = Energy withdrawal factor for energy source  $j$  [ $km^3/GJ$ ]

$GCAM_j$  = GCAM energy production for energy source  $j$  [ $GJ/y$ ]

$Total\ GCAM_i$  = Total GCAM energy production of energy sources  $i$  [ $GJ/y$ ]

By reformulating the industrial water withdrawal in this way, energy production is connected to water demand in the ANEMI3 model, and projected technological changes for industrial water demand are incorporated from the GCAM projections.

Agricultural water demand depends on the amount of agricultural area that is being used for food production, as well as the level of technological change with respect to water usage for food production. Change in global surface temperature is also included as an additional factor affecting water demand for food production. Increased temperatures will lead to higher evapotranspiration rates in agricultural soils thereby leaving less water for utilization for the crops and thus boosting irrigation water requirements (Yuan et al. 2016). Agricultural water demand is represented mathematically as,

$$W_{agr} = PHW \cdot A_l \quad [km^3/y] \quad (3.41)$$

$W_{agr}$  = Agricultural water demand [ $km^3/y$ ]

$PHW$  = Per hectare water withdrawals [ $km^3/(ha \cdot y)$ ]

$A_l$  = Net arable land [ha]

Where per hectare water withdrawals is represented as,

$$PHW = BW_{agr} \cdot Technology_{agr} \cdot T_{feedback} \quad [km^3/(ha \cdot y)] \quad (3.42)$$

$BW_{agr}$  = Base specific water withdrawals for agriculture [ $km^3/(ha \cdot y)$ ]

$Technology_{agr}$  = Exogenous technological change factor for irrigation

$T_{feedback}$  = Temperature feedback multiplier from climate sector

The modifications to the water demand sector from the previous version include improvements to the representation of industrial water demand. Originally, the industrial water demand was based on the product of the industrial structural water demand curve, representing the water demand from per unit of electricity production (Figure 1.1b), and the electricity production represented by an exogenous growth rate. In ANEMI3, the industrial water demand is determined through the use of modelled energy production amounts for coal, oil and gas, hydro and nuclear, and renewables, combined with water withdrawal factors for these energy types from Larsen and Drews (2019). This modification allows for the research objectives number 2 and 3 from Section 2.6 to be addressed, as it creates another feedback water supply development and the energy-economy sectors, as well as provides more plausible industrial water demand projections.

### 3.2.9 Energy-Economy Sector

The energy-economy sector used in ANEMI2 was based on the traditional Solow neoclassical growth model where economic output is represented as a function of capital and labor in the form of a Cobb-Douglas production function (Prescott 1988). The growth of capital is dependent on investment, which is determined by a Solow rule where a fraction of output is invested in new capital every time period, while population growth increases the labor force, thereby boosting output and the capital stocks over time. This reinforcing behaviour on the output is combined with a computable general equilibrium (CGE) model where the global economy consists of a representative household and a representative firm. The representative household encapsulates the World's population whose preferences are captured by a utility function based on consumption. The household generates income by renting capital and selling energy services to the firm, as well as earning income from the labor force. This income provides a budget constraint to the household for which it maximizes its utility function. The firm on the other hand, seeks to minimize the total cost of producing energy amongst different sources. As these two dynamics unfold, prices for energy production move to clear the market and achieve equilibrium between energy supply and demand for each time step. The structure of this model allows for the examination of long run economic growth of aggregate capital stock as well as the production paths for fossil fuels and renewable energies.

In ANEMI3, water supply was to be added as an additional service to be sold to the firm, and the firm would seek to minimize the total cost of production by considering the prices of supplying water. This would be based on the current level of capital stocks in water supply infrastructure for surface water, groundwater, wastewater reuse, and desalination water supplies. The capital stocks include infrastructure such as reservoirs, treatment plants, and distribution networks for example in the case of surface water supplies. Connections between energy and water production would be incorporated into the model by including energy as a key component in the production of water and vice-versa, forming a nexus between energy and water production in the global economy. The implementation of this structure into the energy-economy sector of ANEMI2 however, proved difficult as the clearing of the energy and water markets had a very narrow pathway and was extremely unstable. Therefore, in ANEMI3 a new energy-economy model was incorporated for which water supply could be integrated.

The new energy-economy sector in the ANEMI3 model is based on that developed by Fiddaman (1997), which incorporates the energy and economy models from Sterman (1980), and Nordhaus (1992). Many of the dynamics related to economic growth and resource depletion from previous approach are captured now, but there are some key structural differences. The first being that the macroeconomic assumption of market equilibrium that is used previously is no longer present, as the model being used here is a disequilibrium model. Instead of energy prices being set to equate supply and demand at every time step, there are negative feedbacks which constantly drive supply to meet the demand as they change over time.

The following sub-sections summarize the new energy-economy sector that is incorporated into the ANEMI3 model based on the Feedback-Rich Energy Economy Model (FREE) from Fiddaman (1997) as a basis for the new water supply development sector.

### 3.2.9.1 Goods Production and Capital

The dynamics of the aggregated capital stock of the global economy is shown in in Figure 3.20, consisting of five main feedback loops. The first and second loop depict the adjustment of the desired capital stock in response to the relative cost and marginal product of capital. The gap between the desired and actual capital stock is corrected in the third loop. The fourth loop illustrates the incorporation of expected output growth rate on investment, and the fifth loop factors capital depreciation into investment in additional capital.

The stock and flow structure that is used to drive the global capital stock is shown in Figure 3.21. The capital stock is the main state variable which is affected by investment and depreciation, corresponding to the flows of investment and capital discard rates.

Economic output is determined using a Cobb-Douglas production function in the following form,

$$Y = Y_0 A_t \Omega \left( \frac{L}{L_0} \right)^\alpha \left( \frac{KO}{KO_0} \right)^{1-\alpha} \quad [$/year] \quad (3.43)$$

$Y =$  Gross output [\$/year]

$Y_0 =$  Reference gross output [\$/year]

$A_t =$  Factor productivity

$\Omega =$  Climate damages

$\alpha =$  Value share of labor

$L =$  Labor [persons]

$L_0 =$  Initial labor [persons]

$KO =$  Operating capital [\$]

$KO_0 =$  Initial operating capital [\$]



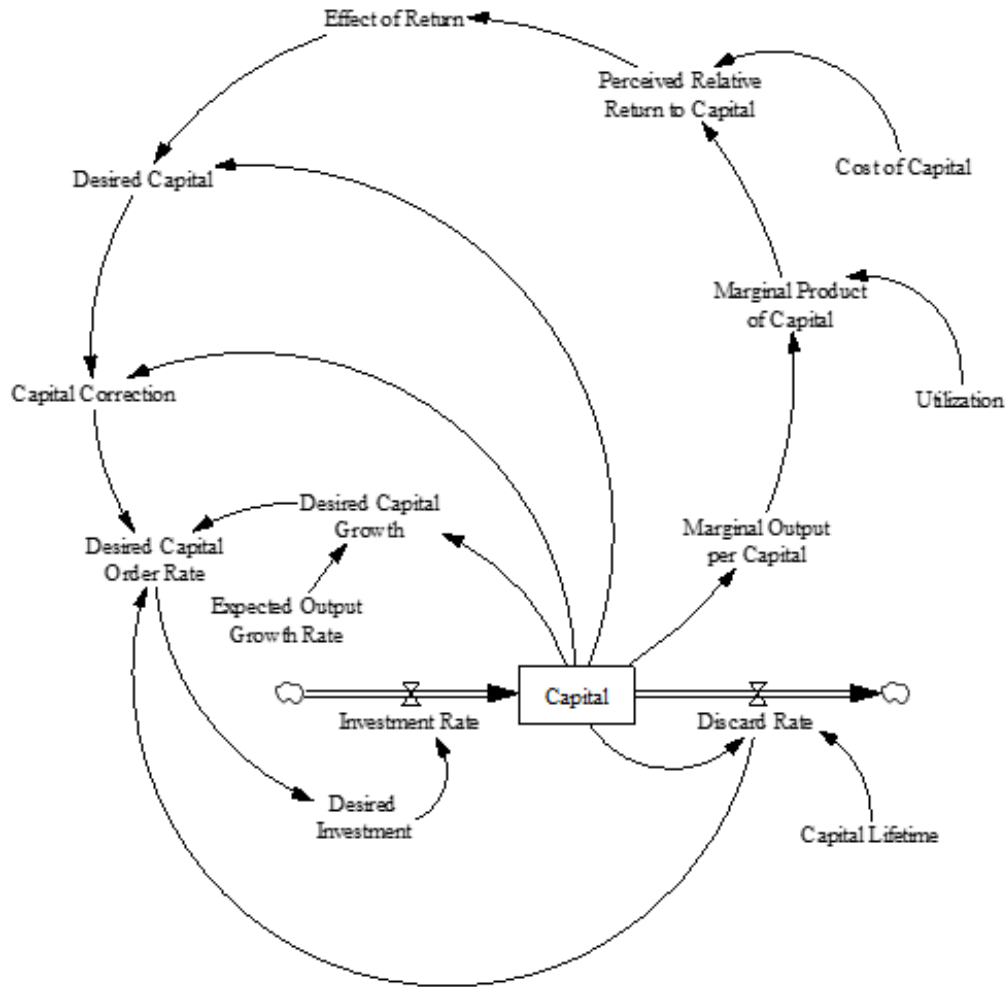


Figure 3.21. Stock and flow diagram of the ANEMI3 capital sector of the economy

Labor will increase over time as the working population increases, as will capital as the economy grows thereby increasing economic output. As global temperatures increase, so too will climate damages and will reduce economic output through the following equation:

$$\Omega = \frac{1}{1 + \theta} * \left( \frac{T - T_a}{T_{ref}} \right)^\phi \quad (3.44)$$

- $\theta$  = Climate damage scale factor
- $T$  = Atmospheric temperature [°C]
- $T_a$  = Adapted temperature [°C]
- $T_{ref}$  = Reference temperature [°C]
- $\phi$  = Climate damage non – linearity factor

This formulation allows for economic climate damages to take place only when there is a deviation from the adapted temperature. The adapted temperature approaches the current atmospheric temperature with a delay according to the fractional adaptation rate,  $T_{frac}$  in units of °C:

$$T_a(t) = \int (T_{frac} \cdot (T - T_a)) \cdot dt \quad [^{\circ}C] \quad (3.45)$$

The aggregate capital stock for the production of goods increases with investment and is depleted by depreciation, which is a fixed fraction of capital,

$$K(t) = \int (I - \delta K) \cdot dt \quad [\$] \quad (3.46)$$

$K$  = Capital aggregate [\\$]

$I$  = Investment rate [\$/year]

$\delta$  = Fractional depreciation rate

Depreciation acts as a first-order exponential decay, and is compensated by the first term of the investment equation which takes the following form,

$$I = \delta K + \frac{(K_D - K)}{\tau_k} + KG \quad [$/year] \quad (3.47)$$

$K_D$  = Desired capital [\\$]

$\tau_k$  = Capital correction time [y]

$G$  = Perceived fractional growth rate of output

In addition to compensating for depreciation, investment is driven by the perceived growth in output. Otherwise, capital would lag the optimal value for each time step. Lastly, investment in capital is determined by the deviation between desired capital and its current value over a correction time. Desired capital is defined as,

$$K_D = \frac{KM_k}{r} \quad [\$] \quad (3.48)$$

$M_k$  = Marginal product of capital [\$/(\$  
· year)]

$r = \text{Interest rate}$

Which amounts to the current level of capital adjusted for the relative cost and marginal product of capital.

### 3.2.9.2 Energy Production

Energy is produced to meet the demands for the production of goods and services (i.e. economic output). The production of energy is disaggregated into four types; coal, oil and gas, hydro and nuclear power, and renewables. Hydro and nuclear energy sources are combined into a single energy source because they have similar carriers (i.e. generation of electricity to a grid) and long-term characteristics including diminishing returns to expansion as the best sites are used first, and are subject to political and environmental constraints (Fiddaman 1997).

The capacity of energy production is set by the amount of capital stock that has been accumulated into each energy source and is influenced by production pressures and profit incentives. The rate of variable inputs determines the utilization of production capacity. Limitations on energy production are in the form of depletion and saturation for non-renewable and renewable energy sources. Depletion refers to the use of limited resource stocks (i.e. fossil fuels) thereby increasing effort and cost required to extract the resources. Saturation in this context refers to diminishing returns to energy production effort. For example, the most ideal sites are taken first to implement wind and solar farms or dams for hydropower generation, thereby making it more difficult and/or expensive to implement additional sites. These concepts are illustrated in the causal loop diagram in Figure 3.22.

Feedback loop number 1 illustrates the effect of resource depletion on energy production. As more energy is produced, energy resources begin to deplete. This affects the ratio of energy resources remaining which acts as a reduction factor on energy production, creating a negative feedback loop. The second loop is a positive loop, which illustrates the increasing efficiency of energy production through technological improvements over time, driven by cumulative energy production. The third loop represents the perpetual production of energy to meet demand. As energy is produced resources begin to deplete, causing a reduction in production through the resource depletion effect. This in turn causes production pressure to meet demand, resulting in further investment in energy capital stocks thereby increasing production again. The fourth loop is a negative feedback loop, which limits the

increase in energy production as technological improvements are made thereby boosting energy production and reducing production pressure.

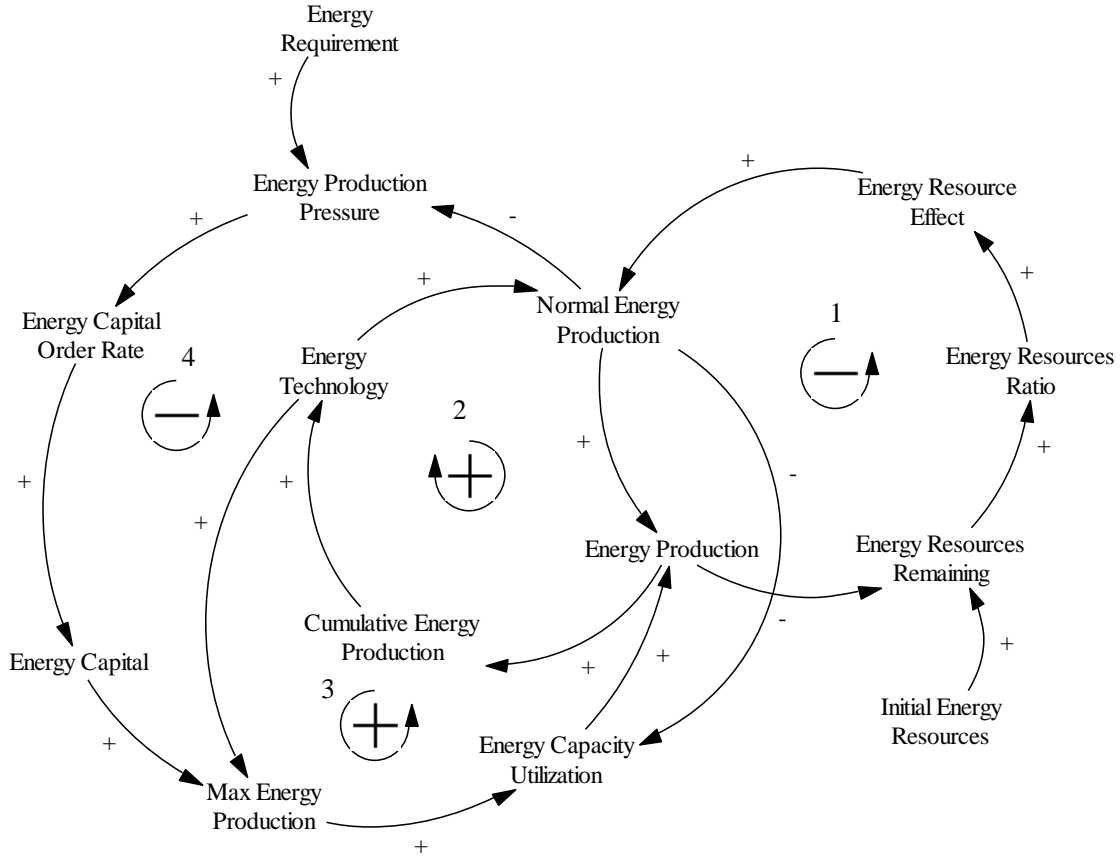


Figure 3.22. Causal loop diagram for the energy production sub-system of the ANEMI3 energy-economy sector.

The equation used to represent energy production in the model takes the following form:

$$EP_i = EP_{i,0} \left( \alpha_i \left( \frac{R_i}{R_{i,0}} \right)^{\rho_i} + (1 - \alpha_i) EII_i^{\rho_i} \right)^{\frac{1}{\rho_i}} \quad [GJ/y] \quad (3.49)$$

$EP_i$  = Energy production [GJ/year]

$EII_i$  = Effective input intensity

$EP_{i,0}$  = Initial energy production [GJ/year]

$\alpha_i$  = Resource share

$R_i$  = Resource remaining [GJ]

$\rho_i$  = Resource substitution coefficient

$R_{i,0}$  = Initial resource remaining [GJ]

In this equation,  $i$  is used to denote the energy source under consideration. The resource share provides an upper limit on energy production by representing the minimum time required for resource extraction in the case of non-renewables, and the maximum resource flux in the case of renewables.

$$\alpha_{nonrenewable} = \left( \frac{R_{i,0}}{\tau_r EP_{i,0}} \right)^{\rho_{nonrenewable}} \quad \alpha_{renewable} = \left( \frac{R_{i,0}}{EP_{i,0}} \right)^{\rho_{renewable}} \quad (3.50)$$

Where  $\tau_r$  is the minimum resource depletion time in years. As energy resources are consumed for example in the case of fossil fuels, there is a depletion effect present that acts to decrease energy production unless there is a change in the effective input intensity. The effective input intensity depends on the level of technology development as well as capital and variable inputs put into production.

$$EI_i = TE_i \left( \frac{KE_i}{KE_{i,0}} \right)^{\beta_{i,kv}} \left( \frac{V_i}{V_{i,0}} \right)^{1-\beta_{i,kv}} \quad (3.51)$$

$TE_i = \text{Energy technology}$

$V = \text{Variable input}$

$KE_i = \text{Energy capital [\$]}$

$V_{i,0} = \text{Initial variable input}$

$KE_{i,0} = \text{Initial energy capital [\$]}$

$\beta_{i,kv} = \text{Capital share}$

The stock and flow diagram for the energy production sector is depicted in Figure 3.23.. The production of energy depletes the energy stock over time thereby accumulating into the cumulative energy production. In the case of coal production and oil and gas production, depleted energy resources results in an energy resource effect that reduces the normal energy production rate over time, creating a negative feedback loop on production with a goal of zero in the case of full depletion.

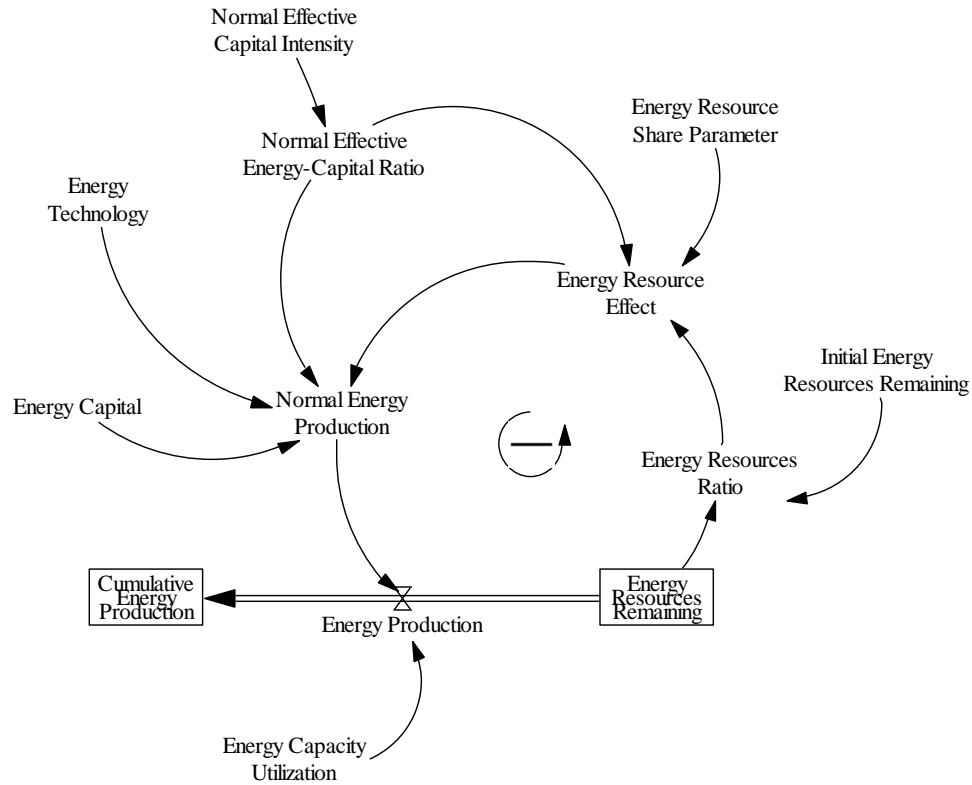


Figure 3.23. Stock and flow diagram for the ANEMI3 energy production sector

### 3.2.9.3 Energy Capital

The capital stocks for the different energy sources are structured in a similar way to that of the goods production capital stock. The main difference is that there is a stock which represents energy capital under construction which after a delay time becomes new energy capital.

There are six feedback loops in total in the energy capital sector (Figure 3.24). The first loop is a negative feedback loop that drives the process of energy capital depreciation which slowly depletes the energy capital stock. The second loop, being a positive feedback loop compensates for depreciation by factoring it into the desired energy capital order thus boosting the energy capital order rate and energy capital. The third loop moves energy capital from the construction phase to the completion phase. The fourth loop reduces energy orders by taking into consideration capital that is currently under construction when determining the desired energy capital order rate. The fifth loop is a positive feedback loop which increases capital investment based on perceived returns. The sixth loop reduces the effect of perceived returns, thereby limiting the positive effect of the fifth. This is because more energy capital results in reduced the marginal product of capital, thereby reducing the

return on energy capital investment. These feedback loops in combination drive the energy production of the ANEMI3 model.

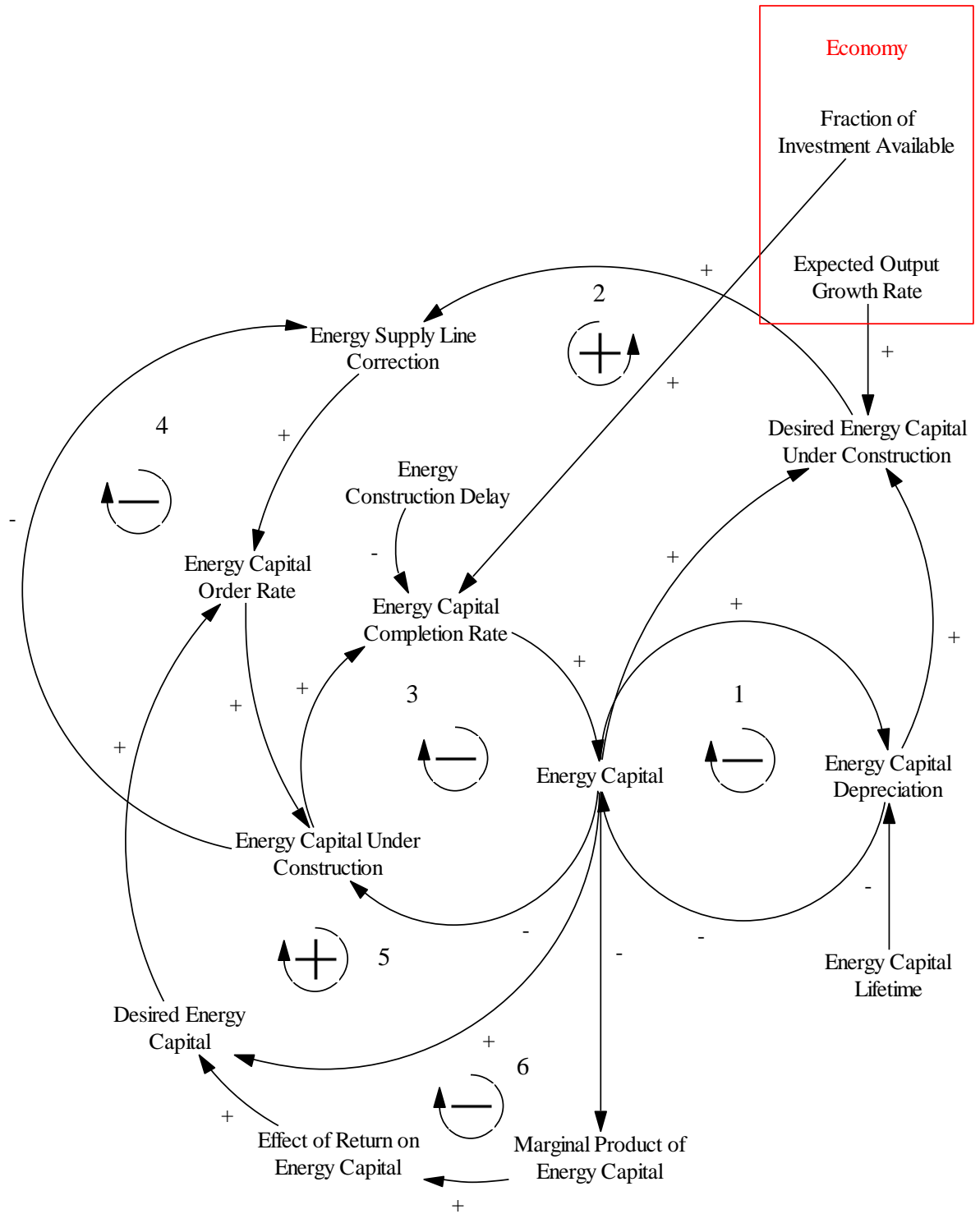


Figure 3.24. Causal loop diagram for the energy capital sub-sector of the energy-economy sector.

The corresponding stock and flow diagram is depicted in Figure 3.25. It illustrates the main feedbacks present in the energy capital sector. There are two stocks which denote energy capital that is either under construction or completed. By dividing the capital stock in this way, a delay is formed from the time that investment in energy supply is made, to when it is completed and contributing to energy production.

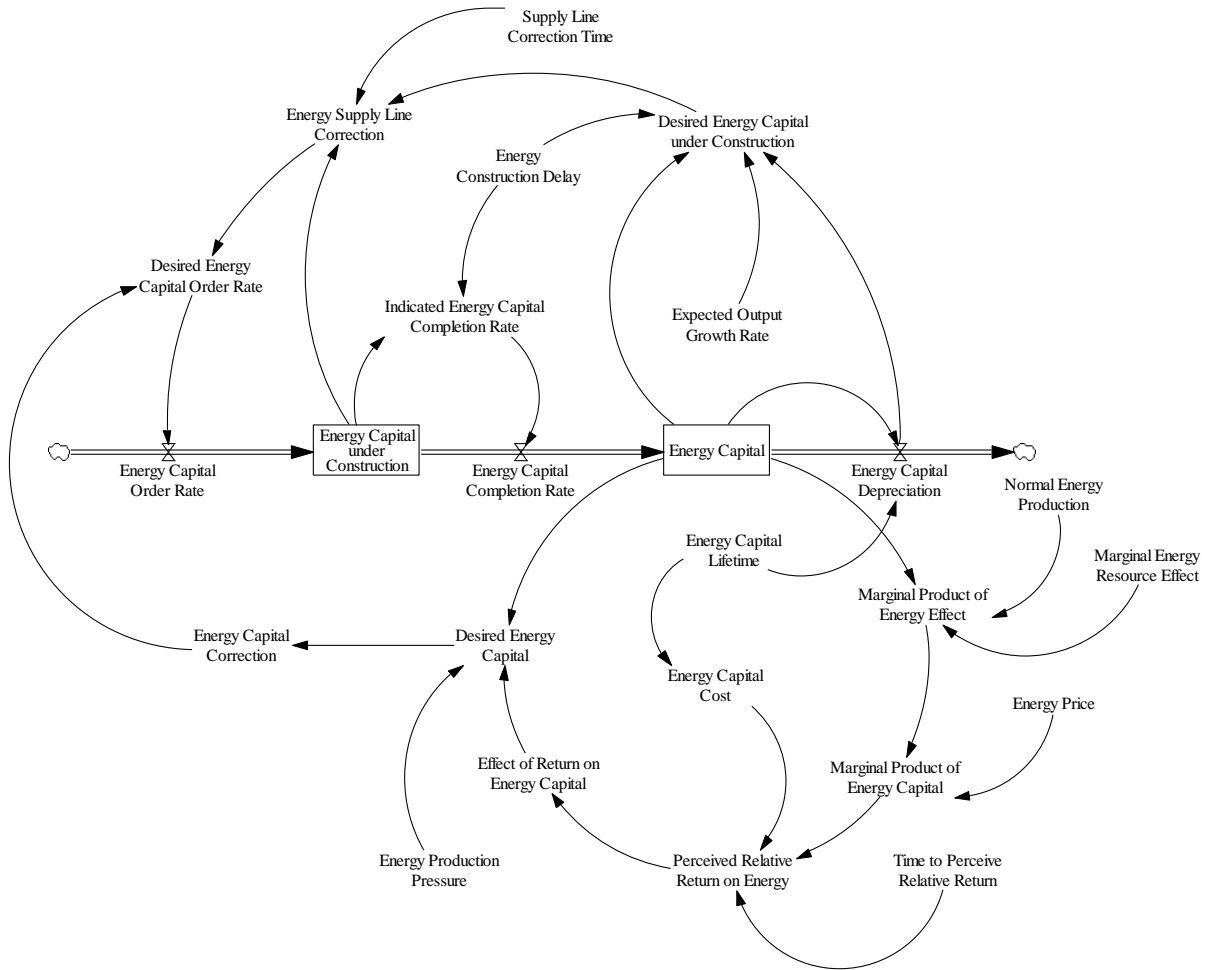


Figure 3.25. Stock and flow diagram of the ANEMI3 energy capital sector

The energy capital stock can be represented mathematically by,

$$KE_i = \int \frac{KC_i}{\tau_c} - \frac{KE_i}{\delta_i} \quad [\$] \quad (3.52)$$

$KE_i = \text{Energy capital for energy source } i \text{ [\$]}$

$KC_i = \text{Energy capital under construction for energy source } i \text{ [\$]}$

$\tau_c = \text{Capital construction delay [y]}$

$\delta_i = \text{Energy capital lifetime [y]}$

$$KC_i = \int EKO_i - \frac{KC_i}{\tau_c} \quad [\$] \quad (3.53)$$

$EKO_i = \text{Energy capital order rate [$/y]}$

The energy capital order rate prompts the construction of new capital and thereby increases the capacity for energy production. It is formulated in the same way as capital investment for goods production in that it compensates for capital depreciation, adjusts for perceived growth in energy orders, and responds to discrepancies in desired versus current energy capital stock.

$$EKO_i = \delta_i KE_i + \frac{DKC_i - KC_i}{\tau_{kc}} + \frac{DKE_i - KE_i}{\tau_k} + KE_i * GE_i \quad [$/year] \quad (3.54)$$

$DKC_i = \text{Desired energy capital under construction [\$]}$

$DKE_i = \text{Desired energy capital [\$]}$

$\tau_{ke} = \text{Time to correct capital under construction [y]}$

$GE_i = \text{Perceived growth rate of energy orders}$

$$DKE_i = \frac{KE_i M_{i,k} EO_i}{r NEP_i} \quad [\$] \quad (3.55)$$

$M_{i,k} = \text{Marginal product of energy capital [$/(\$ \cdot y)]}$

$EO_i = \text{Energy order rate [$/y]}$

$r = \text{Interest rate}$

$NEP_i = \text{Normal energy production [GJ/y]}$

$$DKC_i = KE_i (\delta_i + GE_i) \tau_{kc} \quad [\$] \quad (3.56)$$

### 3.2.9.4 *Energy Requirements*

One of the unique features of the FREE model in contrast to other climate-energy-economy models of its kind is the embodiment of energy requirements, or demand, in the capital stock (Fiddaman 1997). This means that when capital is constructed, it has a fixed energy intensity. In the real world, this equates to energy consumption being dependent on products that persist with time. For example, once an electric stove is manufactured its energy efficiency cannot be changed. This contrasts with other models like DICE (Nordhaus 1994) which assume that appliances like an electric stove could be converted to one that uses natural gas. In the FREE model, transitioning between energy sources requires gradual substitution of energy capital due to price changes even if the current allocation of capital is suboptimal.

The feedbacks that are governing the energy requirement subsystem are shown in Figure 3.26. Five main feedback loops govern the behaviour of this subsystem. The first, represents a negative feedback of diminishing energy requirement. The second is a negative feedback loop where an increase in energy requirements (or demand), results in an increase in price and thus a lower energy requirement install rate. The third loop acts in a similar way as the second, but the energy price is decreased, creating a positive feedback loop on energy requirement. The fourth is a positive feedback loop which shows that an increase in energy requirement causes energy intensity of capital to increase thereby resulting in greater energy requirement. The corresponding stock and flow diagram is presented in Figure 3.27.

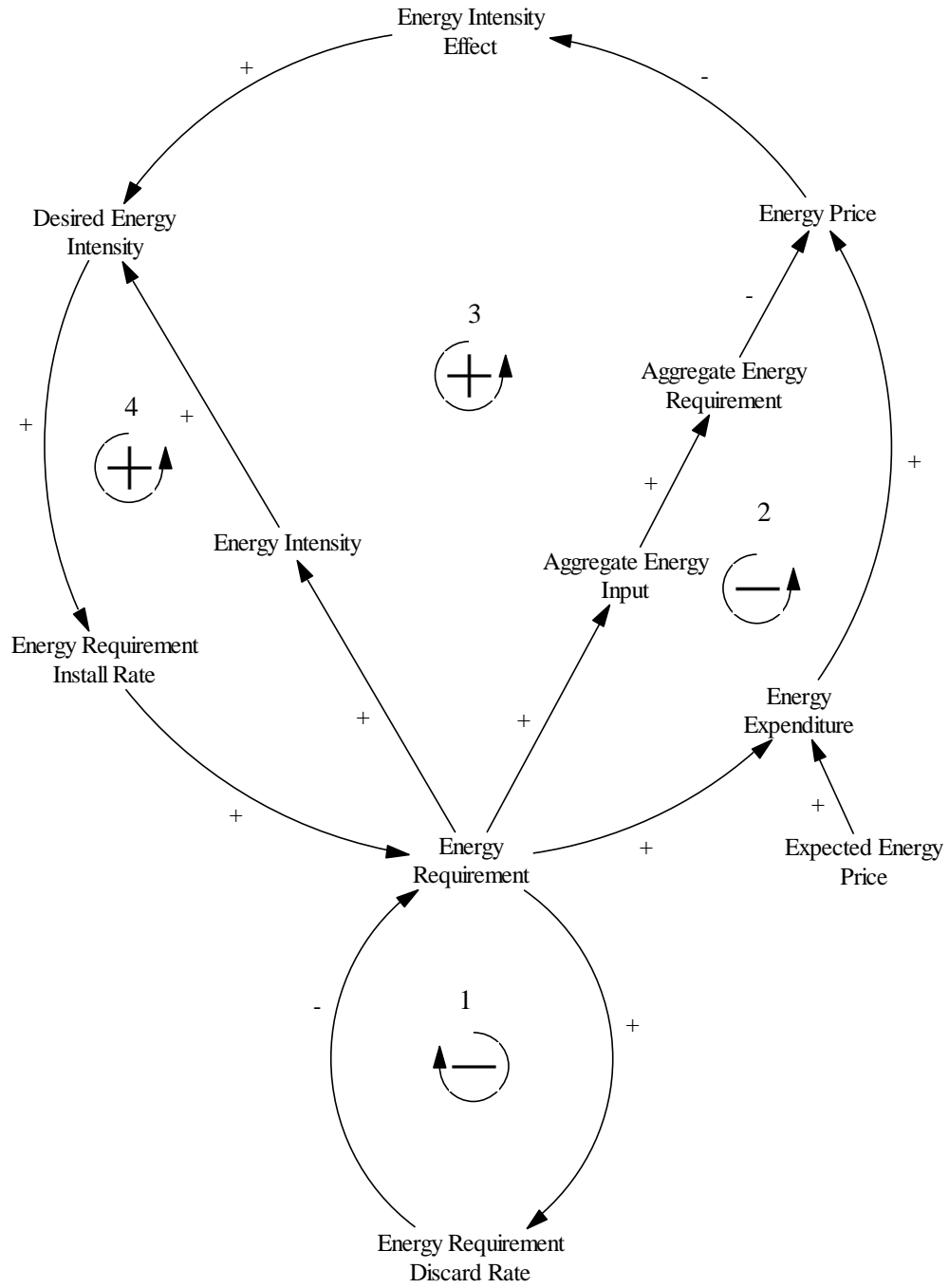


Figure 3.26. Causal loop diagram for energy requirements sub-system in the ANEMI3 energy-economy sector.

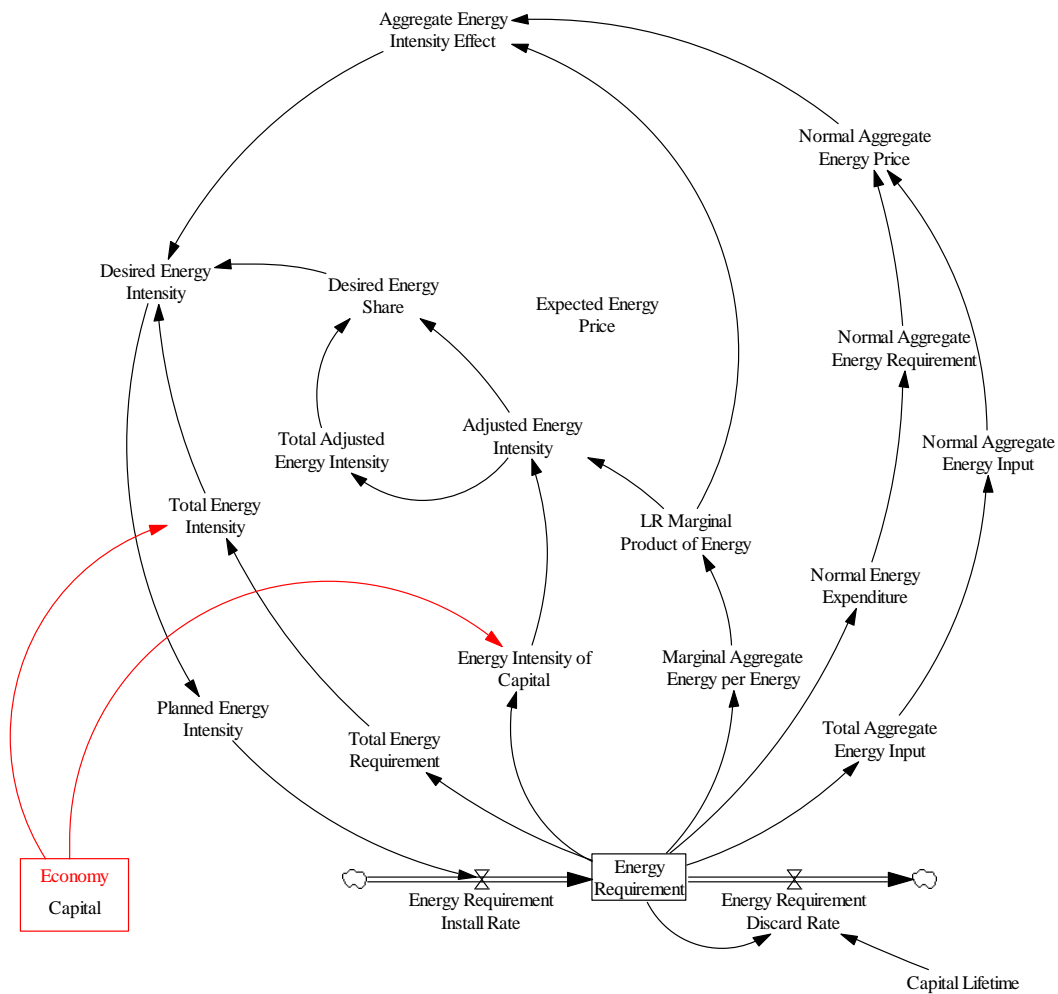


Figure 3.27. Stock and flow diagram of energy requirements sub-system of ANEMI3 energy-economy sector.

Changes in energy requirements are co-flows with capital investment and depreciation of the energy capital stocks, and retrofitting can gradually adjust the energy intensity of existing capital to that of the planned energy intensity of new capital,

$$ER_i = \int (N_i(I + \varepsilon K) - (\delta + \varepsilon)ER_i) \cdot dt \quad [GJ/y] \quad (3.57)$$

$ER_i = \text{Energy requirements for capital corresponding to energy source } i \text{ [GJ/y]}$   
 $N = \text{Planned energy intensity of new capital corresponding to energy source } i \text{ [GJ/(\$} \cdot \text{y)]}$   
 $I = \text{Investment rate [$/y]}$   
 $\varepsilon = \text{Fractional retrofit rate [1/y]}$   
 $\delta = \text{Fractional discard rate [1/y]}$

Planned energy intensity adjusts to the desired intensity with a delay period. The delay period is meant to represent the time taken to incorporate the desired energy intensity into new products,

$$N_i = \int \frac{ND_i - N_i}{\tau_n} \cdot dt \quad [\text{GJ/(\$} \cdot \text{y)}] \quad (3.58)$$

$ND_i = \text{Desired energy intensity of new capital } i \text{ [GJ/(\$} \cdot \text{y)]}$   
 $\tau_n = \text{Energy intensity planning delay [y]}$

The energy intensity is adjusted based on the aggregate energy intensity and the relative shares of individual energy sources. This is done by introducing multipliers for relative price and the marginal product of energy to the current energy intensity,

$$ND_i = N_T \cdot AE \cdot DS_i \quad [\text{GJ/(\$} \cdot \text{y)}] \quad (3.59)$$

$N_T = \text{Total energy intensity of capital [GJ/(\$} \cdot \text{y)]}$   
 $AE = \text{Aggregate energy intensity adjustment}$   
 $DS_i = \text{Desired share for energy source } i$

Where,

$$N_T = \frac{\sum_i ER_i}{K} \quad [\text{GJ/(\$} \cdot \text{y)}] \quad (3.60)$$

The adjustment to aggregate energy intensity is calculated by comparing the long-run marginal product of the aggregate energy good to that of the perceived aggregate energy price from all sources,

$$AE = \left( \frac{M_T}{P_T} \right)^{\omega \sigma_{ke,lr}} \quad (3.61)$$

$M_T =$  Long-run marginal product of aggregate energy [\$/GJ]

$P_T =$  Normal aggregate energy price for energy source  $i$  [\$/GJ]

$\omega =$  Energy intensity adjustment coefficient

$\sigma_{ke,lr} =$  Long-run capital-energy substitution elasticity

With this formulation, higher marginal product of aggregate energy (more economic output per unit of energy) or lower prices will result in a higher desired energy intensity of new capital. The desired share for energy source,  $i$  is calculated as the share of adjusted energy intensity that energy source  $i$  has compared against the total for all energy sources.

$$DS_i = \frac{AI_i}{\sum_i AI_i} \quad (3.62)$$

$AI_i =$  Adjusted energy intensity of energy source  $i$  [\$/( $y \cdot GJ$ )]

$$AI_i = \frac{ER_i \cdot \left( \frac{M_{i,lr}}{P_i} \right)^{\omega \sigma_{ke,lr}}}{K} \quad [$/( $y \cdot GJ$ )] \quad (3.63)$$

$M_{i,lr} =$  Long-run marginal product of energy [\$/GJ]

$P_i =$  Perceived energy price [\$/GJ]

If  $\omega$  in Equation 49 and 51 is set to a value of 1, the substitution of energy sources will behave in a similar way to a general equilibrium model. That is, a change to the energy prices will result in immediate changes to the energy intensity of new capital.

### 3.2.9.5 Energy Pricing

Energy pricing varies with the cost of energy producer prices along with distribution costs, total taxes, and depletion rent. The dynamics of the energy pricing sub-system are illustrated by the causal loop diagram shown in Figure 3.28. There are three feedback loops that govern the behaviour of energy pricing in the model. The first feedback loop regulates the energy price. An increase in energy price results in a decrease in the order rate, thereby reducing production pressure and dampens the initial increase. The second is a positive feedback loop, where an increase in producer price is perpetuated by increasing the indicated price, thereby reinforcing the initial increase. The third loop regulates the second by gradually allowing the gap between the current and indicated producer price over time. This sub-system has connections with the energy production sub-system in establishing the level of production pressure as the ratio of energy production (supply) to the energy order rate (demand), as well as the energy capital sub-system in establishing the average energy cost.

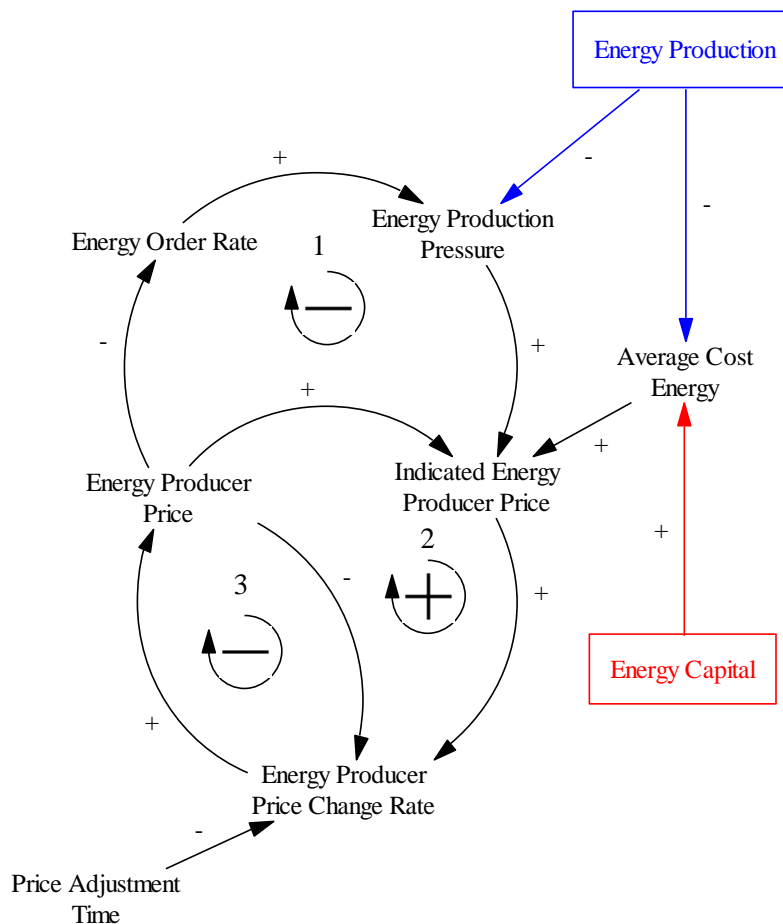


Figure 3.28. Causal loop diagram of ANEMI3 energy pricing sector.

The stock and flow diagram for the energy pricing sub-system is presented in Figure 3.29. From this diagram it is shown that the price acts as a stock or state variable which is changing in response to the indicated price over the price adjustment time. The final energy price is determined by the producer price in addition to distribution costs and total taxes on energy source. This could include the implementation of a carbon tax on fossil fuel production, however this is not considered in this work.

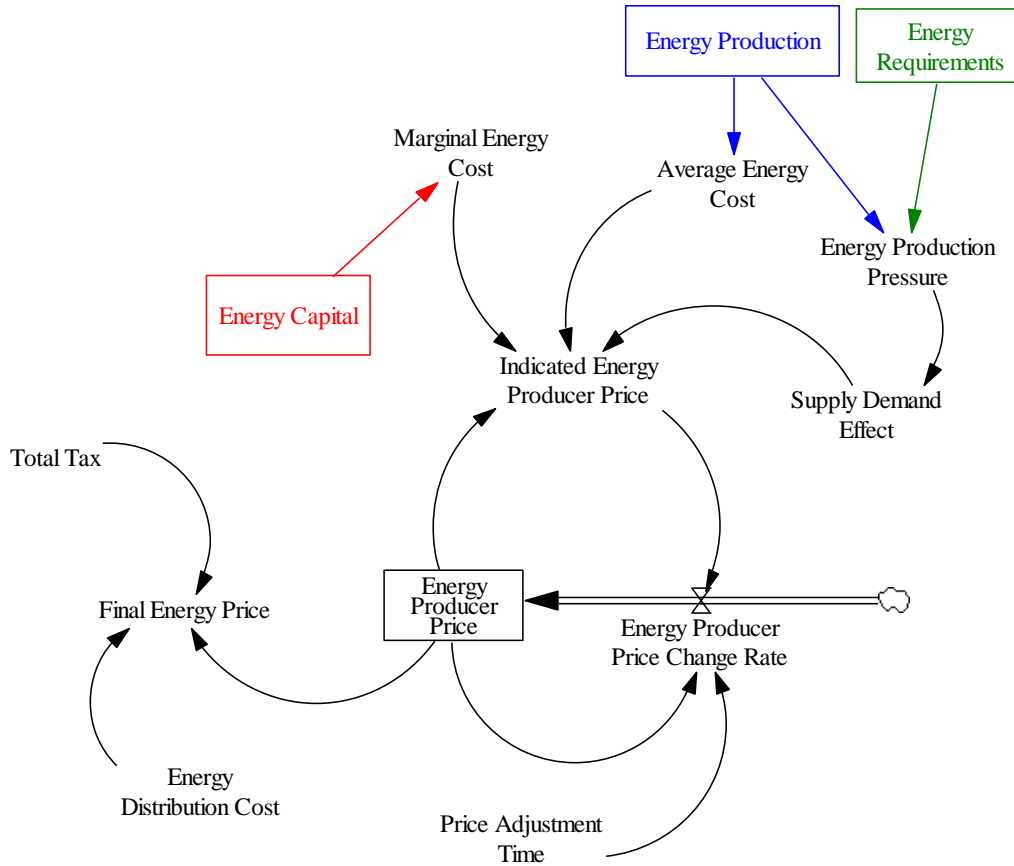


Figure 3.29. Stock and flow diagram for the energy pricing sub-system of the ANEMI3 energy-economy sector.

The energy price can be represented mathematically by,

$$P_i = PP_i + \mu_i + D_i + T_i \quad [$/GJ] \quad (3.64)$$

$P_i = \text{Energy price } [\$/\text{GJ}]$

$D_i = \text{Distribution cost } [\$/\text{GJ}]$

$PP_i = \text{Producer price } [\$/\text{GJ}]$

$T_i = \text{Total taxes } [\$/\text{GJ}]$

$\mu_i = \text{Depletion rent } [\$/\text{GJ}]$

$$PP_i = \int \frac{IP_i - PP_i}{\tau_p} \quad [\$/\text{GJ}] \quad (3.65)$$

$IP_i = \text{Indicated producer price } [\$/\text{GJ}]$

$\tau_p = \text{Price adjustment time } [y]$

The producer price is adjusted by its previous value to approach the indicated producer price over an adjustment time,  $\tau_p$ . The indicated producer price changes with the average and marginal costs of energy production as well as with the ratio of energy orders to production. This is where supply and demand of energy are equated to influence the price in place of a market clearing mechanism that would be used in traditional macroeconomic models.

$$IP_i = PP_i \left( \frac{AC_i}{PP_i} \right)^{\gamma_a} \left( \frac{MC_i}{PP_i} \right)^{\gamma_m} \left( \frac{EO_i}{NEP_i} \right)^{\gamma_d} \quad [\$/\text{GJ}] \quad (3.66)$$

$AC_i = \text{Average cost of energy production } [\$/\text{GJ}]$

$\gamma_a = \text{Weight to average cost } [\$/\text{GJ}]$

$MC_i = \text{Marginal cost of energy production } [\$/\text{GJ}]$

$\gamma_m = \text{Weight to marginal cost}$

$EO_i = \text{Energy order rate } [GJ/y]$

$NEP_i = \text{Energy production at normal capacity utilization } [GJ/y]$

$\gamma_d = \text{Weight to demand pressure}$

### 3.2.9.6 Energy Technology

Technological progression plays a role in the production of energy through the effective input intensity, which acts to increase the production of energy for the same level of inputs. The causal loop

diagram illustrates the feedbacks involved that govern the endogenous representation of energy technology in the model (Figure 3.30).

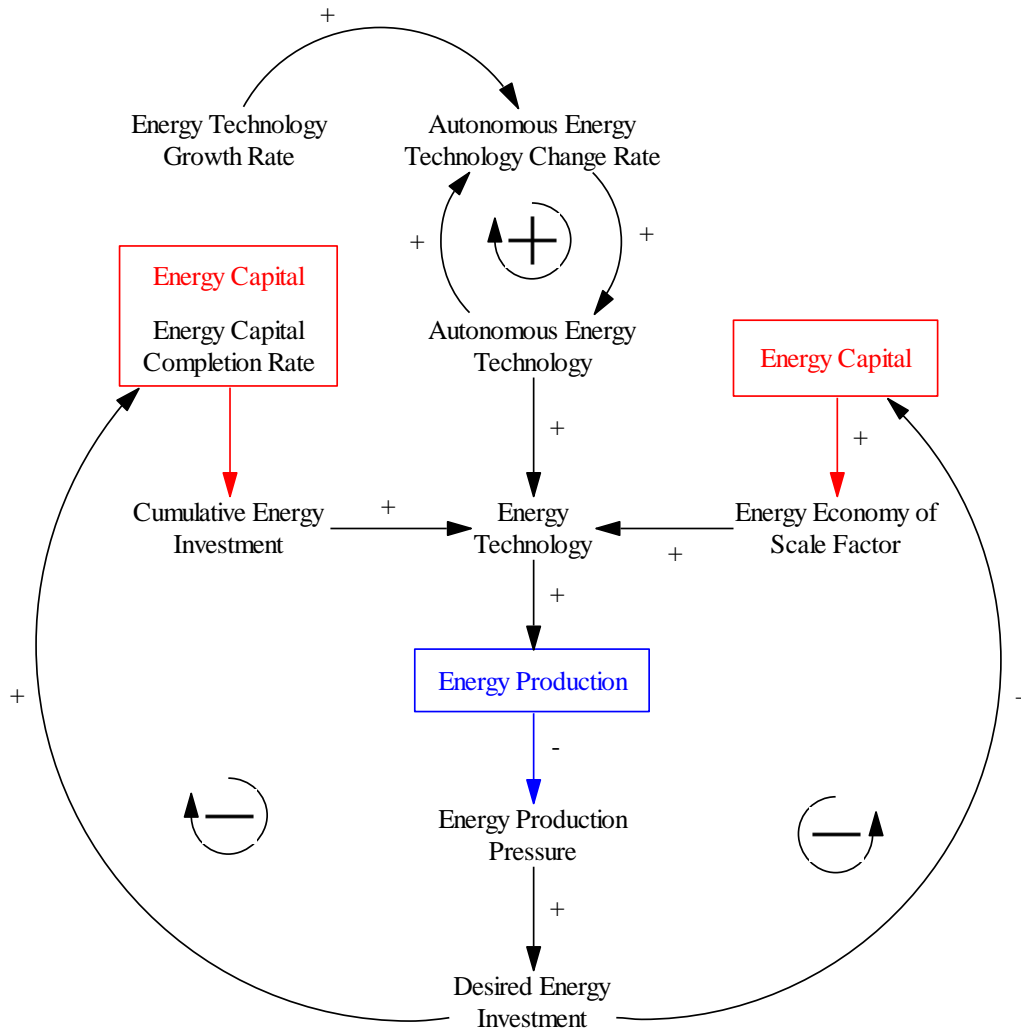


Figure 3.30. Causal loop diagram for the technological change sub-system of the ANEMI3 energy-economy sector.

The positive feedback loop drives technological progress in energy production exogenously over time with the application of a growth rate factor. As energy is produced, the production pressure which takes into account the ratio of supply to demand, acts to decrease the level of desired investment in new energy capital. This decrease in desired energy investment slows the rate at which the cumulative energy investment grows, thereby slowing down technological advancement in energy production. Economy of scale (the proportionate saving in costs through increased production) is also factored

into energy technology. As desired energy investment decreases with increased production, the growth in economy of scale will increase at a slower rate, thereby creating another negative feedback loop on the progression of energy technology.

The corresponding stock and flow diagram illustrates the system structure of the technological change sub-system (Figure 3.31). The level of autonomous energy technology is represented as a stock and grows exogenously based from its initial value and the specified growth rate. This is the only feedback loop that exists directly within this sub-system, while the other come from different sub-systems within the energy-economy sector. The endogenous portion of the energy technology sub-system is represented by incorporating cumulative energy investment stock as an indicator of technological change, as it is assumed that more investment in a given energy source over time will result in faster rates of technological change.

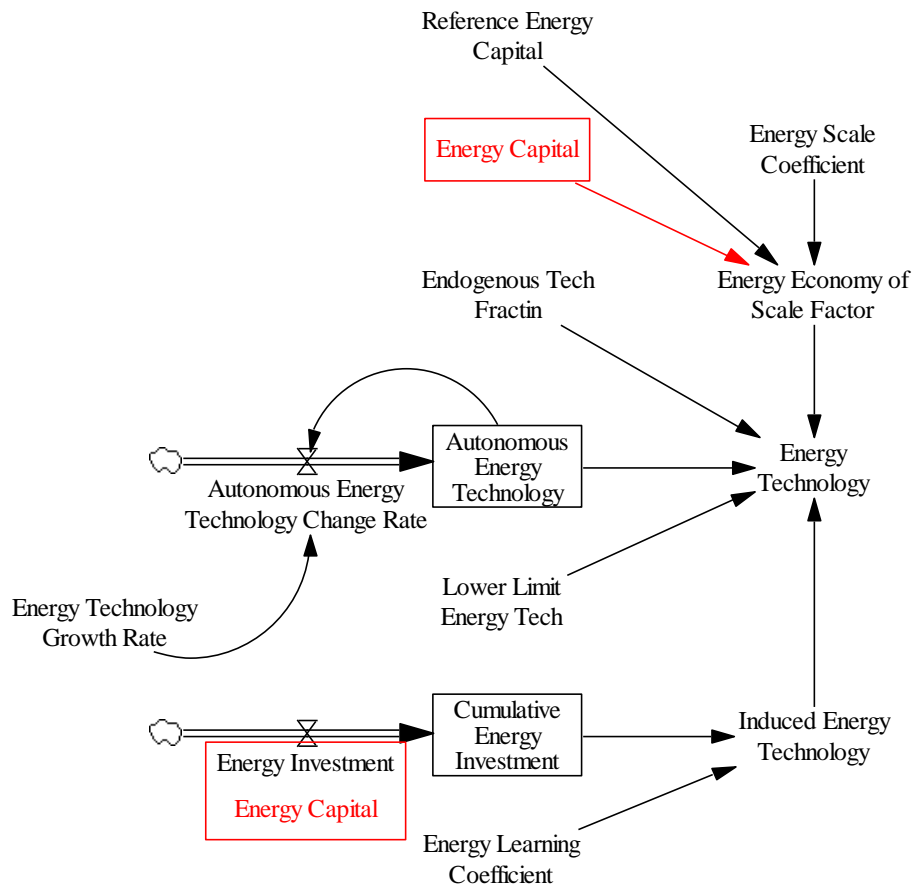


Figure 3.31. Stock and flow diagram of energy technology sub-system within the ANEMI3 energy-economy sector.

Here, technological change is represented by a standard learning curve, that progresses with cumulative investment in energy capital. The functional form is given as,

$$ET_i = \beta_t \ln \left( \frac{C_i}{C_{i,0}} \right) \quad (3.67)$$

$ET_i$  = Endogenous technological change

$\beta_t$  = learning curve coefficient

$C_i$  = Cumulative investment [\$]

$C_{i,0}$  = Initial cumulative investment [\$]

The learning curve function for technological change in energy production is then used to calculate the energy technology level which factors into energy production (Equation 3.49).

$$TE_i = \frac{1}{LL_i + \frac{(1 - LL_i)}{ET_i^v AT_i^{1-v} S_i}} \quad (3.68)$$

$TE_i$  = Energy technology level

$LL_i$  = Lower limit to cost reductions from technology

$ET_i$  = Endogenous learning curve

$AT_i$  = Autonomous technology

$S_i$  = Scale economy effect

$v$  = Fraction of technology endogenous

$$AT_i = e^{\alpha_t t} \quad (3.69)$$

$\alpha_t$  = Fractional autonomous energy technology growth rate

$$S_i = \left( \frac{KE_i}{KE_{i,0}} \right)^{\gamma_s} \quad (3.70)$$

$KE_i = \text{Energy capital [\$]}$

$KE_{i,0} = \text{Initial energy capital [\$]}$

$\gamma_s = \text{Scale coefficient}$

This formulation allows for the energy technology level to increase over time as more capital is invested into energy production.

### 3.2.10 Water Supply Development

The water supply sector in ANEMI3 was developed by incorporating water supply as a new production sector within the newly added energy-economy sector. This has been achieved by adding capital stocks to produce water supply in the form of surface, ground, wastewater reclamation, and desalination water sources. The basic structure of the energy sector, described in the previous section of the document, was adopted as a starting point from which changes were made to accommodate the development of water supply.

The causal loop diagram presented in Figure 3.32 illustrates the dynamics that are governing the behaviour of the water supply development sector. The first feedback loop acts as a negative feedback on water supply capital through depreciation. With regards to water supply, this would represent the cost of maintaining supply infrastructure including pumps, distribution networks, dams and reservoirs, and treatment facilities. The second feedback loop counteracts the first, by having a positive feedback effect on water supply capital. With more water supply capital there is more depreciation, which in turn increases the water capital order rate (investment in water supply) thus adding more water supply capital. The third feedback loop is of a negative sign that counteracts water stress by prompting investment in water capital to increase water supplies. The fourth and last feedback incorporates the effects of depletion and saturation into water supply development.

As available water resources become depleted, the production of water supply is reduced for the same input intensity. This means that more effort is required to produce the same rate of water supplies, which also makes a given type of water supply that is depleted more expensive. For example, when the groundwater elevation decreases from over abstractions, more pumping is required to extract the same amount of water resource. The effect of saturation is also included in this relationship, assuming the best or most cost-effective sites are used first for water supply infrastructures. An example of

which could include the construction of additional reservoirs, source water intakes, of groundwater wells in areas that are less suitable or cost effective than those that were previously constructed.

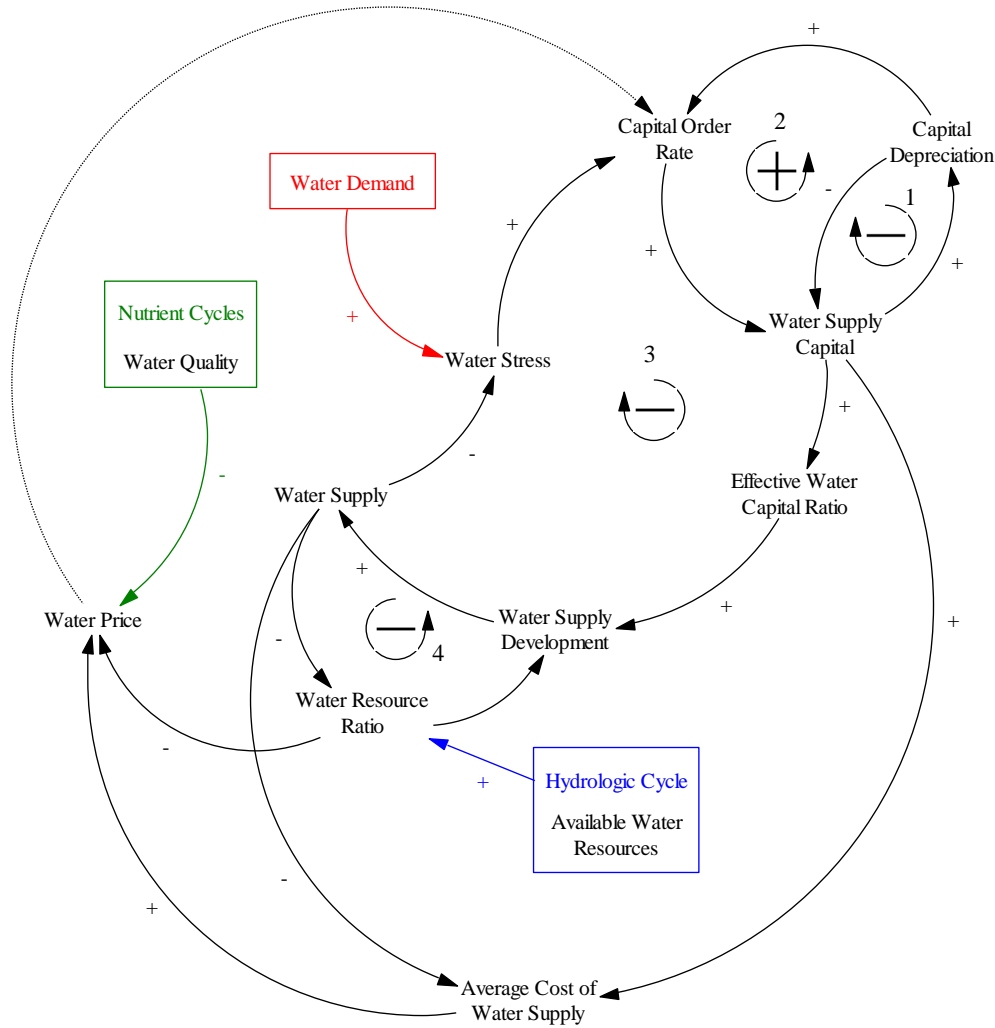


Figure 3.32. Causal loop diagram of the ANEMI3 water supply development sector. The dotted arrow from water price to water supply indicates a causality that is neither positive nor negative

The dotted causal link from water price to the capital order rate in Figure 3.32 indicates a connection that is neither positive nor negative. Instead, this link is used to determine the amount of investment that is made in the capital stocks of the different supply types (surface, ground, wastewater reclamation, and desalination water sources). Inputs from the nutrient cycle, hydrologic cycle, and water demand sectors are used to define the water price, water stress, and water resource ratio variables respectively in the water supply development sector.

The stock and flow diagram for the water supply development sector is shown in Figure 3.33.

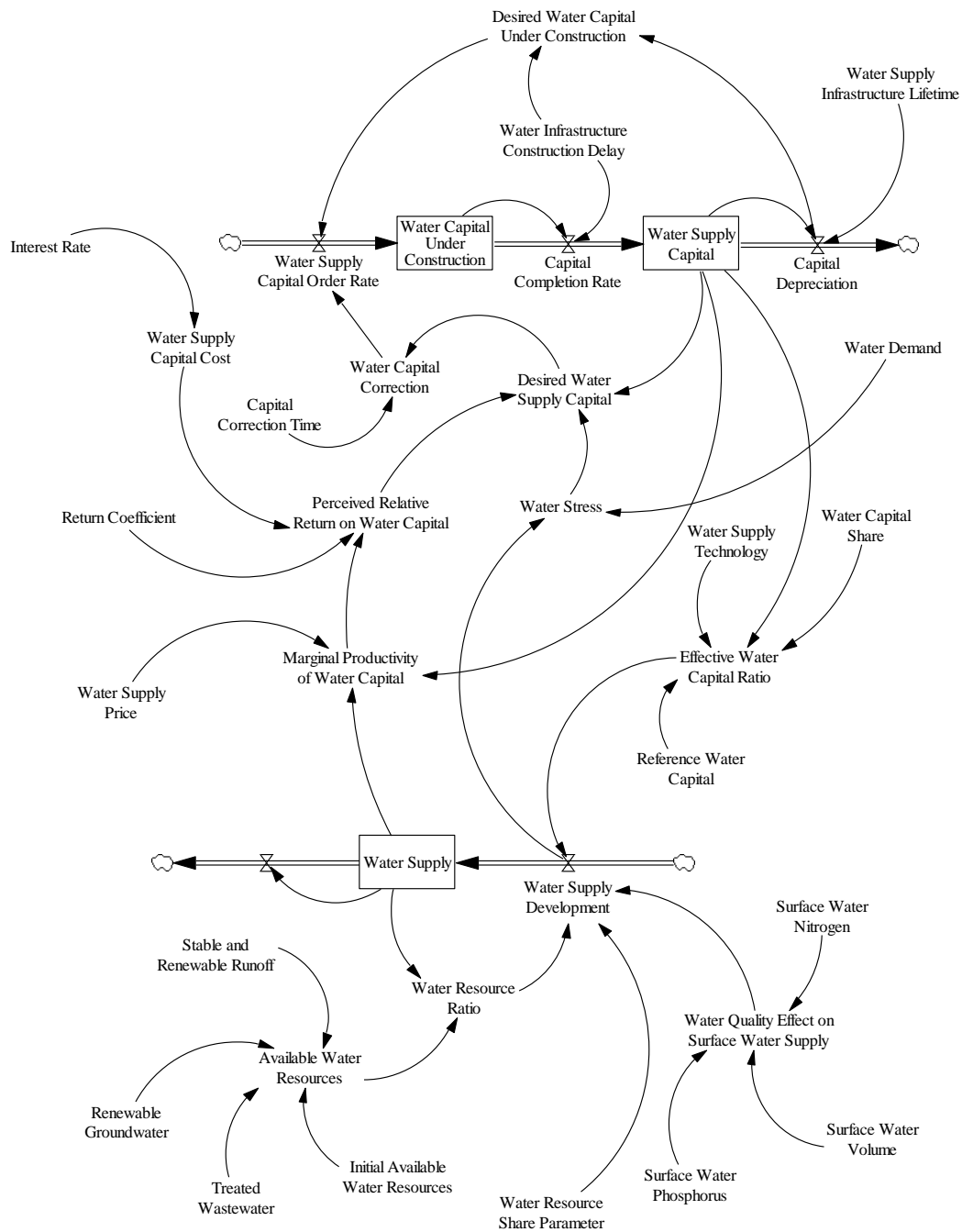


Figure 3.33. Stock and flow diagram of the ANEMI3 water supply development sector. The main stocks in the water supply development sector consist of those for the water supply, water supply price, and water supply capital, both established and under construction. The purpose of having two stocks to represent water supply under construction and currently established is to add a time

delay to the water development of water supplies. The time delay represents a lag in water capital in response to the stimulus of investment, which in this case is the water supply capital order rate. Water supply is represented as a stock, even though this value is a rate or flow that represents the volume of water being supplied by a given source in a year. This was done to mitigate the occurrence of circular references in the model, as the development of water supplies is dependent on the water resource ratio and vice versa. Water supply does not accumulate, only the capital that represents the level of infrastructure associated with water supply. Because of this, an additional unnamed outflow is added which releases the current value of water supply from the water supply stock, preventing any accumulation.

Water pricing within the water supply development sector is shown in Figure 3.34.

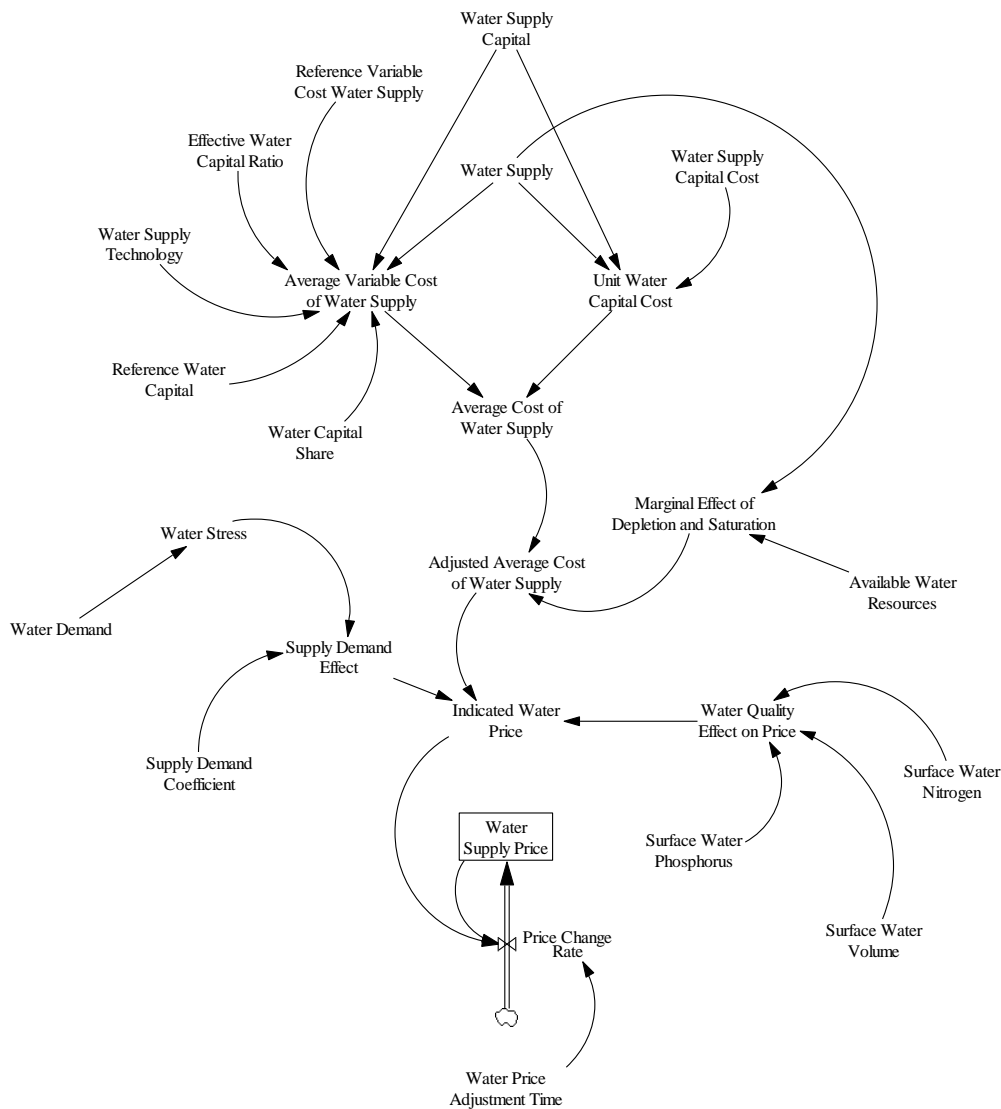


Figure 3.34. Water pricing component of the ANEMI3 water supply development sector.

Water resources,  $R_i$  are used in the production of water supplies, where the subscript  $i$ , denotes the type of water supplies for which the water resources are being used.

$$R_{sw} = S_r * TRF - URW * WPF \quad [km^3/y] \quad (3.71)$$

$$R_{gw} = Q_{perc} - Q_{discharge} \quad [km^3/y] \quad (3.72)$$

$$R_{ww} = TDW + TIW \quad [km^3/y] \quad (3.73)$$

$$R_{ds} = Oceans \quad [km^3] \quad (3.74)$$

$R_{sw}$  = Surface water resources [ $km^3/y$ ]

$R_{gw}$  = Groundwater resources [ $km^3/y$ ]

$R_{ww}$  = Wastewater resources [ $km^3/y$ ]

$R_{ds}$  = Desalination water resources

$S_r$  = Stable and reusable runoff fraction

$TRF$  = Total renewable flow [ $km^3/y$ ]

$WPF$  = Wastewater pollution factor

$Q_{perc}$  = Percolation to groundwater [ $km^3/y$ ]

$Q_{discharge}$  = Groundwater discharge [ $km^3/y$ ]

$TDW$  = Treated domestic wastewater [ $km^3/y$ ]

$TIW$  = Treated industrial wastewater [ $km^3/y$ ]

$URF$  = Untreated Returnable Waters [ $km^3/y$ ]

The amount of water resources available for the development of water supplies is dependent on the hydrologic cycle, water demand, and water quality sectors of the model. In the case of surface water, the stable and reusable portion of runoff is taken from the total renewable streamflow and is adjusted for untreated wastewater discharge. The adjustment for wastewater discharge is based on IHP (2000) which estimates that for every cubic meter of contaminated wastewater discharged into water bodies and streams, makes unsuitable 8-10 cubic meters of fresh water. The difference in groundwater percolation and discharge is used for the consideration of groundwater resources as this refers to renewable groundwater. Only renewable groundwater resources are considered for the global scale. The inclusion of non-renewable or fossil groundwater resources should be considered at the regional scales. For the potential reuse of wastewater, industrial and domestic wastewaters are considered. Although the reuse of wastewater is highly dependent on the type of wastewater and the use for which it is being treated, it is considered here as a supplementary type of water supply in the case of

groundwater and surface water depletion. Water resources used for desalination are considered primarily from the ocean stock in the hydrologic cycle. This results in a virtually limitless supply; however, it is very energy intensive resulting in a high effective input intensity thereby limiting production.

The concept of resource depletion in energy production is also applicable to water supply development. For example, in the case of surface water and groundwater resources, depleted water resources will mean less suitable locations for water extraction and treatment plants. This might mean that source waters could be further from where the water is being used, thus increasing distribution costs. Pumping costs could also be increased by using deeper aquifers or surface water supplies that have a greater difference in elevation from their point of use. Water resource depletion factors into the water supply development process in much the same way as energy production, however there is one key difference. The depletion effect for energy production in Equation 3.49 is based on the ratio of current energy resources remaining to the initial amount. In contrast, water resources are renewable to varying degrees. Therefore, simply taking the ratio of the available water resources to the initial water resources is insufficient. Here, the ratio of available water resources to the current production level is used. In order to accomplish this structure, water production was changed to a stock variable (Figure 3.33) to avoid creating an indeterminate system (introduction of a new negative feedback by making water production a function of itself).

$$WS_i = \int WS_{i,0} \left( \alpha_{w_i} \left( \frac{WS_i}{AW_i} \right)^{\rho_{w_i}} + (1 - \alpha_{w_i}) EWII_i^{\rho_{w_i}} \right)^{\frac{1}{\rho_{w_i}}} \cdot dt \quad [km^3/y] \quad (3.75)$$

$WS_i$  = Water supply from water resource  $i$  [ $km^3/y$ ]

$WP_{i,0}$  = Initial water production [ $km^3/y$ ]

$AW_i$  = Available water resource remaining [ $km^3/y$ ]

$EWII_i$  = Effective water input intensity

$\alpha_{w_i}$  = Water resource share

$\rho_{w_i}$  = Resource substitution coefficient

In the case of surface water, the available water resources are a rate (runoff minus water quality depletion effects) rather than a stock that can be depleted over time. If production equals this rate,

then there is no more surface water that can be utilized at this time step. For wastewater reuse if the rate of reuse is equal to that of the amount of treated wastewater, then no more wastewater can be reused unless wastewater treatment percentage increases.

In the energy capital sub-system of the energy-economy sector, Equation 3.55 is used to define the desired energy capital, which determines the amount of investment to be made in each type of energy source. In this equation, the desired energy capital for each source is determined by the perceived return on investment, and the production pressure defined as the ratio of the energy order rate or demand to energy production for each source.

In the case of water supply, the term for perceived return on investment is removed, thereby making the primary drive for new water supply capital based on production pressure, which resembles the definition of water stress (withdrawal or demand to availability ratio). This value is multiplied by the current water capital stocks to obtain the desired water capital stocks,

$$DKW_i = KW_i \cdot \frac{W_{di}}{WS_i} \quad [\$] \quad (3.76)$$

$DKW_i =$  Desired water capital for water source  $i$  [ $km^3$   
/y]

$W_{di} =$  Demand for water supply  $i$  [ $km^3$ /y]

$WS_i =$  Water supply from water source  $i$  [ $km^3$ /y]

Where  $i$  denotes the type of water supply for which desired water capital is being determined. In order to obtain the demand for water supply from each source, Wood's algorithm (Wood and Wollenberg 1996) is used to allocate the total water demand (sum of domestic, industrial, and agricultural water demand) to each supplier. The geometric representation of Wood's algorithm is illustrated in Figure 3.35., where each rectangle represents a different supplier (surface, ground, wastewater reclamation, and desalination water supplies). The area of each rectangle represents the capacity for a given supplier to fulfil the demand for a product, while the position and width of each rectangle is based on the "attractiveness" value and "width" parameters respectively. Here, the inverse water supply price is used to represent the attractiveness value, and the area of each rectangle would be the water supply capacity for a given supply type. The total water demand is allocated to each supplier by the black line

in Figure 3.35. which moves from right to left until the area to the right of the line fulfils the demand. The area of each rectangle that lies on the right of the black line represents the level of demand satisfied by each supplier, therefore a water supply type with a high price would be place farther to the left on the attractiveness scale, and would receive less of the total water demand.

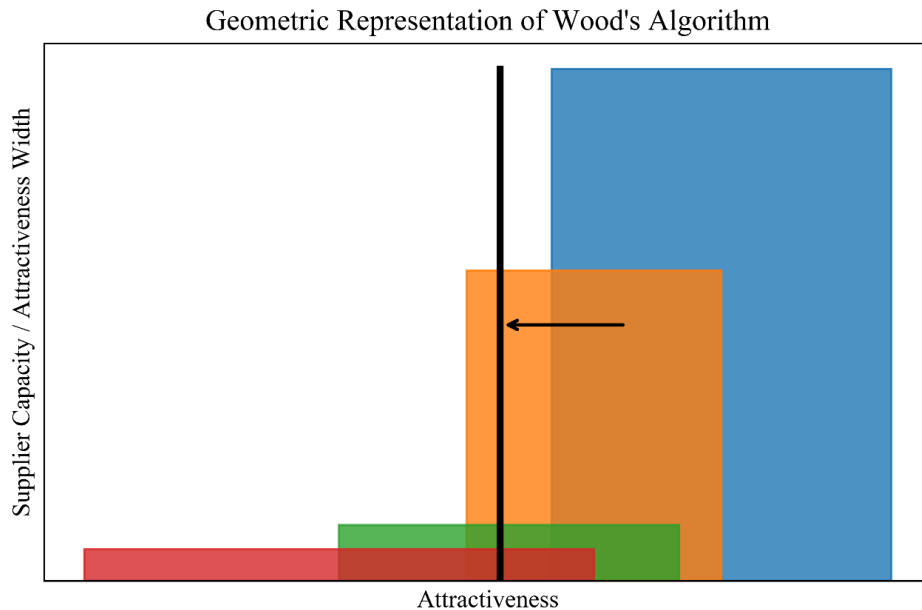


Figure 3.35. Illustration of Wood's algorithm.

The inverse water supply price was chosen as the main driver for changes in supplier attractiveness as this will vary with technological improvements, depletion, saturation, and water quality in the case of surface water supply. This formulation encapsulate the effects of global changes in technology, water resource availability, and water quality on the allocation of capital investments in different types of water supply. The width factor determines how this allocation is distributed to suppliers which are not necessarily the cheapest option. For example, on the global scale, although the use of surface water supplies is likely the most cost-effective option in many regions, groundwater, water reuse, and desalination supplies are all being used simultaneously. For example in areas where surface and groundwater supplies are scarce, desalination is a much more feasible option (Gao et al. 2017). Estimation of the width parameter is discussed in Section 3.3.

The concept of endogenous technological change applied to energy production has analogies to water supply development. In the case of surface water and groundwater supplies, it is assumed that pumping, distribution and treatment technologies will remain largely the same but will show some

improvement over time. However, alternative water supplies such as wastewater reuse and desalination are likely to see vast improvements in the near future as mentioned in the Chapter 2 of the thesis. Factoring in technological change into the water supply development process is what will help make alternative water supplies more feasible in the future, along with depletion and saturation of conventional water supplies. The dynamics and structure for the implementation of technological change in water supply development is the same as that of energy technology in Section 3.2.9.6, however different parameters are used for desalination and water reclamation technologies and are discussed in Section 3.3.

A unique attribute of water resources when considering water supply development is water quality. Degraded water quality can impact the functioning of water treatment facilities as well as maintenance costs and the necessary configuration of unit processes (Schwartz et al. 2000; Eikebrokk et al. 2004; Harasawa et al. 2014). This may also influence the ability to secure adequate source waters for extraction of water resources in the future as a result of pollution and climate change (Ritson et al. 2014). This could negatively impact production of conventional water supplies by increasing the cost of implementing new capital as well as variable inputs needed for treatment and distribution including energy, chemicals, and labor.

In ANEMI3, nutrient concentrations in surface waters are used as an indicator of water quality on a global scale. Wastewater and agricultural inputs are used as the main contributors to water quality degradation, and changes in the levels of nutrients in the form of total nitrogen and phosphorus are used as indicators of water quality from the nutrient cycle sector of the model. The ratio of current to initial nutrient concentrations for surface water resources is used as a multiplier on the water supply price,

$$P_{w_{sw}} = PP_{w_{sw}} \cdot \left( \frac{NCE}{NCE_0} \right)^{\gamma_w} \quad [$/km^3] \quad (3.77)$$

$P_{w_{sw}}$  = Water supply price for surface water [\$/km<sup>3</sup>]

$PP_{w_{sw}}$  = Producer price for surface water [\$/km<sup>3</sup>]

$NCE$  = Nutrient concentration effect [(nN · nP)/(km<sup>3</sup>/y)<sup>2</sup>]

$NCE_0$  = Initial nutrient concentration effect [(nN · nP)/(km<sup>3</sup>/y)<sup>2</sup>]

$\gamma_w = \text{Influence of water quality on surface water supply price}$

Where the nutrient concentration effect takes into consideration the concentration of both total nitrogen and phosphorus,

$$NCE = \frac{N_{N_{River}} \cdot N_{P_{River}}}{SF^2} \quad [(nN \cdot nP)/(km^3/y)^2] \quad (3.78)$$

$N_{N_{River}} = \text{Nitrogen content of river stock } [nN]$

$N_{P_{River}} = \text{Phosphorus content of river stock } [nP]$

$SF = \text{Streamflow } [km^3/y]$

In order to include water supply development as an additional component within the energy-economy sector, key connections needed to be made with the energy-economy sector of the model. Those connections are detailed below and relate to variables mentioned in Section 3.2.8. Establishing these connections effectively closes several feedback loops for water supply development to fit into this sector. Water supply development is treated as an additional horizontal disaggregation of the global capital stock alongside the energy sector (Figure 3.36).

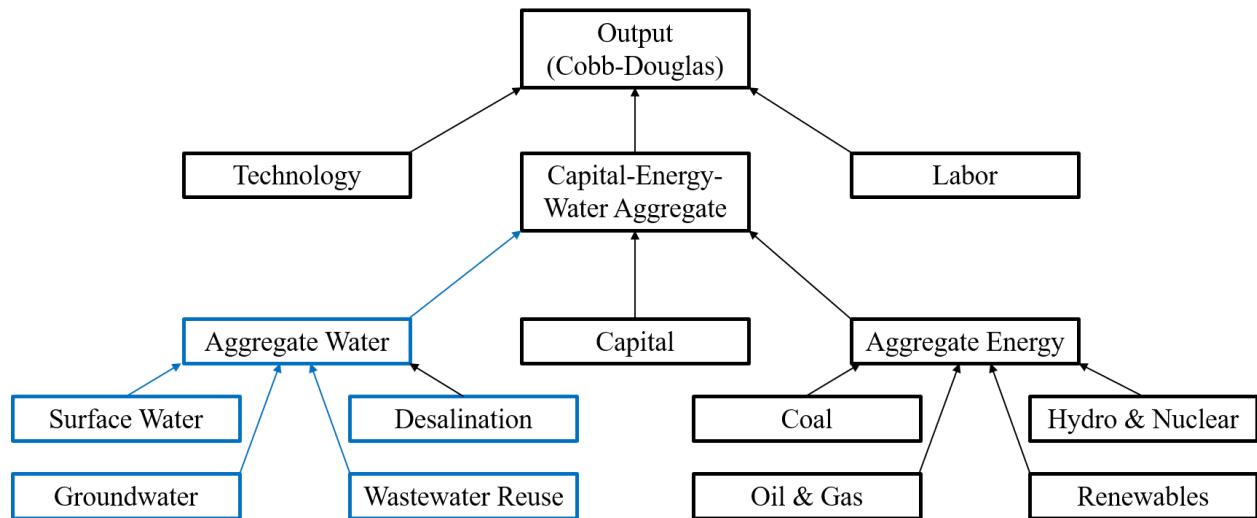


Figure 3.36. Production structure of water supply within the energy-economy-water sector of the ANEMI3.

To accomplish this production structure, water production, capital, technological change, and pricing structures were replicated from that of the energy economy sector. Capital stocks were created to represent water supply infrastructures for surface water, groundwater, wastewater reuse, and desalination. The level of capital for each source refers to any infrastructure that relates to the global capacity of the system to provide water supplies. This includes reservoirs, pumping systems, treatment systems, and distribution networks. Economic output in the energy-economy sector is distributed amongst energy and water production, investment, and consumption. The inclusion of water supply development adds an additional consumer of economic output Figure 3.37.

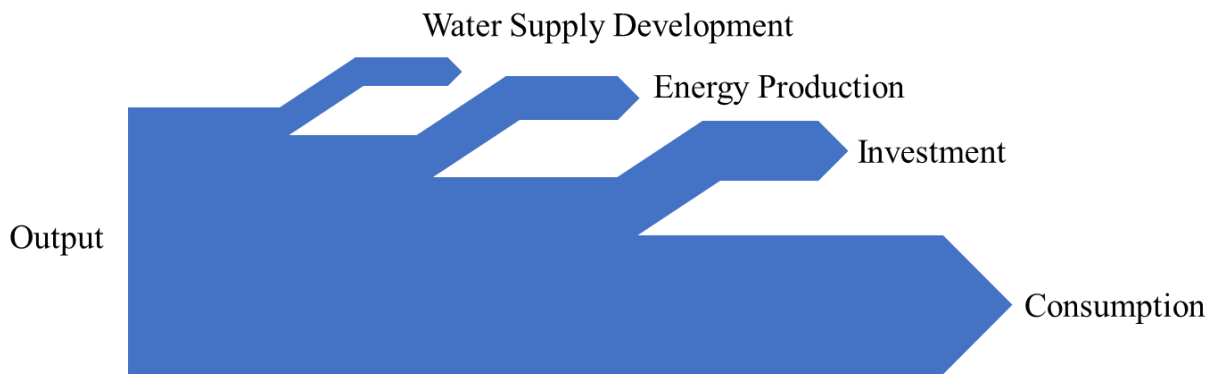


Figure 3.37. Goods allocation in the energy-water-economy sector of the ANEMI3.

The operating capital,  $KO$  signifies the portion of the global capital stock,  $K$  that is used for generating economic output or the production of goods and services in the economic sector. It is represented by the following equation:

$$KO = KO_0 * U * \left( \frac{Aggr_{norm}}{Aggr_{ref}} \right) \quad [\$] \quad (3.79)$$

$U = Utilization$

$Aggr_{norm} = Output\ of\ capital-energy-water\ aggregate\ good\ at\ normal\ capacity\ utilization\ [\$]$

$Aggr_{ref} = Reference\ output\ of\ capital-energy-water\ aggregate\ good\ [\$]$

Utilization refers to the degree to which installed production capacity is being used, or the level of current production versus potential maximum production with full utilization of capital. This was initially only a function of energy production and needed water supply development to be included.

$$U = \frac{1}{2} * (EOC^{\frac{1}{\varepsilon_e}} + WOC^{\frac{1}{\varepsilon_w}}) \quad (3.80)$$

*EOC = Energy operating coefficient*

*WOC = Water operating coefficient*

*$\varepsilon_e$  = Energy elasticity coefficient*

*$\varepsilon_w$  = Water elasticity coefficient*

An average is taken between the utilization of energy and water production capacities. The output of the capital-energy-water aggregate good at normal capacity utilization,  $Aggr_{norm}$  also needed to be modified to include the contribution water supply development to changes in output. This modification is included as the final term in the following equation,

$$Aggr_{norm} = Aggr_{ref} * \left( \alpha_k \left( \frac{K}{K_0} \right)^\gamma + \alpha_e \left( \frac{E_{demand}}{E_{production}} \right)^\gamma + \alpha_w \left( \frac{W_{demand}}{W_{supply}} \right)^\gamma \right)^{\frac{1}{\gamma}} \quad [\$] \quad (3.81)$$

*$Aggr_{norm}$  = Normal capital-energy-water aggregate [\$]*

*$Aggr_{ref}$  = Reference capital-energy-water aggregate [\$]*

*$\alpha_k$  = Capital share parameter*

*$\alpha_e$  = Energy share parameter*

*$\alpha_w$  = Water share parameter*

*$\gamma$  = Capital-energy-water substitution coefficient*

### 3.2.11 Nutrient Cycles

The biogeochemical cycle describes the movement of chemical compounds which drive the biological and geological processes that shape the face of the Earth. These compounds move from various reservoirs including vegetation, soils, rivers and lakes, coastal waters and oceans, and the atmosphere. The processes that drive the movement of these compounds are extremely diverse and occur across widely varied scales of time and space. For example, uplift of the Earth's crust occurs over millions of years, while the delivery of Nitrogen compounds from atmosphere to land through lightning strikes

can occur in seconds. Some of the most important cycles to consider on a global scale are those associated with Nitrogen (N), and Phosphorous (P). These are some of the main elements that make up living matter, and are inextricably linked through the biological processes of respiration and decay (Mackenzie 1999). It is not a coincidence that their cycles are also closely tied to human activities and play a vital role for life on Earth in general.

The cycle of N is important to global change research as it has been identified to be an important rate-limiting element with respect to the biological uptake of CO<sub>2</sub> for land and ocean vegetation, helping to 'balance the budget' of carbon through what is known as the 'fertilization effect' (den Elzen et al. 1997). Most of the processes included in the nitrogen cycle mirror those of the carbon cycle (although the chemical reactions are different). However there are a few key differences: the land and ocean plants and organisms also fixate nitrogen from the air in addition to biological uptake; and rain and lightning are important processes for delivering nitrogen from the atmosphere to the Earth's surface and oceans. Additionally, it should be noted that the vast majority of nitrogen is stored in the air and atmosphere in contrast to the carbon where most of it is stored in the ocean.

Phosphorous compounds act as essential nutrients that support plant life around the globe. The Phosphorous cycle also follows that of the carbon cycle in that the sources and transport processes are similar. The main difference arises in the fact that the primary mechanism associated with the transport of Phosphorous compounds occurs through the attachment to sediments which are transported as runoff or in aerosol form. This is partly why the cycle of Phosphorous does not typically include an atmospheric component. Phosphorous rarely exists in a gaseous state unlike nitrogen and carbon, but can temporarily form as an aerosol which is deposited relatively quickly. Phosphorous also acts as a rate limiting factor for the biological uptake of carbon and nitrogen especially for photosynthesizing marine organisms (den Elzen et al. 1997).

Humans are now having a profound influence on the major nutrient cycles of N, and P with increasing development and industrialization. In many cases N, and P are extracted, consumed, and discharged as waste. This has caused an increase in the amount of these compounds in certain reservoirs, thereby accelerating the flow to others. In addition, many of the processes mentioned previously have been bypassed, thus affecting the timing of the cycles themselves. Examples include increasing fertilizer application and soil erosion rates via intensified agriculture, discharging wastewater to streams, and

mining P ore for use on land. These human activities have the potential to destabilize the nutrient cycles in ways that have not been seen previously. As a result we are now able to detect impacts such as climate change, loss of aquatic biodiversity as a result of poor water quality and limited water quantity (Schuster-Wallace et al. 2008), and acid deposition due to the oxidation of sulfur and nitrogen gases in the atmosphere increasing the pH of rainwater (Mackenzie 1999). The extent of these impacts is largely unknown today and less so in the future. However, their potential to impact various aspects of the Earth system, such as population, economy, water quality, land cover, food production, and climate are likely.

The structure of the N and P nutrient cycle model of Mackenzie et al. (1993) that captures the natural processes that move these elements through their respective cycles at various timescales, is used as the basis for the development of nutrient cycles in the ANEMI3 (Breach and Simonovic 2018). This part of the model is based on the assumption of an initial quasi-steady state condition from which the model is to be perturbed to account for human influence on the element cycles. The stock and flow diagrams for the nutrient cycles of N and P are shown in Figures 3.38. and 3.39 respectively.

Each flow in the model is represented as a negative feedback with a first-order material delay and an implicit goal of zero. The mathematical representation of the nutrient cycles is given as,

$$N_i = \int (k_{ijN} \cdot N_i + F_{ijN}) \cdot dt \quad [nN] \quad (3.82)$$

$$P_i = \int (k_{ijP} \cdot P_i + F_{ijP}) \cdot dt \quad [nP] \quad (3.83)$$

*i* = Index for originating nutrient reservoir

*j* = Index for receiving nutrient reservoir

$k_{ijN}$  = Rate constant matrix for N flows from nutrient reservoir *i* to *j* [1/y]

$k_{ijP}$  = Rate constant matrix for P flows from nutrient reservoir *i* to *j* [1/y]

$N_i$  = Nitrogen reservoir *i* [nN]

$P_i$  = Phosphorus reservoir *i* [nP]

$F_{ijN}$  = Constant nitrogen flow from reservoir *i* to *j* [nN/y]

$F_{ijP}$  = Constant phosphorus flow from reservoir *i* to *j* [nP/y]

As each stock is drained it will be transferred to another in a continuous chain of higher order delays. Because the system is closed and represents a continuous cycle, it will attempt to reach a steady state, which can also change as a result of a change in model structure. This change in the model structure

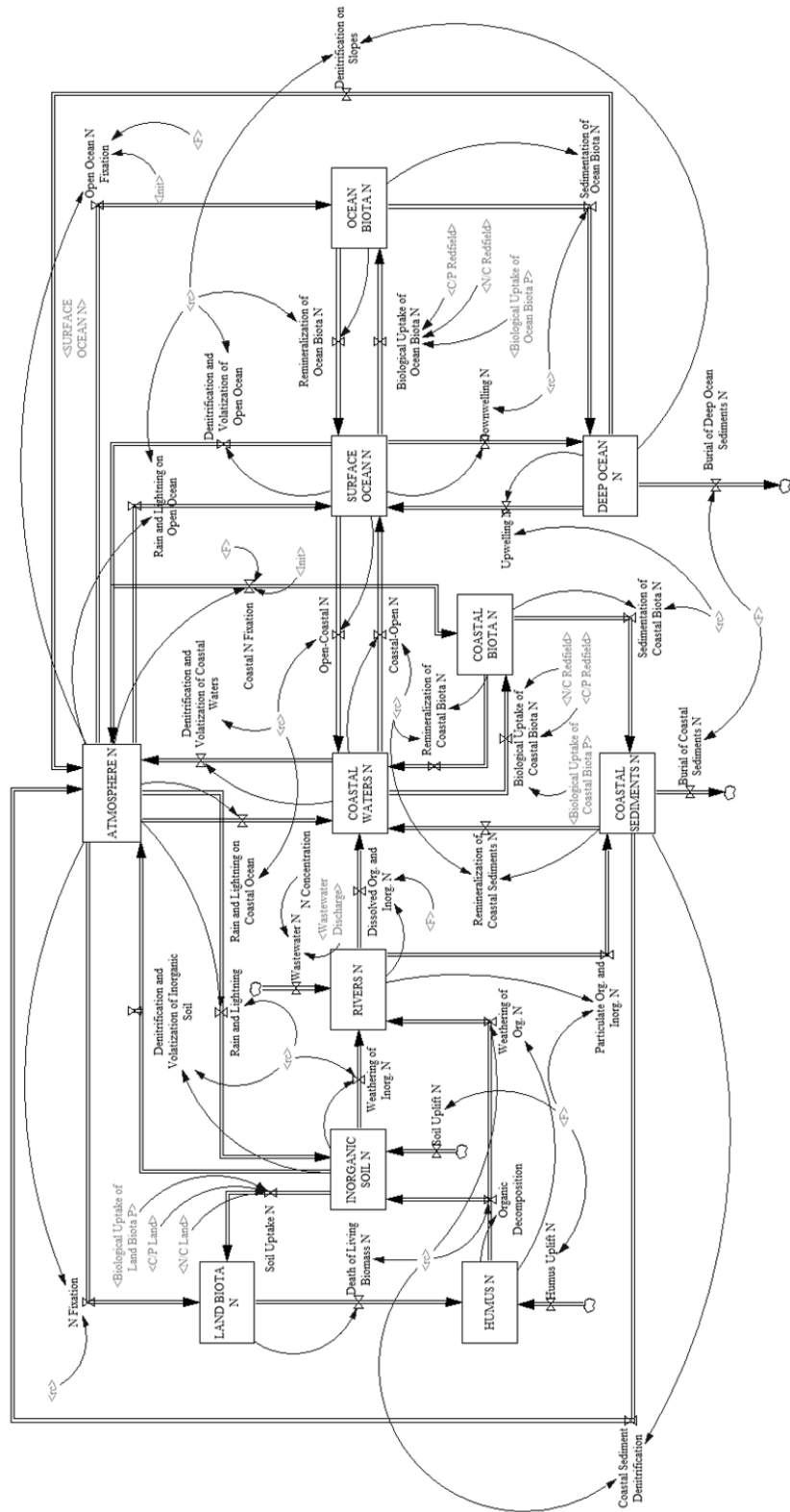


Figure 3.38. Stock and flow diagram of the ANEMI3 nitrogen cycle.



is represented by the influence of human development in the form of wastewater discharge to the N and P river stocks. Due to the presence of higher order delays, the system is also likely to be susceptible to large fluctuations and oscillations when perturbed. Initial values for the stocks to create the initial steady state condition in the model and rate constants (or decay fractions) describing the flow of a particular element from one stock to another. The inverse of the rate constant is the time constant, which represents the time associated with the first-order delay for one mole of a particular element to travel from a particular stock. The initial values for the nutrient reservoirs as well as rate constants and constant flows are given in Appendix A.

The input of N and P in the nutrient cycles from wastewater is calculated for domestic and industrial wastewaters as well as agricultural returnable waters. For domestic and industrial wastewaters, the nutrient input is calculated based on the amount of untreated wastewater adjusting for wastewater reuse, as well as treated wastewater with exogenous removal efficiencies applied,

$$NE_{N_{dom}} = \left( DW_{untreated} - W_{ww_{dom}} + DW_{treated} \cdot (1 - N_{removal_{eff}}) \right) \cdot N_{conc_{dom}} [nN/y] \quad (3.84)$$

$$NE_{P_{dom}} = \left( DW_{untreated} - W_{ww_{dom}} + DW_{treated} \cdot (1 - P_{removal_{eff}}) \right) \cdot P_{conc_{dom}} [nP/y] \quad (3.85)$$

$$NE_{N_{ind}} = \left( IW_{untreated} - W_{ww_{ind}} + IW_{treated} \cdot (1 - N_{removal_{eff}}) \right) \cdot N_{conc_{ind}} [nN/y] \quad (3.86)$$

$$NE_{P_{ind}} = \left( IW_{untreated} - W_{ww_{ind}} + IW_{treated} \cdot (1 - P_{removal_{eff}}) \right) \cdot P_{conc_{ind}} [nP/y] \quad (3.87)$$

*NE* = Nutrient emission

*DW* = Domestic wastewater [ $km^3/y$ ]

*IW* = Industrial wastewater [ $km^3/y$ ]

*W<sub>ww</sub>* = Wastewater reuse from water production sector [ $km^3/y$ ]

*N<sub>removal<sub>eff</sub></sub>* = Exogenous N removal efficiency

*P<sub>removal<sub>eff</sub></sub>* = Exogenous P removal efficiency

*N<sub>conc</sub>* = Concentration of N in wastewater [ $nN/km^3$ ]

*P<sub>conc</sub>* = Concentration of P in wastewater [ $nP/km^3$ ]

Agricultural nutrient inputs to surface water are based on the net amount of arable land that is used for food production. This is paired with nutrient leaching factors that are used to determine the amount of nutrients that reach surface waters,

$$NE_{N_{agr}} = A_l \cdot N_{leaching} \quad [nN/year] \quad (3.88)$$

$$NE_{P_{agr}} = A_l \cdot P_{leaching} \quad [nP/year] \quad (3.89)$$

$A_l$  = Net arable land [ha]

$N_{leaching}$  = Leaching factor for N from net arable land [nN/y]

$P_{leaching}$  = Leaching factor for P from net arable land [nP/y]

The input of nutrients to surface waters in the nutrient cycle is based only on the excess amount from the initial nutrient inputs. This is because the nutrient cycle sub-system is assumed to start at a quasi-steady state solution. The parameter values used in calculation nutrient inputs to the nutrient cycles are given below in Table 3.8.

Table 3.7. Parameters used nutrient inputs to nutrient cycles.

Parameter	Value	Units	Source
Nitrogen concentration of domestic wastewater	60	g/L	Henze and Comeau (2008)
Nitrogen concentration of industrial wastewater	60	g/L	
Phosphorus concentration of domestic wastewater	15	g/L	
Phosphorus concentration of industrial wastewater	15	g/L	
Nitrogen leaching coefficient of agricultural runoff	18.65	kg/ha/year	FAO (2019a)
Phosphorus leaching coefficient of agricultural runoff	0.415	kg/ha/year	

The nutrient cycles sector is an entirely new addition to the ANEMI model. In the previous version, water quality was represented only by the subtracting wastewater and agricultural runoff from the available water resources with a dilution factor applied. In ANEMI3, the nutrient concentration of

surface waters provides an indicator of water quality that is used to influence the development of surface water supplies as discussed in Section 3.2.10.

### 3.2.12 Persistent Pollution

An additional sector to represent the level of persistent pollution in the Earth system was added in ANEMI3. This sector is used to describe the generation and assimilation of pollutants over time that may be harmful to the global biosphere (Thissen and De Mol 1978). It is based on the persistent pollution sector of the WORLD3 model and is used to form an additional negative feedback on population growth (Meadows et al. 1974). The main drivers for the generation of persistent pollution are industrial and agricultural activity, while the current population and economic output are used to scale these effects in global system. Technological change acts as a reduction factor for the levels of persistent pollution generation from these activities, while natural rate of assimilation represents the environmental capacity to cope with and break down these pollutants over time. The causal structure of the persistent pollution sector is shown in Figure 3.40.

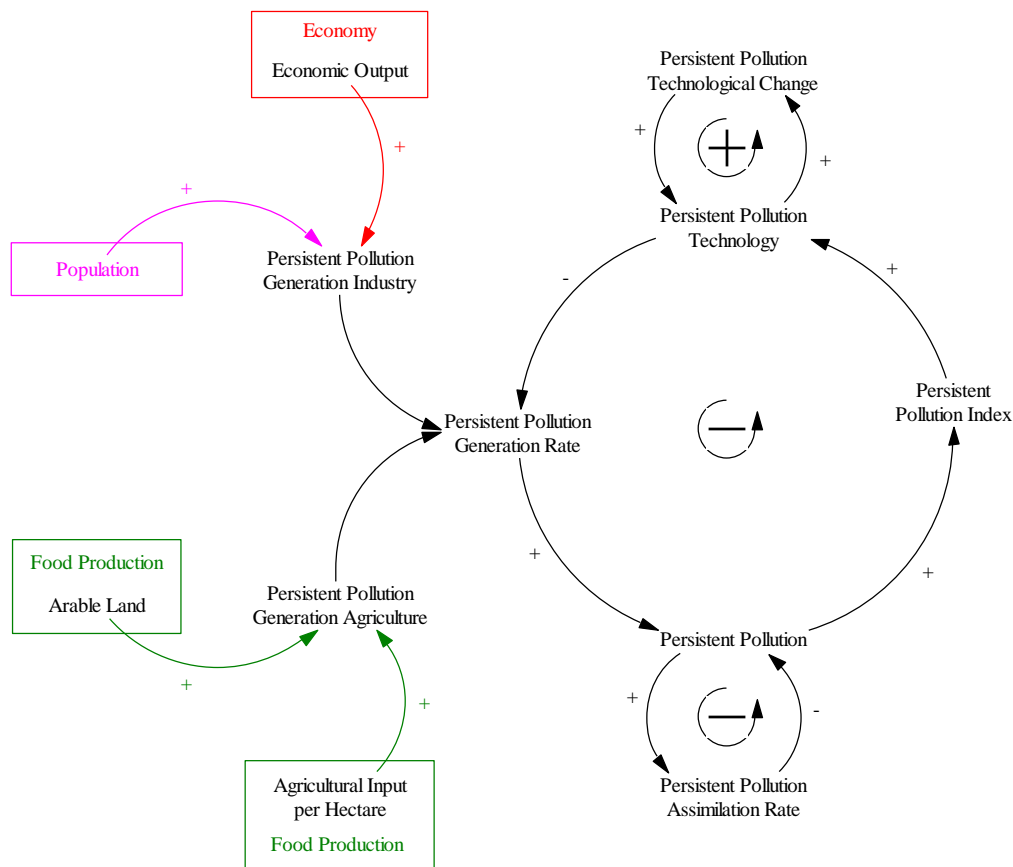


Figure 3.40. Causal structure of the ANEMI3 persistent pollution sector.

There are three feedback loops that drive the dynamics of persistent pollution. The loop connecting persistent pollution with persistent pollution technology acts as a negative feedback on persistent pollution. As the levels of persistent pollution increase, so too does the persistent pollution index, creating a greater need for technological change for dealing with pollution. The changes in technology reduce the generation rate from industry and agriculture, which results in less persistent pollution. The positive loop driving technological change represents an accumulation of knowledge, whereby more technological progress leads to a faster accumulation of new developments in persistent pollution technology. The final loop represents a negative feedback on persistent pollution through the natural assimilation rate. Overtime, assimilation leads to a decrease in persistent pollution, acting as a form of exponential decay.

The stock and flow diagram for the persistent pollution sector is presented in Figure 3.41.

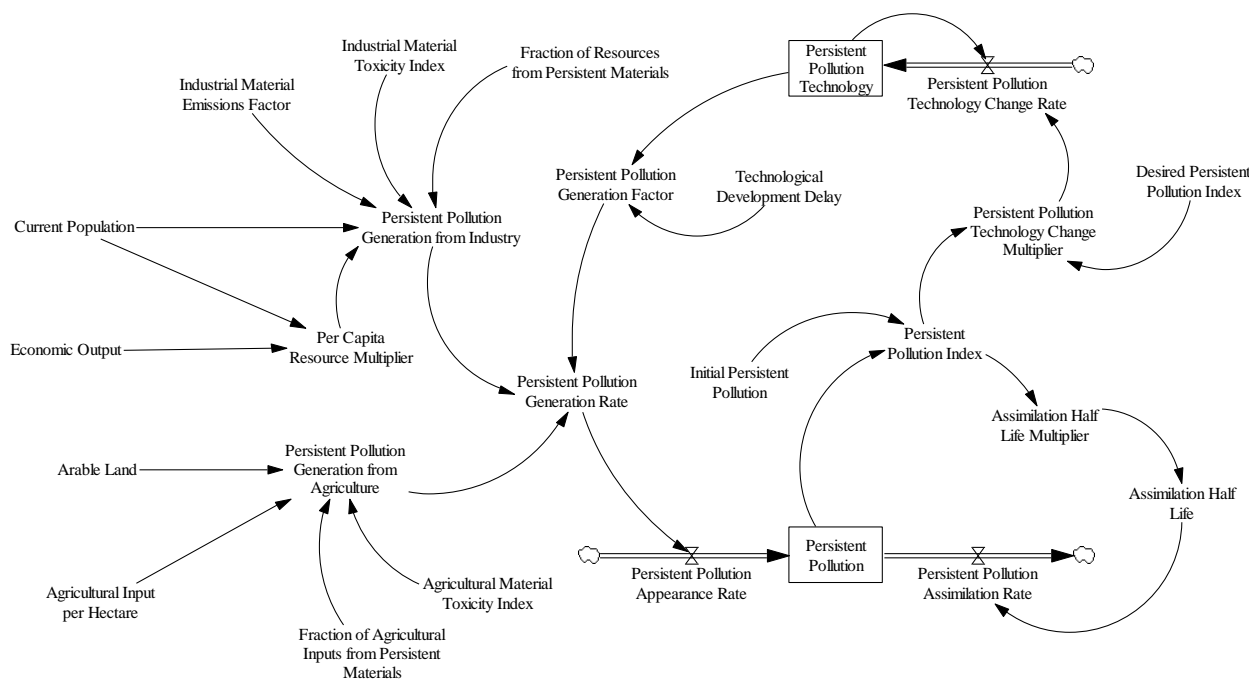


Figure 3.41. Stock and flow diagram of the ANEMI3 persistent pollution sector.

The state of the persistent pollution sub-system is represented by the two stock variables of persistent pollution and persistent pollution technology. The flows that alter the state of the system are based on the rates at which pollution is generated by the industrial and agricultural sectors as well as the natural assimilation rate in the case of persistent pollution. For persistent pollution technology, the

rate of change is driven by the previous level of technology as well as the current level of persistent pollution.

The persistent pollution stock can be represented mathematically by the following equation,

$$PP = \int (PP_{Appearance} - PP_{assimilation}) \cdot dt \quad [Pollution\ units] \quad (3.90)$$

$PP = Persistent\ pollution\ [Pollution\ units]$

$PP_{appearance} = Persistent\ pollution\ appearance\ rate\ [Pollution\ units]$

$PP_{assimilation} = Persistent\ pollution\ assimilation\ rate\ [Pollution\ units]$

The assimilation rate is calculated based on the current level of persistent pollution along with the assimilation half-life,

$$PP_{assimilation} = \frac{PP}{\tau_{assimilation}} \quad [Pollution\ units/y] \quad (3.91)$$

$\tau_{assimilation} = Assimilation\ half-life\ [y]$

The assimilation half life changes with the persistent pollution index,

$$\tau_{assimilation} = f(PP_{index}) \quad [y] \quad (3.92)$$

$PP_{index} = Persistent\ pollution\ index$

The  $PP_{index}$  is simply calculated as the current  $PP$  divided by its initial value. The rate at which persistent pollution is accumulated is defined below,

$$PP_{appearance} = \frac{PP_{gr}}{\tau_{transmission}} \quad (3.93)$$

$PP_{gr} = Persistent\ pollution\ generation\ rate\ [Pollution\ units/y]$

$\tau_{transmission} = Persistent\ pollution\ transmission\ delay\ [y]$

The generation rate depends on persistent pollution generated from agriculture, industry, and includes a generation factor that encapsulates the effect of technological change,

$$PP_{gr} = PP_{gr_{factor}} \left( PP_{gr_{ind}} + PP_{gr_{agr}} \right) \quad [Pollution\ units/y] \quad (3.94)$$

$PP_{gr_{factor}}$  = Persistent pollution generation factor

$PP_{gr_{ind}}$  = Persistent pollution industrial generation [Pollution units/y]

$PP_{gr_{agr}}$  = Persistent pollution agricultural generation [Pollution units/y]

Industrial generation is driven by population,

$$PP_{gr_{ind}} = M_{resource} \cdot P_{total} \cdot F_{pm} \cdot M_{e_{ind}} \cdot M_{t_{ind}} \quad [Pollution\ units/y] \quad (3.95)$$

$M_{resource}$  = Per capita resource use multiplier [Resource unit/(person · y)]

$P_{total}$  = Total population [persons]

$F_{pm}$  = Fraction of resources from persistent materials

$M_{e_{ind}}$  = Industrial material emissions factor

$M_{t_{ind}}$  = Industrial material toxicity index [Pollution unit/Resource unit]

Agricultural pollution generation is calculated in a similar way, except it is based on the arable land and agricultural inputs,

$$PP_{gr_{agr}} = Ag_{input} \cdot L_{ar} \cdot F_{pm_{ind}} \cdot M_{t_{agr}} \quad [Pollution\ units/y] \quad (3.96)$$

$Ag_{input}$  = Agricultural input per hectare [\$(/ha · y)]

$L_{ar}$  = Arable land [ha]

$F_{pm_{ind}}$  = Fraction of agricultural inputs from persistent materials

$M_{t_{agr}}$  = Agricultural material toxicity index [Pollution units/y]

The persistent pollution generation factor is equal to the level of persistent pollution technology with an information delay of  $\tau_{technology}$ , that is applied in the form of exponential smoothing. This is done to represent the time it takes for technological change to take effect,

$$PP_{gr\_factor} = SMOOTH(PP_{tech}, \tau_{technology}) \quad (3.97)$$

$PP_{tech}$  = Persistent pollution technology

$\tau_{technology}$  = Technology development delay [y]

The level of persistent pollution technology is an accumulation of the persistent pollution technology change rate,

$$PP_{tech} = \int PP_{tech\_rate} \cdot dt \quad (3.98)$$

$PP_{tech\_rate}$  = Persistent pollution technology change rate

The rate of change of persistent pollution technology is a function of the persistent pollution index,

$$PP_{tech\_rate} = f\left(1 - \frac{PP_{index}}{DPP_{index}}\right) \quad [1/y] \quad (3.99)$$

$PP_{index}$  = Persistent pollution index

$DPP_{index}$  = Desired persistent pollution index

The values of the parameters used in the persistent pollution sector are given in Table 3.9. below.

This sector is an entirely new addition to the ANEMI model. The inclusion of the persistent pollution sector in ANEMI3 provides an additional negative feedback on population growth based on the work of Meadows et al. (1974).

Table 3.8. Parameters values used in the persistent pollution sector.

Parameter	Symbol	Units	Value
Persistent pollution transmission delay	$\tau_{transmission}$	year	20
Technology development delay	$\tau_{technology}$	year	20
Industrial material emissions factor	$M_{eind}$	dimensionless	0.1
Industrial material toxicity index	$M_{tind}$	pollution units/resource units	10
Agricultural material toxicity index	$M_{tagr}$	pollution units/\$	1
Fraction of agricultural inputs from persistent materials	$F_{pmagr}$	dimensionless	0.001
Fraction of resources from persistent materials	$F_{pmind}$	dimensionless	0.02

## 4 Model Validation

This section presents the process of model parameter estimation and model validation simulation.

### 4.1 Parameter Estimation

Due to the large number of feedbacks in the ANEMI3 model any changes made in one sector affects all others. This is also true when incorporating and coupling new sectors into the model as additional feedbacks are formed. In order to ensure that realistic values and system behaviours are generated, some of the parameters needed to be re-estimated. Parameters within the water supply development sector and the energy production sector were re-estimated as they are newly added sectors in the model and have a large influence on the other sectors. The population sector also contained parameters relating to life expectancy and fertility that needed re-estimation so that more realistic population values could be obtained, as population growth is a key driver for every sector of the model. Water demand data are included in the optimization due to the use of inputs from the new economic and energy sectors for the determination of domestic and industrial water demands. The variables that were optimized are listed in Table 4.1. together with their optimal values.

Table 4.1. Model constants and their optimal values with corresponding sectors.

Model Sector	Decision Variable	Optimal Value	Units	
Water Supply	Specific Water Intake Factor	0.95	-	
	Water Resource Elasticity	Surface water	0.469	-
		Groundwater	0.413	-
		Wastewater	0.770	-
		Desalination	0.691	-
	Water Capital Share	Surface water	0.987	-
		Groundwater	0.01	-
		Wastewater	0.937	-
		Desalination	0.658	-
	Initial Water Producer Price	Surface water	15740	\$/km <sup>3</sup>
		Groundwater	68509	\$/km <sup>3</sup>
Wastewater		119114	\$/km <sup>3</sup>	
Desalination		132786	\$/km <sup>3</sup>	
	Short-Run Water Elasticity	0.239	-	
	Water Quality Share Parameter	0.097	-	
Energy Production	Energy Adjustment Coefficient	0.133	-	
	Energy Order Adjustment Coefficient	0.050	-	
	Energy Return Coefficient	1.07	-	
	Energy Substitution Elasticity	2.25	-	
	Energy Resource Elasticity	Coal	0.700	-
		Oil and Gas	0.700	-
		Hydro and Nuclear	0.650	-
		Renewables	0.520	-
	Initial Energy Production	Coal	7.58e10	GJ/year
		Oil and Gas	2.01e11	GJ/year
		Hydro and Nuclear	1.00e10	GJ/year
		Renewables	3.32e8	GJ/year
	Initial Energy Producer Price	Coal	1.28	\$/GJ
Oil and Gas		1.37	\$/GJ	
Hydro and Nuclear		10	\$/GJ	
Renewables		50	\$/GJ	
Population	Crowding Factor	0.86	-	
	GDP Factor	1.41	-	
	Lifetime Perception Delay	22.4	years	
	Social Adjustment Delay	18.7	years	
	Max Total Fertility	13.1	-	
	Reproductive Lifetime	33.2	years	

The procedure for selecting the re-estimated model values is based on the optimization procedure that minimizes errors in historical datasets for population, water supply, energy production, and water demands. Objective function is extremely non-linear due to the coupled non-linear nature of the

model. Modifying any of the decision variables listed in Table 4.1 will affect all other aspects of the model to some degree. The solution space is assumed to be one that has many valleys and peaks creating the potential find suboptimal solutions. Because of this, a global optimization algorithm needs to be used, rather than a gradient based method. The differential evolution algorithm (Storn and Price 1995) was selected for this reason, in addition to the fact that derivatives are not needed for the objective function. This algorithm is evolutionary and stochastic by nature, which can lead to results that are close to the global optimum but not necessarily exact. The minimum solution obtained by the differential evolution algorithm was used as a starting point for a deterministic local minimizer to finish the optimization. Details regarding this algorithm and the procedure for how it was applied can be found in Appendix B. A software package has been developed to link the algorithm to the Vensim system dynamics simulation software (available on the ANEMI GitHub platform under the name VenPy).

## 4.2 Model Validation

A series of tests from Sterman (2000) is used to evaluate the ANEMI3 plausibility of the baseline scenario with regards to the dynamics that take place. The absolute values are important, however the emphasis here is on the model behaviour so that we can analyze the feedback mechanisms that are driving the model to future states. Each test is performed for a selection of the ANEMI3 model variables in each model sector. They are listed in Table 4.2.

All the validation results are available in Breach (2020). For the purpose of this report we will focus only on (a) behavior reproduction; and (b) comparison to future projections.

### 4.2.1 Behaviour Reproduction

Many of the variables in ANEMI3 do not have historically observed counter parts on a global scale, but there are key variables in each sector that can be compared to historical data. One thing to note in this comparison is that on a global scale, there are many datasets that are incomplete (data is only recorded for certain regions), inconsistent (different recording methodologies used across regions, recording is done at irregular intervals), and at times, unreliable. However, there is still value in comparing the model to the real world in any way possible to see that it reproduces the behaviour of the sub-systems that are being represented. With this being said, the goal is not to reproduce the numbers from the data, but build confidence in the model's ability to generate realistic system

Table 4.2. Model testing procedures based on Sterman (2000).

<b>Test</b>	<b>Purpose of Test</b>	<b>Procedure</b>
<b>Behaviour Reproduction</b>	Compare modelled variables to historically observed data.	Plot modelled and historical observed variables in each model sector to ascertain whether modelled variable exhibits similar behaviour when compared to observed. Compute statistical measures of correspondence between model and data.
<b>Projected Comparison</b>	Compare ANEMI3 modelled variables to projected variables in other studies.	Plot ANEMI3 results for variables in each sector against projections from other studies. Identify if ANEMI3 results are within the range of other studies. If not, explain why.
<b>Integration Error</b>	Test the extent to which changes in the model time step affect the results.	Half the time step and run ANEMI3. Plot the result for model variables in each sector. Use different integration methods.
<b>Sensitivity Analysis</b>	Test for changes in behavioural modes when assumptions about parameters, model boundaries, and aggregations are varied over the plausible range of uncertainty.	Identify variables in each sector that are uncertain, may have a high degree of heterogeneity in the Earth system, or are assumed constant but could change over time. Apply Monte Carlo simulation to test the likelihood that these variables could alter model behaviour.
<b>Extreme Conditions</b>	Test whether the model responds plausibly when subjected to extreme policies, shocks, or parameter changes.	Test the response to extreme values in key inputs, alone and in combination.

behaviours in order to build confidence in future behaviours that arise, as well as policies that are implemented to alter them. The ANEMI3 variables that have been selected, along with the datasets used for comparison are in Table 4.3.

Table 4.3. Comparison datasets for baseline model run.

Model Sector	Variable	Datasets
Population	Total Population	UN World Population Prospects 2019
	Population (0-14)	UN World Population Prospects 2019
	Population (15-44)	UN World Population Prospects 2019
	Population (45-65)	UN World Population Prospects 2019
	Population (65+)	UN World Population Prospects 2019
Climate	Global Atmospheric Temperature	NASA (2019)
Economy	World GDP	World Bank and OECD National Accounts
Water Demand	Domestic Water Withdrawal	International Hydrological Programme (2000)
	Industrial Water Withdrawal	
	Agricultural Water Withdrawal	
Water Supply	Surface Water Withdrawal	Wada and Bierkens (2014a)
	Ground Water Withdrawal	
Energy Production	Coal Energy Production	World Nuclear Association (2018)
	Oil and Gas Energy Production	
	Hydro and Nuclear Energy Production	Ritchie and Roser (2018a)
	Renewable Energies	Ritchie and Roser (2018b)
Land Use and Cover	Agricultural Area	HYDE (2016)
	Urban Area	

Selected results of the behaviour reproduction are in Figure 4.1. The growth of human population one of the most important feedback loops in the ANEMI3 model as it is a key driver of the global change. When comparing the simulated and observed total population in Figure 4.1 (top row, panel 1), we see that they start at the same initial value and follow a similar path to 2019. However, the paths start to diverge slightly between the years 2010 to 2019. This discrepancy is relatively minor and there is not a major difference in the overall behaviour of the historical population. When the population is subdivided further (Figure 4.1, top row, panel 2), it is shown that the simulated population for all age

groups except for 15 to 44, follow historical trends, where the 15 to 44 age group is slightly underestimated.

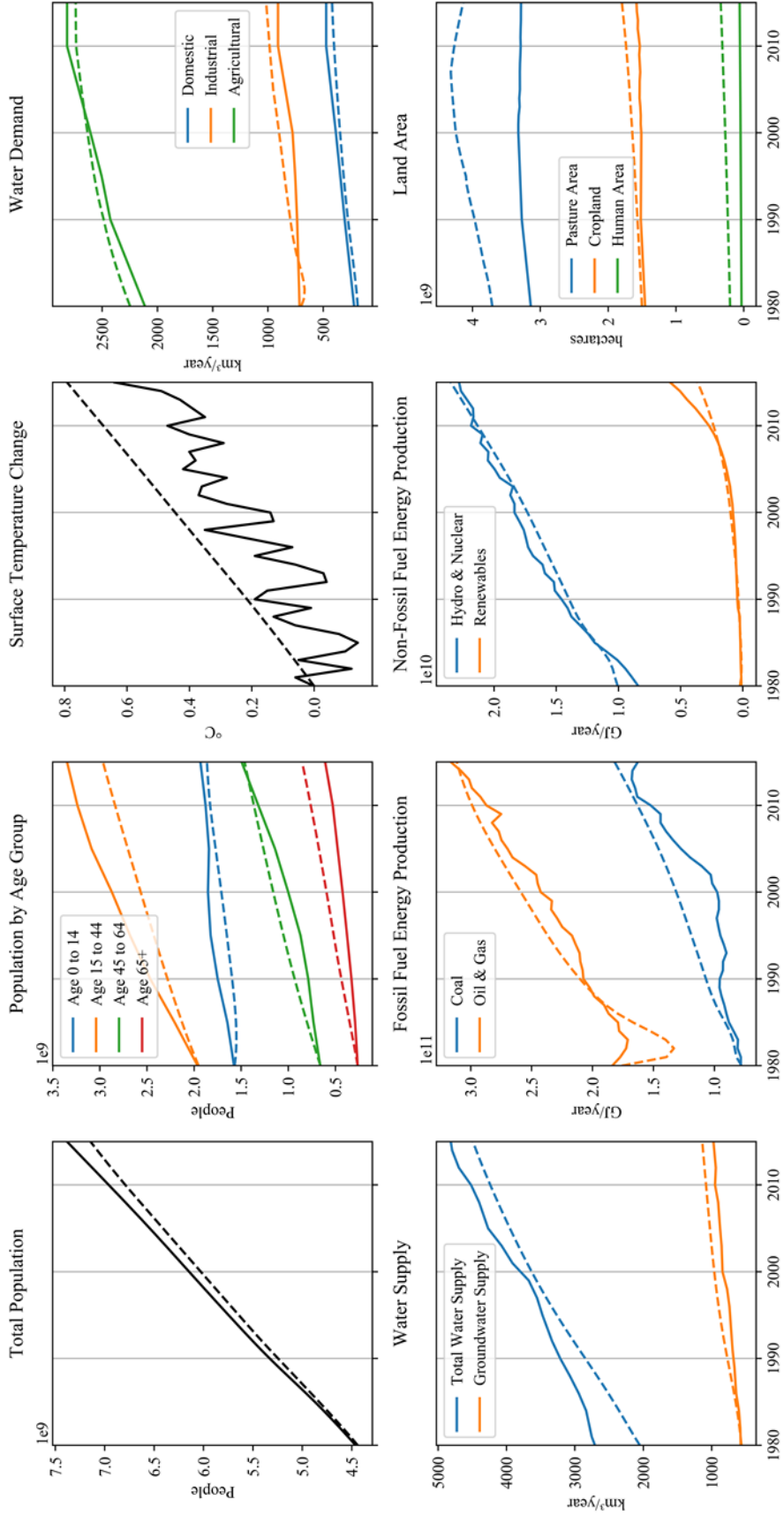


Figure 4.1. ANEMI3 model behavior reproduction

The variation in global temperatures due to climate change from the year 1980 are shown in Figure 4.1 (top row, panel 3) . From 1980 to 2018 the ANEMI3 model predicts a global temperature change of 0.87 degrees, while the observed NASA data reports a value of 0.6 degrees. The simplified climate system in ANEMI3 is not able or designed to capture the annual variation in global temperatures that are present in the observed NASA data.

Water demand projections from ANEMI3 are compared to estimates from IHP (2000) in Figure 4.1 (top row, panel 4). Agricultural demand in 1980 and 2010 is slightly lower than the historical values before the year 1990 and slightly higher after, while industrial water demand provides a good match and domestic water demand is slightly lower than historical. The water demand values are driven by food production in the case of agricultural demands, energy production for the industrial water demand, and population along with economic output for domestic demand. Considering the integrated nature of water demand in ANEMI3, the trend of increasing water demands is accurately captured from 1980-2010.

The water production sector in ANEMI3 is compared against estimates provided by Wada and Bierkens (2014a). Available global data for the withdrawal of surface water and groundwater is scarce, however in Wada and Bierkens (2014a) a global hydrologic model was used in conjunction with a global water demand model to generate estimates for surface water and groundwater withdrawal amounts. Comparison between the ANEMI3 simulated values and the estimates (Figure 4.1, bottom row, panel 1) shows good agreement in the trends although the ANEMI3 value for surface water withdrawal is slightly lower.

Energy production in the ANEMI3 model is based on that of the FREE model in Fiddaman (1997) which is intended for long term simulations of energy production for the purpose of policy analysis (such as for example, the application of carbon taxes on fossil fuels.) The simulated values for oil and gas production are presented in Figure 4.1 (bottom row, panel 2). There is an initial drop in production in the year 1986. From this point onward, the trajectory of oil and gas production is successfully captured.

Hydro and nuclear energy production are very close to the historical data, capturing the absolute values and trend over time (Figure 4.1, bottom row, panel 3). However, in the case of renewable energy

production the simulated renewable energy values show an increase, but not on the scale that has been observed. The reason for this is most likely the sensitivity of the ANEMI3 model to initial conditions for renewable energy production, because the initial values are small relative to the amount of growth that is made in a short period of time.

Land area comparisons are made between the ANEMI3 model results and data obtained from HYDE (2016) for agricultural and built land areas during the historical period (Figure 4.1, bottom row, panel 4). Simulated values for cropland, grazing land, and human built areas appear to be slightly overestimated by the ANEMI3 when compared to the historical values. This may be due to minor differences in the categorization of land use types embedded in the initial land values used in ANEMI3 from (Goudriaan and Ketner 1984a). However, the rates of change in each category are similar.

#### 4.2.2 Future Model Performance

Models and data have been used to analyze future behaviour of various components of the Earth system that are also being modelled by ANEMI3. Comparing the ANEMI3 future behavior to these models and data provides some context as to where the ANEMI3 results lie amongst the range of available future behaviors, as well as providing an additional test of plausibility for the model. The goal is not to reproduce the results shown from the other models. The models are using different datasets, time horizons, and model structures in comparison to ANEMI3. The Table 4.4 lists the variables that are being used from each sector in ANEMI3 for comparison with other future Earth system behaviors available in the literature.

The trajectories of the main stocks in the baseline scenario that define the state of the ANEMI3 model are shown in Figure 4.2. The total population (Figure 4.2, top row, panel 1) varies from 4.4 billion to 9.5 billion in 1980 and 2100 respectively. Population increases almost linearly at the start of the simulation, then the increase slows down as negative feedbacks on population begin to limit the growth. The peak population is reached in the year 2085. After this point the death rate exceeds that of the birth rate and there is a gradual decrease in population until the end of the simulation. The 2019 revision of the UN World Population Prospects (UN WPP) report (United Nations 2019b) contains future population scenarios defined by projected variants in fertility, mortality, and migrations rates to the year 2100. When ANEMI3 is compared to the projections, the results are shown to lie between the low and medium projections.

Table 4.4. Datasets used for comparison of the ANEMI3 model future behaviour

Model Sector	Variable	Dataset
Population	Total Population	UN World Population Prospects 2019
Climate	Global Atmospheric Temperature	Krinner et al. (2013)
Economy	Gross Economic Output	DICE 2013R
	Per Capita Consumption	ANEMI2
Water Demand	Domestic Water Withdrawal	Wada et al. (2016)
	Industrial Water Withdrawal	Chaturvedi et al. (2013)
	Agricultural Water Withdrawal	
Water Supply	Surface Water Production	Wada et al. (2014b)
	Groundwater Production	
	Desalination Production	Hanasaki et al. (2016) Fichtner GmbH (2011)
Energy Production	Total Energy Production	ANEMI2
	Coal Energy Production	Ito et al. (2000)
	Oil and Gas Energy Production	Mohr et al. (2009)
	Hydro and Nuclear Energy Production	
	Renewable Energies	

The change in global surface temperatures resulting from running the ANEMI3 model with the RCP scenarios, is shown in Figure 4.2 (top row, panel 2). The ANEMI3 results are found to be within what is projected with the RCP scenarios, between those of RCP6 (2.6°C by 2100) and RCP8.5 (4.3°C by 2100) corresponding to a 2.7°C temperature change by the year 2100.

Comparing the CO<sub>2</sub> concentrations of the RCP scenarios to that of the ANEMI3 model also shows a similar result, with a very close trajectory to RCP6 (Figure 4.2, top row, panel 3). This indicates that the overall socioeconomic pathway of the ANEMI3 baseline run is between one that is medium to high in terms of emissions with some climate change mitigation present, and is similar to that of the AIM integrated assessment model (van Vuuren et al. 2011).

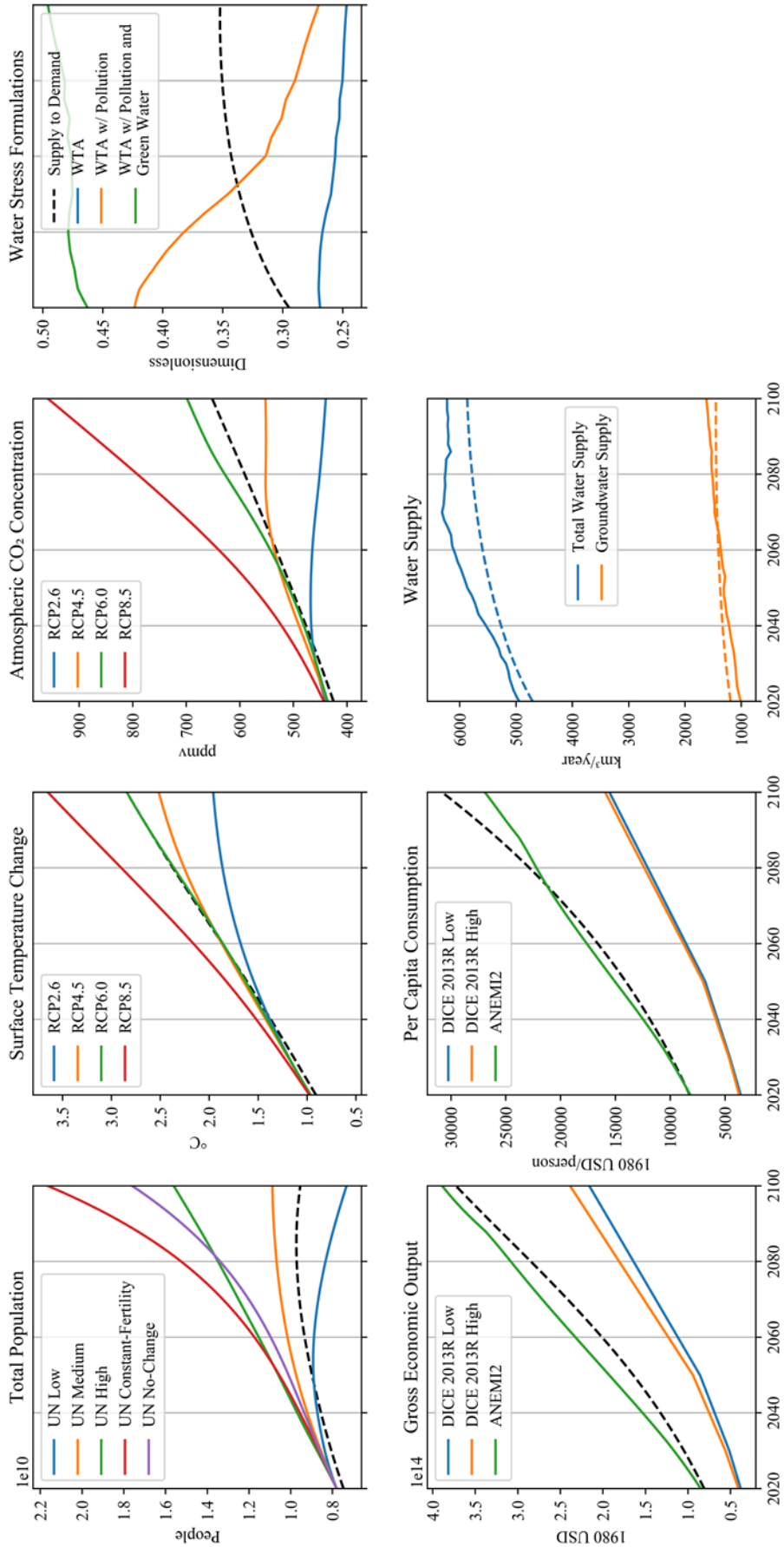


Figure 4.2. ANEM13 model future behavior

Thresholds of water stress have been defined by United Nations (1997). Low, moderate, medium-high, and high levels of water stress corresponds to values of less than 0.1, 0.1 to 0.2, 0.2 to 0.4, and greater than 0.4 respectively, where water stress ( $WTA$ ) is defined as the ratio of surface water withdrawals ( $SWW$ ) to availability (ASW),

$$WTA = \frac{SWW}{ASW} \quad (4.1)$$

In the ANEMI3 model, water stress can be calculated using different formulations. Water pollution and green water dilution effects ( $WTA_{poll}$  and  $WTA_{poll+gw}$ ) can be applied to the WTA ratio in order to gain a more conservative measure of water stress (Davies and Simonovic 2011).

$$WTA_{pollution} = \frac{SWW + URW \cdot WDF}{Total\ Renewable\ Flow} \quad (4.2)$$

$$WTA_{pollution+gw} = \frac{SWW + URW \cdot WDF + GWR}{Total\ Renewable\ Flow} \quad (4.3)$$

$URW = Untreated\ returnable\ water\ [km^3/y]$

$WPF = Water\ pollution\ factor$

$GWR = Green\ water\ requirement\ for\ crops\ and\ pasture\ [km^3/y]$

In this report, an additional representation is used based on the ratio of total water supply to the amount of available conventional water resources of surface water ( $R_{sw}$ ) and groundwater ( $R_{gw}$ ).

$$WTA_{water\ supply} = \frac{\sum WS_i}{R_{sw} + R_{gw}} \quad (4.4)$$

The total amount of water supply includes both, conventional and alternative water resources, allowing for increased alternative water resources to reduce water stress. The projected water stress

values using the formulations (4.1) – (4.4) are shown in Figure 4.2 (top row, panel 4). When the effects of pollution and green water dilution are included, water stress values are much higher. Using only the WTA ratio, water stress values start initially at a value of 0.21 and rise up to 0.24, which is on the low end of the medium-high water stress category. In contrast, when pollution and green water effects are considered, the starting values range between 0.32 to 0.35. As the simulation progresses, water stress with only pollution effects considered on top of the WTA reaches a peak in the year 2010 and declines afterwards. This is because in this case the pollution effects are represented only through wastewater inputs, which decrease as domestic and industrial water demands decrease in the model due to reduced water intensities with greater global economic output. When water pollution in the form of agricultural runoff or green water is included, water stress values continue to rise to a value of 0.5 by the end of the simulation. This indicates severe levels of water stress. Using the ratio of water supply to available water resource levels as an indicator of water stress result in a starting value of 0.15 which follows S-shaped growth to 0.35. This indicates a shift from low levels of water stress to the high end of the medium-high water stress category.

Despite economic damages from climate change, economic output increases exponentially from 19.4 to 372 trillion 1980 USD (Figure 4.2, bottom row, panel 1). When compared with the ANEMI2 model, it is interesting to note that the simulated values follow a similar trajectory. The same initial value of the global capital stock was used between the two models, but the model structure of the economic sectors of ANEMI2 and ANEMI3 are entirely different. The second version of ANEMI uses a computable general equilibrium model to generate economic output and investment in capital stocks, while the ANEMI3 uses the system dynamics simulation approach based on the FREE model of Fiddaman (1997). Although the projections from the DICE2013R (Nordhaus 2013) model show values that are considerably lower than that of ANEMI versions 2 and 3, the general pattern of consistent exponential growth is the same, and the differences likely stem from the choice of initial values.

The rates of per capita consumption show a similar pattern as well amongst the models (Figure 4.2, bottom row, panel 2).

The simulated water supply rates for the ANEMI3 model and that of Wada et al. (2014b) are compared for surface and groundwater supply (Figure 4.2, bottom row, panel 3). The trajectories for both surface

water and groundwater are similar, however the water supply rates are higher for surface water over the duration of the simulation in Wada et al. (2014b). Groundwater supply rates are similar between the two models, but diverge after the year 2040. This is likely due to increased utilization of alternative water supplies in the form of wastewater reuse and desalination.

## 5 Closing Remarks

The report provides the detailed introduction to the ANEMI3 model of global change developed at the University of Western Ontario. The focus of the report is on the model structure and its details with the presentation of the model validation results.

With the new complex structure of the ANEMI3 model, various experiments can be conducted in order to; examine the impacts of climate change throughout the Earth system, evaluate potential limits to population growth through the depletion of food and water supplies and the generation of pollution, assess the potential impacts of water quality on the development of water supplies, and analyze the role of water supply development of conventional and alternative water supplies in adapting to global water stress. The role of alternative water supplies in the form of desalination and wastewater reuse can be also assessed to fulfill future water demands beyond conventional water supplies of surface and groundwater. Detailed presentation of all simulated scenarios is available in Breach (2020, Chapter 4).

The entire model code is provided in the “ANEMI” GitHub repository located at <https://github.com/FIDS-UWO/anemi> as a Vensim model file titled “ANEMI3.mdl”. This file can be opened using the Vensim software in order to view the model structure. A free Vensim PLE licence can be obtained from <https://vensim.com>, which can be used to view the stock and flow diagram that makes up the model structure. Due to the advanced features used in the ANEMI3 model, a Vensim DSS license is required to run the model.

## 6 References

- Akhtar MK, Wibe J, Simonovic SP, MacGee J (2013) Integrated assessment model of society-biosphere-climate-economy-energy system. *Environ Model Softw* 49:1–21 . doi: 10.1016/j.envsoft.2013.07.006
- Alcamo J, Döll P, Henrichs T, et al (2003) Development and testing of the WaterGAP 2 global model of water use and availability. *Hydrol Sci J* 48:317–337 . doi: 10.1623/hysj.48.3.317.45290
- Aulakh R (2014) China wakes up to its water crisis. *Star*
- Breach PA (2020) Water Supply Capacity Building in the Context of Global Change. PhD Dissertation, Western University, Department of Civil and Environmental Engineering.
- Breach PA, Simonovic SP (2018) Wastewater Treatment Energy Recovery Potential For Adaptation To Global Change: An Integrated Assessment. *Environ Manage* 61:624–636 . doi: 10.1007/s00267-018-0997-6
- Calvin K, Patel P, Clarke L, et al (2019) GCAM v5.1: Representing the linkages between energy, water, land, climate, and economic systems. *Geosci Model Dev* 12:677–698 . doi: 10.5194/gmd-12-677-2019
- Chaturvedi V, Hejazi M, Edmonds J, et al (2013) Climate mitigation policy implications for global irrigation water demand. *Mitig Adapt Strateg Glob Chang* 20:389–407 . doi: 10.1007/s11027-013-9497-4
- Chen J, Mueller V (2018) Climate change is making soils saltier, forcing many farmers to find new livelihoods. *Conversat*.
- Cox P, Nakicenovic N (2004) Assessing and Simulating the Altered Functioning of the Earth System in the Anthropocene. In: Schellnhuber H, Crutzen P, Clark W, et al. (eds) *Earth system analysis for sustainability*. MIT Press, pp 293–312
- Davies EG (2007) *Modelling Feedback in the Society-Biosphere-Climate System*. University of Western Ontario
- Davies EGR, Simonovic SP (2010) ANEMI: a new model for integrated assessment of global change. *Interdiscip Environ Rev* 11:127–161 . doi: 10.1504/IER.2010.037903
- Davies EGR, Simonovic SP (2011) Global water resources modeling with an integrated model of the social-economic-environmental system. *Adv Water Resour* 34:684–700 . doi: 10.1016/j.advwatres.2011.02.010
- Davies EGR, Kyle P, Edmonds JA (2013) An integrated assessment of global and regional water demands for electricity generation to 2095. *Adv Water Resour* 52:296–313 . doi:

10.1016/j.advwatres.2012.11.020

- den Elzen MGJ, Beusen AHW, Rotmans J (1997) An integrated modeling approach to global carbon and nitrogen cycles: Balancing their budgets. *Global Biogeochem Cycles* 11:191–215 . doi: 10.1029/96GB03938
- Dowgert M (2010) The Impact of Irrigated Agriculture on a Stable Food Supply. *Proc 22nd Annu Cent Plains Irrig Conf* 1–11
- Dunford R, Harrison P a., Rounsevell MD a (2014) Exploring scenario and model uncertainty in cross-sectoral integrated assessment approaches to climate change impacts. *Clim Change*. doi: 10.1007/s10584-014-1211-3
- Eikebrokk B, Vogt RD, Liltved H (2004) NOM increase in Northern European source waters: Discussion of possible causes and impacts on coagulation/contact filtration processes. *Water Sci Technol Water Supply* 4:47–54
- FAO, IFAD, UNICEF, et al (2019) *The State of Food Security and Nutrition in the World: Safeguarding Against Economic Slowdowns and Downturns*. Rome, FAO
- (FAO) Food and Agriculture Organization of the United Nations (2018) *The future of food and agriculture – Alternative pathways to 2050*
- (FAO) Food and Agricultural Organization (2019a) *Eutrophication of Surface Waters*. In: *Fertilizers as Pollutants*. <http://www.fao.org/3/w2598e/w2598e06.htm>. Accessed 15 Oct 2017
- (FAO) Food and Agriculture Organization of the United Nations (2019b) *FAOSTAT Crop Database*. <http://www.fao.org/faostat/en/#data/QC>. Accessed 10 Dec 2019
- Fichtner GmbH (2011) *MENA Regional Water Outlook Part II: Desalination Using Renewable Energy*. Fichtner, Stuttgart, Germany
- Fiddaman TS (2002) Exploring policy options with a behavioral climate-economy model. *Syst Dyn Rev* 18:243–267 . doi: 10.1002/sdr.241
- Fiddaman TS (1997) Feedback Complexity in Integrated Climate-Economy Models. *Proc 1998 Syst Dyn Conf* 1:32
- Gao L, Yoshikawa S, Iseri Y, et al (2017) An economic assessment of the global potential for seawater desalination to 2050. *Water (Switzerland)* 9: . doi: 10.3390/w9100763
- Goudriaan J, Ketner P (1984a) A simulation study for the global carbon cycle, including man's impact on the biosphere. *Clim Change* 6:167–192 . doi: 10.1007/BF00144611
- Goudriaan J, Ketner P (1984b) A simulation study for the global carbon cycle, including man's impact on the biosphere. *Clim Change* 6:167–192 . doi: 10.1007/BF00144611

- Hamilton SH, Elsawah S, Guillaume JH a, et al (2015) Integrated assessment and modelling : Overview and synthesis of salient dimensions. *Environ Model Softw* 64:215–229 . doi: 10.1016/j.envsoft.2014.12.005
- Hanasaki N, Yoshikawa S, Kakinuma K, Kanae S (2016) A seawater desalination scheme for global hydrological models. *Hydrol Earth Syst Sci* 20:4143–4157 . doi: 10.5194/hess-20-4143-2016
- Harasawa H, Lal M, Wu S, et al (2014) Freshwater Resources. In: *Climate Change 2014: Impacts, Adaptation, and Vulnerability. Part A: Global and Sectoral Aspects*. pp 229–269
- Henze M, Comeau Y (2008) Wastewater Characterization. In: *Biological Wastewater Treatment: Principles Modelling and Design*. IWA Publishing, London, UK, pp 33–52
- (HYDE) History Database of the Global Environment (2016) Land Use Data. <https://themasites.pbl.nl/tridion/en/themasites/hyde/landusedata/index-2.html>. Accessed 10 Aug 2019
- (IHP) International Hydrological Programme (2000) World Freshwater Resources. *UNESCO Int* 25:11–32
- (IHP) International Hydrological Programme (2000) World Freshwater Resources. CD-ROM prepared by I.A. Shiklomanov, International Hydrologic Programme, UNESCO
- Ionesco D, Mokhnacheva D, Gemenne F (2017) *The Atlas of Environmental Migration*. Routledge Taylor & Francis Group
- IPCC (2013) *Climate Change 2013: The Physical Science Basis. Contribution of Working Group I to the Fifth Assessment Report of the Intergovernmental Panel on Climate Change*. Geneva, Switzerland
- IPCC (2014) *Climate Change 2014: Impacts, Adaptation, and Vulnerability. Part A: Global and Sectoral Aspects. Contribution of Working Group II to the Fifth Assessment Report of the Intergovernmental Panel on Climate Change*. Cambridge University Press, Cambridge, United Kingdom and New York, NY, USA, 1132 pp.
- Ito K, Murota Y, Econometrics S, et al (2000) Ultra-Long Term Global Energy Supply / Demand Models And Simulation. 1–19
- Janetos AC (2008) *Science Challenges and Future Directions: Climate Change Integrated Assessment Research*. U.S. Department of Energy
- Jevrejeva S, Jackson LP, Grinsted A, et al (2018) Flood damage costs under the sea level rise with warming of 1.5°C and 2°C. *Environ Res Lett* 13: . doi: 10.1088/1748-9326/aacc76
- Jin S, Yu W, Jansen HGP, Lansing E (2012) The impact of Irrigation on Agricultural Productivity :

- Evidence from India The impact of Irrigation on Agricultural Productivity : Evidence from India 1 ) Department of Agricultural , Food , and Resource Economics , Michigan State University , 2 ) World
- Kauffman DLJ (1980) *Systems One : An Introduction to Systems Thinking*, 2nd edn. Future Systems, Inc., Saint Paul, MN
- Keyfitz N, Flieger W (1971) *Population: facts and method of demography*. San Francisco
- King M, Altdorff D, Li P, et al (2018) Northward shift of the agricultural climate zone under 21 st - century global climate change. *Sci Rep* 8:1–10 . doi: 10.1038/s41598-018-26321-8
- Klohn W, Faurès J, Vallée D, et al (2003) Securing food for a growing population. In: *The World Water Development Report*. UNESCO-WWAP
- Kotir JH, Smith C, Brown G, et al (2016) A system dynamics simulation model for sustainable water resources management and agricultural development in the Volta River Basin, Ghana. *Sci Total Environ* 573:444–457 . doi: 10.1016/j.scitotenv.2016.08.081
- Krinner G, Germany F, Shongwe M, et al (2013) Long-term climate change: Projections, commitments and irreversibility. *Clim Chang* 2013 Phys Sci Basis Work Gr I Contrib to Fifth Assess Rep Intergov Panel Clim Chang 9781107057:1029–1136 . doi: 10.1017/CBO9781107415324.024
- Larsen MAD, Drews M (2019) Water use in electricity generation for water-energy nexus analyses: The European case. *Sci Total Environ* 651:2044–2058 . doi: 10.1016/j.scitotenv.2018.10.045
- Lipton M, Litchfield J, Faures M (2003) The Effects of Irrigation on Poverty: A Framework for Analysis. *J Water Policy* 5:413–427 . doi: 10.2166/wp.2003.0026
- Mackenzie FT (1999) *Global Biogeochemical Cycles and the Physical Climate System*. Hawaii
- Mackenzie FT, Ver LM, Sabine C, Lane M (1993) C, N, P, S Global Biogeochemical Cycles and Modeling of Global Change. In: *Interactions of C, N, P and S Biogeochemical Cycles and Global Change*. Springer, Verlag, pp 1–61
- Masterson W, Hurley C (2009) *Chemistry: Principles and Reactions*, 6th edn. Brooks/Cole Cengage Learning
- Matsuoka Y, Morita T, Kainuma M (2001) Integrated Assessment Model of Climate Change : The AIM Approach. In: Matsuno T, Kida H (eds) *Present and Future of Modeling Global Environmental Change: Toward Integrated Modeling*. TerraPub, pp 339–361
- Meadows D, Behrens W, Meadows D, et al (1974) *Dynamics of Growth in a Finite World*. Wright-Allen Press, Inc., Cambridge, MA

- Meadows DH, Jorgen R (1992) *Beyond the Limits: Confronting Global Collapse, Envisioning a Sustainable Future*. Chelsea Green Pub., Hartford, VT
- Moss RH, Edmonds J a, Hibbard K a, et al (2010) The next generation of scenarios for climate change research and assessment. *Nature* 463:747–756 . doi: 10.1038/nature08823
- (NASA) National Aeronautics and Space Administration (2019) Global Temperature. In: *Global Land-Ocean Temp. Index*. <https://climate.nasa.gov/vital-signs/global-temperature/>. Accessed 17 Oct 2019
- Nordhaus WD (1992) *The “DICE” Model: Background and Structure of a Dynamic Integrated Climate-Economy Model of the Economics of Global Warming*
- Nordhaus WD (1994) *Managing the Global Commons: The Economics of Climate Change*. MIT Press, Cambridge, MA
- Nordhaus WD (2013) *DICE 2013R: Introduction and User’s Manual*. Yale Univ Press 102
- Piguat É, Pecoud A, and Guchteneire P (2008) *Migration and climate change*. Cambridge University Press, Cambridge, United Kingdom.
- Prescott EC (1988) Robert M . Solow’s Neoclassical Growth Model : An Influential Contribution to Economics. *Scand J Econ* 90:7–12
- Price MF (1989) Global change: Defining the ill-defined. *Environ Sci Policy Sustain Dev* 31:18–44 . doi: 10.1080/00139157.1989.9928971
- Rahmstorf S (2007) A Semi-Empirical Approach to Projecting Future Sea-Level Rise. *Science* (80-) 315:368–370
- Ritchie H, Roser M (2018a) *Energy Production & Changing Energy Sources*. In: *Our World Data*. <https://ourworldindata.org/energy-production-and-changing-energy-sources>. Accessed 15 Sep 2019
- Ritchie H, Roser M (2018b) *Renewable Energy*. In: *Our World Data*. <https://ourworldindata.org/renewable-energy>. Accessed 15 Sep 2019
- Ritson JP, Graham NJD, Templeton MR, et al (2014) The impact of climate change on the treatability of dissolved organic matter (DOM) in upland water supplies: A UK perspective. *Sci Total Environ* 473–474:714–730 . doi: 10.1016/j.scitotenv.2013.12.095
- Roberts N, Anderson D, Deal R, et al (1983) *Introduction to Delays*. In: *Introduction to Computer Simulation: A System Dynamics Modeling Approach*1. Productivity Press, Portland, Oregon, pp 301–333
- Rotmans J, Dowlatabadi H (1998) *Integrated Assessment of Climate Change: Evaluation of*

- Methods and Strategies. In: Rayner S, Malone EL (eds) *Human Choices and Climate Change: A State of the Art Report*
- Rotmans J, van Asselt M (1999) *Integrated Assessment Modelling*. 239–275 . doi: 10.1007/0-306-47982-6\_7
- Schuster-Wallace CJ, Grover VI, Adeel Z, et al (2008) *Safe Water as the Key to Global Health*. UNU-INWEH, Tokyo
- Schwartz J, Levin R, Goldstein R (2000) Drinking water turbidity and gastrointestinal illness in the elderly of Philadelphia. *J Epidemiol Community Health* 54:45–51 . doi: 10.1136/jech.54.1.45
- Searchinger T, Waite R, Hanson C, Ranganathan J (2019) *Creating a Sustainable Food Future: a Menu of Solutions to Feed Nearly 10 Billion People by 2050*. *World Resour Rep* 558
- Shiklomanov I (2000) *Appraisal and Assessment of World Water Resources*. *Water Int* 25:11–32 . doi: 10.1080/02508060008686794
- Simonovic SP (2002a) World water dynamics: global modeling of water resources. *J Environ Manage* 66:249–267 . doi: 10.1006/jema.2002.0585
- Simonović SP (2012) *Managing water resources: Methods and tools for a systems approach*. UNESCO, Paris and Earthscan James & James, London
- Steffan W, Sanderson A, Tyson P, et al (2004) *Global Change and the Earth System: A Planet Under Pressure*. Springer, Berlin, Heidelberg, New York, Hong Kong, London, Milan, Paris, Tokyo
- Stehfest E, van Vuuren D, Kram T, Bouwman L (2014) Overview of IMAGE 3.0. In: *Integrated Assessment of Global Environmental Change with IMAGE 3.0: Model description and policy applications*. PBL Netherlands Environmental Assessment Agency, pp 32–54
- Sterman JD (1980) *The Use of Aggregate Production Functions in Disequilibrium Models of Energy-Economy Interactions*
- Sterman JD (2000) *Business Dynamics: Systems Thinking and Modeling for a Complex World*. Irwin McGraw-Hill, Boston, MA
- Storn R, Price K (1995) *Differential Evolution - A simple and efficient adaptive scheme for global optimization over continuous spaces*. Berkeley, CA
- Strzepek K, Schlosser A, Gueneau A, et al (2013) Modeling water resource systems within the framework of the MIT integrated global system model: IGSM-WRS. *J Adv Model Earth Syst* 5:638–653 . doi: 10.1002/jame.20044
- Thissen W, De Mol C (1978) The agricultural and persistent pollution subsystems in world. *IEEE Trans Syst Man Cybern* 8:159–172 . doi: 10.1109/TSMC.1978.4309927

- Tol RSJ, Vellinga P (1998) The European forum on integrated environmental assessment. *Environ Model Assess* 3:181–191 . doi: 10.1023/A:1019023124912
- United Nations (2019a) Migration and the climate crisis: the UN's search for solutions. In: UN-News. <https://news.un.org/en/story/2019/07/1043551>
- United Nations (2019b) World Population Prospects 2019: Methodology of the United Nations population estimates and projections
- United Nations (1997) Comprehensive Assessment of the Freshwater Resources of the World. Stockholm
- van Vuuren DP, Edmonds J, Kainuma M, et al (2011) The representative concentration pathways: An overview. *Clim Change* 109:5–31 . doi: 10.1007/s10584-011-0148-z
- Virtanen P, Gommers R, Travis EO, et al (2019) Scipy 1.0-Fundamental Algorithms for Scientific Computing in Python
- Wada Y, Bierkens MFP (2014a) Sustainability of global water use: Past reconstruction and future projections. *Environ Res Lett* 9 . doi: 10.1088/1748-9326/9/10/104003
- Wada Y, Wisser D, Bierkens MFP (2014b) Global modeling of withdrawal, allocation and consumptive use of surface water and groundwater resources. *Earth Syst Dyn* 5:15–40 . doi: 10.5194/esd-5-15-2014
- Wada Y, Flörke M, Hanasaki N, et al (2016) Modeling global water use for the 21st century: The Water Futures and Solutions (WFaS) initiative and its approaches. *Geosci Model Dev* 9:175–222 . doi: 10.5194/gmd-9-175-2016
- Wood A, Wollenberg B (1996) *Power Generation, Operation and Control*, 2nd edn. Wiley, New York
- (WCRP) World Climate Research Programme (2020) About WCRP. <https://www.wcrp-climate.org/about-wcrp/wcrp-overview>. Accessed 19 Dec 2019
- World Commission on Environment and Development (1987) *Our Common Future*. Oxford University Press, Oxford
- World Nuclear Association (2018) *Nuclear Power in the World Today*. <https://www.world-nuclear.org/information-library/current-and-future-generation/nuclear-power-in-the-world-today.aspx>. Accessed 15 Dec 2019
- Yuan Z, Yan D, Yang Z, et al (2016) Impacts of climate change on winter wheat water requirement in Haihe River Basin. *Mitig Adapt Strateg Glob Chang* 21:677–697 . doi: 10.1007/s11027-014-9612-1

Zabel F, Putzenlechner B, Mauser W (2014) Global agricultural land resources - A high resolution suitability evaluation and its perspectives until 2100 under climate change conditions. PLoS One 9: . doi: 10.1371/journal.pone.0107522

Zhao C, Liu B, Piao S, et al (2017) Temperature increase reduces global yields of major crops in four independent estimates. Proc Natl Acad Sci U S A 114:9326–9331 . doi: 10.1073/pnas.1701762114

## Appendix A: Parameters for the Nutrient Cycles

Table A.1. Initial values and residence times of carbon, nitrogen, and phosphorus stocks in their respective cycles from Mackenzie et al. (1993).

Reservoir (No.)	CARBON		NITROGEN		PHOSPHORUS	
	Mass, moles	RT, years	Mass, moles	RT, years	Mass, moles	RT, years
Land Biota (1)	$4.98 \times 10^{16}$	9.5	$7.14 \times 10^{14}$	9	$9.69 \times 10^{13}$	9.5
Humus (2)	$2.05 \times 10^{16}$	4	$2.43 \times 10^{15}$	30	$4.01 \times 10^{14}$	39
Inorganic Soil (3)	$5.98 \times 10^{16}$	1,300	$1.23 \times 10^{14}$	1.4	$1.15 \times 10^{15}$	1,770
Coastal Waters (4)	$6.00 \times 10^{15}$	2.3	$1.08 \times 10^{14}$	1.1	$4.50 \times 10^{12}$	0.75
Coastal Biota (5)	$4.21 \times 10^{13}$	0.07	$6.35 \times 10^{12}$	0.07	$3.76 \times 10^{11}$	0.07
Coastal Sediments (6)	$2.07 \times 10^{17}$	5,400	$2.28 \times 10^{15}$	370	$9.20 \times 10^{15}$	11,000
Surface Ocean (7)	$3.54 \times 10^{17}$	22	$2.05 \times 10^{14}$	0.41	$2.65 \times 10^{14}$	8.8
Ocean Biota (8)	$2.21 \times 10^{14}$	0.07	$3.36 \times 10^{13}$	0.07	$1.97 \times 10^{12}$	0.07
Deep Ocean (9)	$2.75 \times 10^{18}$	1,200	$5.11 \times 10^{16}$	1,500	$2.97 \times 10^{15}$	1,100
Atmosphere (10)	$6.15 \times 10^{16}$	3.6	$2.80 \times 10^{20}$	11,400,000		

Table A.2. Rate constants used to describe flow in the cycles of carbon, nitrogen, and phosphorus from Mackenzie et al. (1993).

$k_{ij}$	CARBON		NITROGEN		PHOSPHORUS	
	Flux, moles/year	k, /year	Flux, moles/year	k, /year	Flux, moles/year	k, /year
k 101	$5.25 \times 10^{15}$	$8.54 \times 10^{-2}$	$9.60 \times 10^{12}$	$3.43 \times 10^{-8}$		
k 103	$3.40 \times 10^{13}$	$5.53 \times 10^{-4}$	$6.90 \times 10^{12}$	$2.46 \times 10^{-8}$		
k 104	$1.51 \times 10^{15}$	$2.45 \times 10^{-2}$	$5.07 \times 10^{11}$	$1.81 \times 10^{-9}$		
k 105			$2.37 \times 10^{12}$	$2.56 \times 10^2$		
k 107	$1.03 \times 10^{16}$	$1.68 \times 10^{-1}$	$4.59 \times 10^{12}$	$1.64 \times 10^{-8}$		
k 108			$6.30 \times 10^{11}$	$1.29 \times 10^2$		
k 12	$5.25 \times 10^{15}$	$1.05 \times 10^{-1}$	$8.33 \times 10^{13}$	$1.17 \times 10^{-1}$	$1.02 \times 10^{13}$	$1.05 \times 10^{-1}$
k 23			$8.15 \times 10^{13}$	$3.35 \times 10^{-2}$		
k 210	$5.22 \times 10^{15}$	$2.54 \times 10^{-1}$				
k 31			$7.37 \times 10^{13}$	$5.99 \times 10^{-1}$		
k 310			$1.42 \times 10^{13}$	$1.15 \times 10^{-1}$		
k 45	$6.00 \times 10^{14}$	$1.00 \times 10^{-1}$	$9.07 \times 10^{13}$	$8.40 \times 10^{-1}$	$5.37 \times 10^{12}$	$1.19 \times 10^0$
k 47	$5.00 \times 10^{14}$	$8.33 \times 10^{-2}$	$7.50 \times 10^{12}$	$6.94 \times 10^{-2}$	$6.40 \times 10^{11}$	$1.42 \times 10^{-1}$
k 410	$1.51 \times 10^{15}$	$2.51 \times 10^{-1}$	$1.10 \times 10^{12}$	$1.02 \times 10^{-2}$		
k 54	$5.76 \times 10^{14}$	$1.37 \times 10^1$	$8.69 \times 10^{13}$	$1.37 \times 10^1$	$5.15 \times 10^{12}$	$1.37 \times 10^1$
k 56	$2.40 \times 10^{13}$	$5.70 \times 10^{-1}$	$6.14 \times 10^{12}$	$9.67 \times 10^{-1}$	$2.20 \times 10^{11}$	$5.85 \times 10^{-1}$
k 64	$3.10 \times 10^{13}$	$1.50 \times 10^{-4}$	$4.39 \times 10^{12}$	$1.93 \times 10^{-3}$	$5.10 \times 10^{11}$	$5.54 \times 10^{-5}$
k 610			$3.33 \times 10^{12}$	$1.46 \times 10^{-3}$		
k 74	$4.29 \times 10^{14}$	$1.21 \times 10^{-3}$	$6.44 \times 10^{12}$	$3.14 \times 10^{-2}$	$3.20 \times 10^{11}$	$1.21 \times 10^{-3}$
k 78	$3.15 \times 10^{15}$	$8.90 \times 10^{-3}$	$4.80 \times 10^{14}$	$2.34 \times 10^0$	$2.82 \times 10^{13}$	$1.06 \times 10^{-1}$
k 79	$2.16 \times 10^{15}$	$6.10 \times 10^{-3}$	$1.14 \times 10^{13}$	$5.57 \times 10^{-2}$	$1.59 \times 10^{12}$	$6.00 \times 10^{-3}$

## Appendix B: Differential evolution algorithm for parameter estimation

The differential evolution algorithm of Storn and Price (1995) was used for parameter estimation of the ANEMI3 model baseline run. This evolutionary algorithm was selected because of its ability to find the global optimum of high-dimensional objective functions without the need for the function derivative to be specified.

Differential Evolution (DE) is a brute-force stochastic algorithm that falls within the family of Evolutionary Algorithms (EA). Within the set of EAs there exists a common set of principles that are used to reach a solution to global optimization problems that are otherwise difficult to obtain from traditional non-linear solvers in certain circumstances. Solutions tend to evolve from an initial population of feasible solutions based on their level of fitness in achieving the goal of the optimization. Each individual of the population is defined by a set of genes, representing the elements of a feasible solution vector. As the evolution process proceeds, individuals' genes are mutated and combined to reach a new generation whose overall level of fitness is increased. Individuals of the population either make it to the next generation or are discarded based on their level of fitness with respect to the objective function. It is this evolutionary principle of “survival of the fittest” that EAs use to progressively improve their set of feasible solutions.

The DE algorithm steps are discussed here while the interested reader is referred to Storn and Price (1995) for details of the original DE algorithm (rand/1/bin).

1. DE starts with an objective function  $F(X)$  where  $X$  represents a set of  $N$  decision variables.
2. Each gene of the  $N$  trial vectors are initialized randomly between a specified set of bounds for which the optimal solution of  $F(X)$  is to be found
3. The evolution process is composed of three steps, mutation (i), crossover (ii), and selection (iii).
  - i. Mutation combines the genes of two randomly selected members of the population with another randomly selected unique member. This is done by taking the difference between the first two randomly selected individuals, applying a mutation factor  $F$ , and adding the result to the third, which defines the mutation vector. One mutation vector is generated for each individual or target vector of the population.

- ii. Crossover transfers genes from the mutated vector to the target vector. For each gene of both the mutated and target vectors a random number,  $r \sim U(0, 1)$  is compared to a predefined crossover probability constant,  $CR$ . If  $r < CR$  the mutated gene replaces the target gene, while if  $r > CR$  the target gene is kept. To ensure that at least one mutated gene is transferred to the new individual, a randomly generated number  $rn \sim U(0, N)$  is compared to the index  $i \in [0, N]$  of each gene. If  $i = rn$  then the mutated gene is transferred regardless of the value of  $r$ . The resulting vector is termed the trial vector.
- iii. Finally, the fitness of the trial vector is compared to the target vector using the by inputting them into the objective function. The vector with the best objective function value is kept in the population for the next generation.

As the evolution proceeds, termination is reached when the maximum number of iterations is met, or a tolerance level is satisfied. At this point the fittest individual in the population at the final generation is retained as the final solution that optimizes the objective function.

This algorithm was incorporated into the parameter estimation process of the Vensim model by using the VenPy automation software. The differential evolution algorithm was implemented using the Scipy software package (Virtanen et al. 2019). The Python code used to run the differential algorithm with the ANEMI3 model is provided below.

```
import venpy as vp
import time
from scipy.optimize import differential_evolution as de

# Parameters were loaded from another .cin file
parameters = {}
Nfeval = 1

def func(x):
    global Nfeval
    print(f"Running parameter estimation simulation number {Nfeval}")
    Nfeval += 1

    # Load the compiled Vensim model
    model = vp.load('ANEMI3.vpm')

    # Set the model parameters
    for xi, p in zip(x, parameters):
```

```

    model[p] = xi

# Run the model and return high number in the case of errors
try:
    model.run('total_parameter_estimation_run')
except:
    print("Error running simulation")
    return 1e10
time.sleep(0.2)
try:
    # Obtain total error of parameter estimation objective function
    defined in Vensim
    error = model.result(names=['Total Error'])
    if len(error) == 121:
        total_error = error.values.sum()
        print(f"Current error is: {total_error}")
        return total_error
    else:
        print(f"Simulation did not finish. Total length is
{len(error)}")
        return 1e10

except IOError:
    print("Could not obtain error for this run")
    return 1e10

# Return the value of the objective function
return error

# Run objective function with bounds for parameter values
result = de(func, list(parameters.values()), disp=True, polish=False)

print("Done.")

```

## Appendix C: Previous Reports in the Series

In addition to 78 previous reports (No. 01 – No. 78) prior to 2012

Samiran Das and Slobodan P. Simonovic (2012). [Assessment of Uncertainty in Flood Flows under Climate Change](#). Water Resources Research Report no. 079, Facility for Intelligent Decision Support, Department of Civil and Environmental Engineering, London, Ontario, Canada, 67 pages. ISBN: (print) 978-0-7714-2960-6; (online) 978-0-7714-2961-3. Rubaiya

Sarwar, Sarah E. Irwin, Leanna King and Slobodan P. Simonovic (2012). [Assessment of Climatic Vulnerability in the Upper Thames River basin: Downscaling with SDSM](#). Water Resources Research Report no. 080, Facility for Intelligent Decision Support, Department of Civil and Environmental Engineering, London, Ontario, Canada, 65 pages. ISBN: (print) 978-0-7714-2962-0; (online) 978-0-7714-2963-7.

Sarah E. Irwin, Rubaiya Sarwar, Leanna King and Slobodan P. Simonovic (2012). [Assessment of Climatic Vulnerability in the Upper Thames River basin: Downscaling with LARS-WG](#). Water Resources Research Report no. 081, Facility for Intelligent Decision Support, Department of Civil and Environmental Engineering, London, Ontario, Canada, 80 pages. ISBN: (print) 978-0-7714-2964-4; (online) 978-0-7714-2965-1.

Samiran Das and Slobodan P. Simonovic (2012). [Guidelines for Flood Frequency Estimation under Climate Change](#). Water Resources Research Report no. 082, Facility for Intelligent Decision Support, Department of Civil and Environmental Engineering, London, Ontario, Canada, 44 pages. ISBN: (print) 978-0-7714-2973-6; (online) 978-0-7714-2974-3.

Angela Peck and Slobodan P. Simonovic (2013). [Coastal Cities at Risk \(CCaR\): Generic System Dynamics Simulation Models for Use with City Resilience Simulator](#). Water Resources Research Report no. 083, Facility for Intelligent Decision Support, Department of Civil and Environmental Engineering, London, Ontario, Canada, 55 pages. ISBN: (print) 978-0-7714-3024-4; (online) 978-0-7714-3025-1.

Roshan Srivastav and Slobodan P. Simonovic (2014). [Generic Framework for Computation of Spatial Dynamic Resilience](#). Water Resources Research Report no. 085, Facility for Intelligent Decision Support, Department of Civil and Environmental Engineering, London, Ontario, Canada, 81 pages. ISBN: (print) 978-0-7714-3067-1; (online) 978-0-7714-3068-8.

Angela Peck and Slobodan P. Simonovic (2014). [Coupling System Dynamics with Geographic Information Systems: CCaR Project Report](#). Water Resources Research Report no. 086, Facility 56 for Intelligent Decision Support, Department of Civil and Environmental Engineering, London, Ontario, Canada, 60 pages. ISBN: (print) 978-0-7714-3069-5; (online) 978-0-7714-3070-1.

Sarah Irwin, Roshan Srivastav and Slobodan P. Simonovic (2014). [Instruction for Watershed Delineation in an ArcGIS Environment for Regionalization Studies](#). Water Resources Research Report no. 087, Facility for Intelligent Decision Support, Department of Civil and Environmental

Engineering, London, Ontario, Canada, 45 pages. ISBN: (print) 978-0-7714-3071-8; (online) 978-0-7714-3072-5.

Andre Schardong, Roshan K. Srivastav and Slobodan P. Simonovic (2014). [Computerized Tool for the Development of Intensity-Duration-Frequency Curves under a Changing Climate: Users Manual v.1](#). Water Resources Research Report no. 088, Facility for Intelligent Decision Support, Department of Civil and Environmental Engineering, London, Ontario, Canada, 68 pages. ISBN: (print) 978-0-7714-3085-5; (online) 978-0-7714-3086-2.

Roshan K. Srivastav, Andre Schardong and Slobodan P. Simonovic (2014). [Computerized Tool for the Development of Intensity-Duration-Frequency Curves under a Changing Climate: Technical Manual v.1](#). Water Resources Research Report no. 089, Facility for Intelligent Decision Support, Department of Civil and Environmental Engineering, London, Ontario, Canada, 62 pages. ISBN: (print) 978-0-7714-3087-9; (online) 978-0-7714-3088-6.

Roshan K. Srivastav and Slobodan P. Simonovic (2014). [Simulation of Dynamic Resilience: A Railway Case Study](#). Water Resources Research Report no. 090, Facility for Intelligent Decision Support, Department of Civil and Environmental Engineering, London, Ontario, Canada, 91 pages. ISBN: (print) 978-0-7714-3089-3; (online) 978-0-7714-3090-9.

Nick Agam and Slobodan P. Simonovic (2015). [Development of Inundation Maps for the Vancouver Coastline Incorporating the Effects of Sea Level Rise and Extreme Events](#). Water Resources Research Report no. 091, Facility for Intelligent Decision Support, Department of Civil and Environmental Engineering, London, Ontario, Canada, 107 pages. ISBN: (print) 978-0-7714-3092-3; (online) 978-0-7714-3094-7.

Sarah Irwin, Roshan K. Srivastav and Slobodan P. Simonovic (2015). [Instructions for Operating the Proposed Regionalization Tool "Cluster-FCM" Using Fuzzy C-Means Clustering and LMoment Statistics](#). Water Resources Research Report no. 092, Facility for Intelligent Decision Support, Department of Civil and Environmental Engineering, London, Ontario, Canada, 54 pages. ISBN: (print) 978-0-7714-3101-2; (online) 978-0-7714-3102-9. 57

Bogdan Pavlovic and Slobodan P. Simonovic (2016). [Automated Control Flow Generation Procedure: Cheakamus Dam Case Study](#). Water Resources Research Report no. 093, Facility for Intelligent Decision Support, Department of Civil and Environmental Engineering, London, Ontario, Canada, 78 pages. ISBN: (print) 978-0-7714-3113-5; (online) 978-0-7714-3114-2.

Sarah Irwin, Slobodan P. Simonovic and Niru Nirupama (2016). [Introduction to ResilSIM: A Decision Support Tool for Estimating Disaster Resilience to Hydro-Meteorological Events](#). Water Resources Research Report no. 094, Facility for Intelligent Decision Support, Department of Civil and Environmental Engineering, London, Ontario, Canada, 66 pages. ISBN: (print) 978-0-7714-3115-9; (online) 978-0-7714-3116-6.

Tommy Kokas, Slobodan P. Simonovic (2016). [Flood Risk Management in Canadian Urban Environments: A Comprehensive Framework for Water Resources Modeling and Decision-Making](#). Water Resources Research Report no. 095. Facility for Intelligent Decision Support,

Department of Civil and Environmental Engineering, London, Ontario, Canada, 66 pages. ISBN: (print) 978-0-7714-3117-3; (online) 978-0-7714-3118-0.

Jingjing Kong and Slobodan P. Simonovic (2016). [Interdependent Infrastructure Network Resilience Model with Joint Restoration Strategy](#). Water Resources Research Report no. 096, Facility for Intelligent Decision Support, Department of Civil and Environmental Engineering, London, Ontario, Canada, 83 pages. ISBN: (print) 978-0-7714-3132-6; (online) 978-0-7714-3133-3.

Sohom Mandal, Patrick A. Breach and Slobodan P. Simonovic (2017). [Tools for Downscaling Climate Variables: A Technical Manual](#). Water Resources Research Report no. 097, Facility for Intelligent Decision Support, Department of Civil and Environmental Engineering, London, Ontario, Canada, 95 pages. ISBN: (print) 978-0-7714-3135-7; (online) 978-0-7714-3136-4.

R Arunkumar and Slobodan P. Simonovic (2017). [General Methodology for Developing a CFD Model for Studying Spillway Hydraulics using ANSYS Fluent](#). Water Resources Research Report no. 098, Facility for Intelligent Decision Support, Department of Civil and Environmental Engineering, London, Ontario, Canada, 39 pages. ISBN: (print) 978-0-7714-3148-7; (online) 978-0-7714-3149-4.

Andre Schardong, Slobodan P. Simonovic and Dan Sandink (2017). [Computerized Tool for the Development of Intensity-Duration-Frequency Curves Under a Changing Climate: Technical Manual v.2.1](#). Water Resources Research Report no. 099, Facility for Intelligent Decision Support, Department of Civil and Environmental Engineering, London, Ontario, Canada, 52 pages. ISBN: (print) 978-0-7714-3150-0; (online) 978-0-7714-3151-7. 58

Andre Schardong, Slobodan P. Simonovic and Dan Sandink (2017). [Computerized Tool for the Development of Intensity-Duration-Frequency Curves Under a Changing Climate: User's Manual v.2.1](#). Water Resources Research Report no. 100, Facility for Intelligent Decision Support, Department of Civil and Environmental Engineering, London, Ontario, Canada, 52 pages. ISBN: (print) 978-0-7714-3152-4; (online) 978-0-7714-3153-1.

Ayushi Gaur, Abhishek Gaur and Slobodan P. Simonovic (2017). [Modelling of High Resolution Flow from GCM Simulated Runoff using a Mesoscale Hydrodynamic Model: CAMA-FLOOD](#). Water Resources Research Report no. 101, Facility for Intelligent Decision Support, Department of Civil and Environmental Engineering, London, Ontario, Canada, 44 pages. ISBN: (print) 978-0-7714-3154-8; (online) 978-0-7714-3155-5.

Jingjing Kong and Slobodan P. Simonovic (2017). [Multi-hazard resilience model of an interdependent infrastructure system](#). Water Resources Research Report no. 102, Facility for Intelligent Decision Support. Department of Civil and Environmental Engineering, London, Ontario, Canada, 99 pages. ISBN: (print) 978-0-7714-3158-6; (online) 978-0-7714-3159-3.

Andre Schardong, Slobodan P. Simonovic and Dan Sandink (2018). [Computerized Tool for the Development of Intensity-Duration-Frequency Curves Under a Changing Climate: Technical Manual v.3](#). Water Resources Research Report no. 103, Facility for Intelligent Decision Support,

Department of Civil and Environmental Engineering, London, Ontario, Canada, 67 pages. ISBN: 978-0-7714-3107-4.

Andre Schardong, Slobodan P. Simonovic and Dan Sandink (2018). [Computerized Tool for the Development of Intensity-Duration-Frequency Curves Under a Changing Climate: User's Manual v.3](#). Water Resources Research Report no. 104, Facility for Intelligent Decision Support, Department of Civil and Environmental Engineering, London, Ontario, Canada, 80 pages. ISBN: 978-0-7714-3108-1.

Schardong, A., S. P. Simonovic and H. Tong (2018). Use of Quantitative Resilience in Managing Urban Infrastructure Response to Natural Hazards: A Web-Based Decision Support Tool - ResilSIMt. Water Resources Research Report no. 105, Facility for Intelligent Decision Support, Department of Civil and Environmental Engineering, London, Ontario, Canada, 112 pages. ISBN: 978-0-7714-3115-7.

Feitoza Silva D. and S. P. Simonovic (2020). [Development of Non-Stationary Rainfall Intensity Duration Frequency Curves for Future Climate Conditions](#). Water Resources Research Report no. 106, Facility for Intelligent Decision Support, Department of Civil and Environmental Engineering, London, Ontario, Canada, 48 pages. ISBN:.

Braden, J. and S.P. Simonovic (2020). A Review of Flood Hazard Mapping Practices across Canada. Water Resources Research Report no. 107, Facility for Intelligent Decision Support, Department of Civil and Environmental Engineering, London, Ontario, Canada, 64 pages. ISBN:.